Enzyme Inactivation by Photoexcited Titanium Dioxide (TiO_2) and Prevention by Encapsulation

Pascal Turcotte

A Thesis

in

The Department

of

Chemistry

Presented in Partial Fulfillment of the Requirements
For the Degree of Master of Science (Chemistry) at
Concordia University
Montréal, Québec, Canada

September 2003

Your file Votre référence
ISBN: 0-612-83854-4
Our file Notre référence
ISBN: 0-612-83854-4

ABSTRACT

Enzyme Inactivation by Photoexcited Titanium Dioxide (TiO_2) and Prevention by Encapsulation

Pascal Turcotte

Titanium dioxide (TiO_2) is used in sunscreens because it reflects and scatters UV light. However, TiO_2 can catalyze *in vitro* oxidative damage to DNA, to cultured human fibroblasts and can also inactivate the enzyme horseradish peroxidase (HRP) upon photoexcitation by UV light. The effects of photoexcited TiO_2 on two key enzymes involved in the skin's enzymatic antioxidant defense system, copper-zinc superoxide dismutase (CuZnSOD) and catalase, are reported here. Both enzymes are rapidly inactivated upon exposure to photoexcited TiO_2, and their inactivation mechanisms are described. Hydroxyl radicals ($OH^{\bullet}$), generated upon photoexcitation of TiO_2, attack the active sites of the enzymes, leading to their inactivation. Copper release from CuZnSOD and heme destruction in catalase were observed, which explain the loss of activity. Encapsulation of TiO_2 in faujasite and mordenite, two different types of zeolites, greatly reduced the inactivation of CuZnSOD and catalase upon exposure to UVA light. These results suggest that encapsulation may lead to safer sunscreens based on supramolecular chemistry.

ACKNOWLEDGMENTS

I would first like to thank my supervisor, Dr. Ann M. English, for her help and guidance through my project. I also wish to thank Dr. Tito Scaiano for his advice and for the encapsulated TiO_2 sample that was provided by his lab. Many thanks to Dr. Farida Mohamed for her help with cell cultures and for many helpful discussions. John Wright and Heng Jiang are thanked for their help with mass spectrometry and SDS-PAGE, Dr. Marcus Lawrence for allowing me to use his glove box, and all the members of our group for their help and support during my graduate studies, and for tolerating my music over the past two years.

Finally, I want to sincerely thank my parents, Lise and Raymond, and my three brothers, Martin, Stéphane and Robert, who always supported me and believed in my potential. Without them, all this work would not have been possible.

TABLE OF CONTENTS

LIST OF FIGURES

LIST OF TABLES

LIST OF ABBREVIATIONS

ABTS: 2,2-azino-di-[3-ethylbenzthiazoline sulfonate (6)] diammonium salt

CHO cells: chinese hamster ovary cells

CuZnSOD: copper-zinc superoxide dismutase

DDC: diethyldithiocarbamic acid

DHA: dihydroxyacetone

DMEM : Dulbecco's modified eagle's medium

DNA: deoxyribonucleic acid

DTPA: diethylenetriaminepentaacetic acid

DTT: dithiothreitol

FeSOD: iron superoxide dismutase

GSH: glutathione

HeLa cells: Human cervix epitheloid carcinoma cells

HEPES: N-2-Hydroxyethylpiperazine-N'-2-ethanesulfonic acid

HRP: horseradish peroxidase

MnSOD: manganese superoxide dismutase

NADP: nicotinamide adenine dinucleotide phosphate

OMC: octyl methoxycinnamate

PABA: *p*-aminobenzoic acid

PBS: phosphate buffered saline

PBSA: 2-phenyl-benzimidazole-5-sulfonic acid

PMSF: phenylmethylsulfonyl fluoride

RK: rat keratinocytes

ROS: reactive oxygen species

rpm: rotations per minute

SDS-PAGE: sodium dodecylsulfate-polyacrylamide gel electrophoresis

SPF: sun protection factor

UVR: ultraviolet radiation

Chapter 1

1. INTRODUCTION

1.1 Sunscreens

With the constant diminution of the thickness of the ozone layer, sunscreens with higher and higher sun protection factor (SPF) have appeared on the market. Also, the development of new sunscreen ingredients is of much interest.

1.1.1 Types of sunscreens

Table 1 lists the most common ultraviolet radiation (UVR) filters currently used in sunscreens. UVR filters can be grouped in two main categories, those using organic molecules and those using inorganic particles.

1.1.1.1 Organic sunscreens

The function of a sunscreen is to afford protection to the skin from the sun. Organic molecules that absorb and convert UV light into heat through a process known as cyclic photochemistry are the main type of sunscreen used today. The most common sunscreens are octyl methoxycinnamate (OMC) and oxybenzone. These compounds absorb a specific portion of the UV spectrum and protect the skin from that specific irradiation. But no single organic sunscreen agent used at levels currently allowed by the U.S. Food and Drug Administration [Food and Drug Administration (1993)] can provide a high SPF. Hence, organic sunscreens are almost always used in combination.

Table 1. List of UVR filters used in the skin care market in the United States [Gasparro (1998)].

UV filter (approximate rank order)	Comment
Octyl methoxycinnamate (OMC)	Found in over 90% of sunscreen products used in the world
Oxybenzone	Combined with OMC in many beach products
Octyl salicylate	Used in oxybenzone/OMC primarily for its solvent properties
Octocrylene	Found in many recreational sunscreen products
2-Phenyl-benzimidazole-5-sulfonic acid (PBSA)	Used in combination with OMC in daily UV protectant products
Methyl anthranilate	
Homosalate	
2-Ethylhexyl-4-dimethylaminobenzoate (Padimate O)	
Avobenzone	
Zinc oxide	
Titanium dioxide	
p-Aminobenzoic acid (PABA)	Rarely used
Glyceryl aminobenzoate	Rarely used
Amyl *p*-dimethylaminobenzoate (Padimate A)	Rarely used
Ethyl 4-[bis(hydroxypropyl)]amino	Rarely used
Dioxybenzone	Rarely used
Sulisobenzone	Rarely used
Cinoxate	Rarely used
Diethanolamine *p*-methoxycinnamate	Rarely used
Lawsone + dihydroxyacetone (DHA)	Rarely used
Red petrolatum	Rarely used
Sodium 3,4-dimethylphenyl glyoxylate	Rarely used
Benzoate digalloyltrioleate	Rarely used
Triethanolamine salicylate	Rarely used

1.1.1.2 Inorganic sunscreens

The second type of sunscreen ingredient consists of inorganic particles. These are used with increasing frequency, in part, because of their effectiveness in blocking UVA light. Inorganic sunscreens protect from UV light via a mechanism that is quite different from that employed by organic molecules. Effectively, inorganic particles act as light scatterers by reflecting and dispersing UV light. The two main particles used are titanium dioxide (TiO_2) and zinc oxide (ZnO).

1.1.2 Problems associated with sunscreens

Even though sunscreens protect well against UV light, they are not perfect and some problems are still encountered.

1.1.2.1 Organic sunscreens

Organic sunscreens may be absorbed by the skin and can come in contact with biological materials resulting in adverse effects. For example, PABA, which was supposed to be an efficient and safe sunscreen, is now known to be a potential carcinogen when photosensitized [Gasparro (1985), Salter (1993), Shaw (1992), Sutherland (1984)]. Another important property of a sunscreen is its "fatigue resistance". In some cases, the active molecule will be destroyed in the photoprotective process, leading to production of compounds that can also be harmful to living tissues. Moreover, as pointed out earlier, mixtures of sunscreens are often used to give broad UV protection. Some of the different sunscreen components can interact with each other, leading to the degradation of one of them, thus greatly reducing the efficiency of the sunscreen.

1.1.2.2 Inorganic sunscreens

Inorganic sunscreens such as TiO_2 are known to cause photoinduced DNA damage [Dunford (1997)]. Such damage is caused by different reactive oxygen species (ROS) produced upon UV irradiation and will be discussed later. The goal of this project is to develop a new type of sunscreen that would prevent or reduce some of these problems.

1.1.2.3 Sun Protection Factor (SPF)

A major problem related to sunscreens is that the population is not properly informed about their use. Most customers consider only the SPF value when they buy a sunscreen. What does SPF mean and what does it represent? SPF stands for "Sun Protection Factor" and is defined as the ratio of the sun exposure that skin can tolerate before burning or before minimal erythema is apparent with and without sunscreen protection. For example, if someone applies a sunscreen with an SPF of 15, it means that it will take 15 times longer to observe redness of the skin compared to when no sunscreen is applied. Thus, SPF just gives an indication of the protection against sunburns. Since sunburns are mainly caused by UVB irradiation, the SPF factor mainly denotes the efficiency of the sunscreen towards UVB light. Although less energetic, UVA can also be very dangerous for the skin. Thus, people who do not know the real definition of SPF use high SPF sunscreens and stay in the sun for long periods believing that they are fully protected since they do not see any immediate effects on their skin.

Even sunscreens with a high SPF factor do not afford full protection from UV light. The best and safest way to avoid skin cancer and other problems related to UV

exposure remains the use of appropriate clothing and keep the amount of sun exposure to a minimum. Nonetheless, people tend to go out more on bright and sunny summer days, either to relax on the beach or just to soak up the sun. Therefore, it becomes important to use an appropriate sunscreen and that is why this work focuses on the development of a new type of sunscreen.

1.2 UV light

It is first important to understand the nature of UV light to appreciate how sunscreens should protect us against it.

1.2.1 Solar irradiation

The solar irradiation that reaches the earth's surface is composed mainly of UV, visible and infrared light (Figure 1). The total solar radiation that is detected at the earth's surface consists of about 15% UV, 60% visible and 25% infrared radiation. Although UV radiation accounts for the smallest portion, it is the most energetic due to its short wavelength. UV radiation is subdivided in three main regions: UVC (100-280 nm), UVB (280-320 nm) and UVA (320-400 nm). In the last decade, concerns were raised regarding the protection of human skin against UV light because of the reduction in the thickness of the ozone layer. A closer look at Figure 1 shows that no UVC reaches the earth because it is absorbed by the ozone layer. Also, about 70-90 % of UVB is absorbed by the ozone layer, allowing only a small percentage to reach the earth's surface, but all UVA radiation can penetrate the ozone layer.

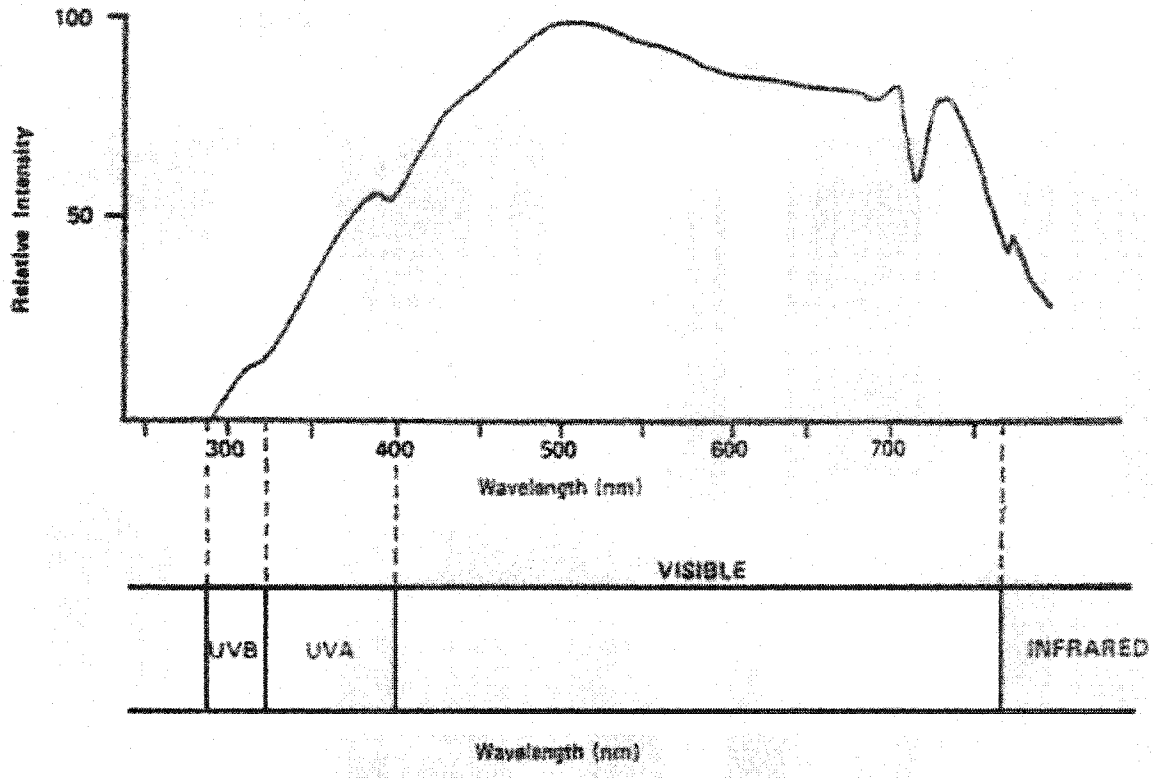

Figure 1. Sunlight spectrum reaching the earth's surface [Frain-Bell (1985)].

1.2.2 Effects of skin exposure to UV light

Because it is very energetic, UV radiation can cause a lot of damage to the skin. Figure 2 shows a diagram of the layers present in human skin and Figure 3 indicates the penetration of UV light into the different skin layers. Although it is less energetic, UVA light penetrates deeper into the skin than UVB. This is because the absorption of light by living tissues is greater at shorter wavelengths. Much of the UVA damage occurs in the epidermis and the dermis while most UVB damage is found only in the epidermis. Effectively, ultraviolet radiation of the shorter wavelength (UVB; 280-320 nm) is mostly absorbed in the epidermis and affects predominantly epidermal cells, *i.e.* keratinocytes, while longer wavelength (UVA; 320-400 nm) penetrate deeper and can interact with both

epidermal keratinocytes and dermal fibroblasts. As noted earlier, UVB is mainly responsible for skin erythema (redness of the skin that leads to sunburn), so its effect on

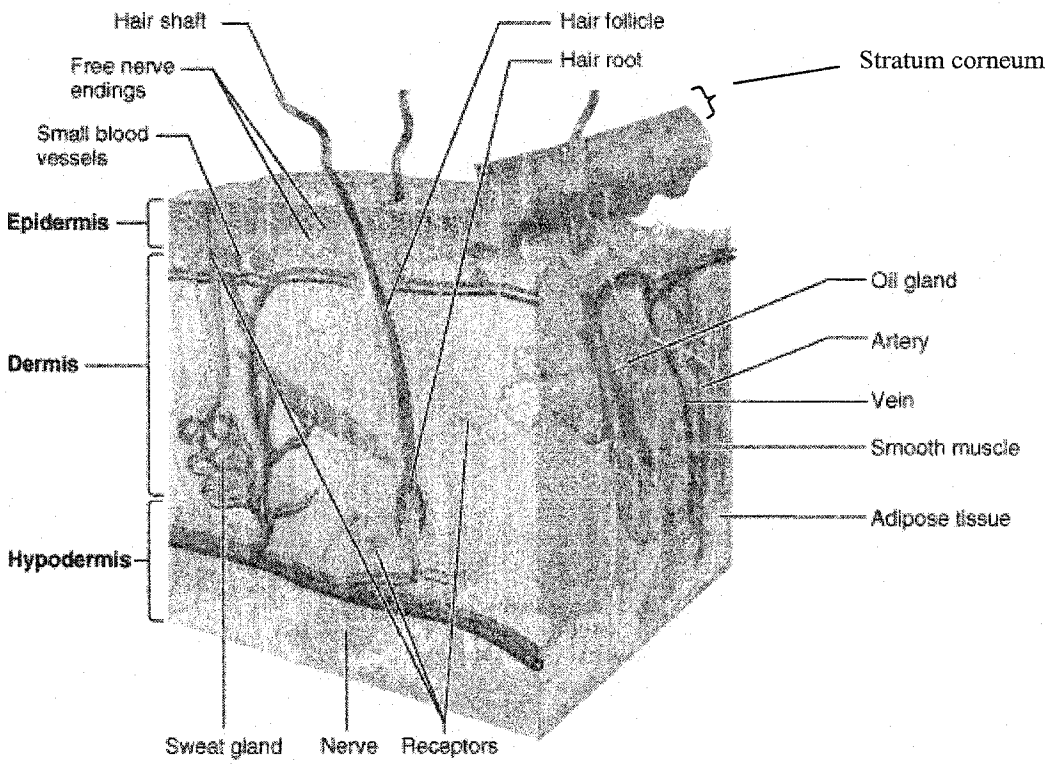

Figure 2. Diagram of the layers present in normal human skin. On top of the skin, there is a layer of dead cells called the *stratum corneum*. Underneath are the *epidermis*, the *dermis* and the *hypodermis* [www.bmb.psu.edu/courses/bisci004a/tissues/tissnote.htm].

the skin is more obvious than that of UVA. Since UVA rays are less energetic and they penetrate deeper into the skin, their effects are harder to detect and may lead to long-term problems. Some of the main effects on health due to overexposure to the sun regardless of skin color include:

- Skin cancer (melanoma, basal-cell carcinoma, and squamous-cell carcinoma).

- Premature aging of the skin and other problems (e.g., actinic keratoses).
- Cataracts and other eye damage (e.g., pterygium, skin cancer around the eyes and degeneration of the macula).
- Suppression of the immune system and the skin's natural defenses (e.g., impaired response to immunizations; increased sensitivity to sunlight; and reactions to certain medications).
- Tanning and sunburn.

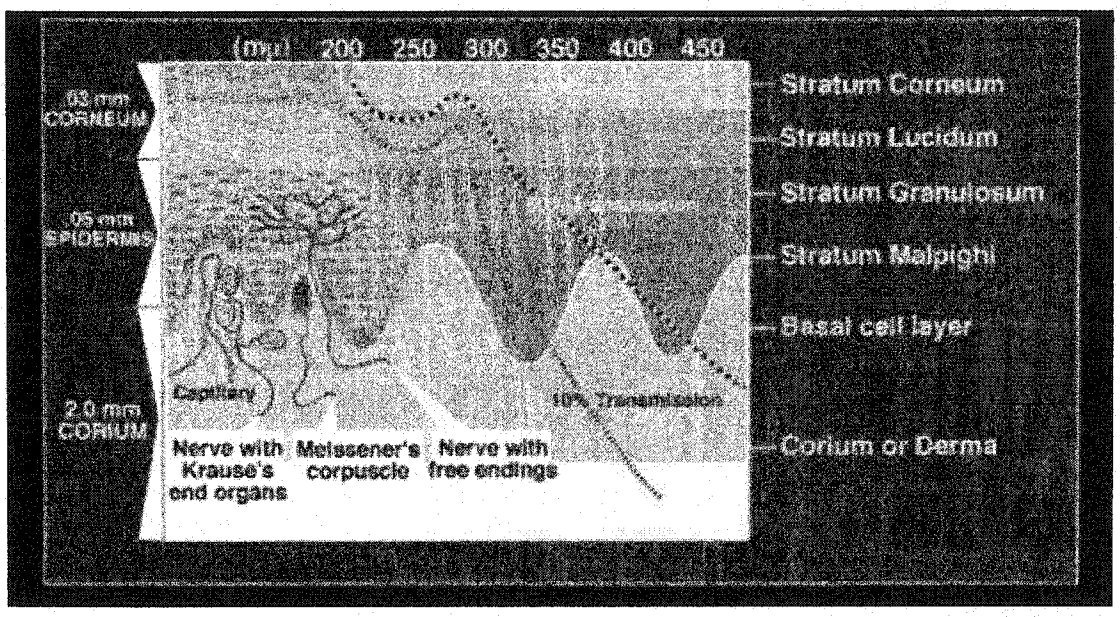

Figure 3. UV light penetration into skin [http://medlib.med.utah.edu/kw/derm/pages/meet_2.htm].

It is well known that UVB and UVA irradiation induce the formation of reactive oxygen species (ROS) in cutaneous tissues [Kitazawa (1997), Scharffetter-Kochanek (1997)]. These oxygen radicals and other activated oxygen species react with amino acid residues in proteins and frequently result in functional changes of structural or enzymatic proteins [Stadtman (1992)]. They can also exert a multitude of other effects such as lipid peroxidation, activation of transcription factors and generation of DNA-strand breaks.

These lead to premature aging of the skin, termed photoaging, which gives the skin a leathery and wrinkled appearance. Photoaging also leads to thickening of the skin.

1.3 Antioxidant enzymes

To protect the skin from harmful ROS, cells contain different enzymes that regulate their concentrations to an acceptable level. The skin's enzymatic antioxidant defense system includes copper-zinc superoxide dismutase (CuZnSOD), manganese superoxide dismutase and catalase. This study investigates the effects of UV irradiation on CuZnSOD and catalase. Since these are key enzymes in protecting the skin from ROS, the results will yield critical information on the effects of photoexcited titanium dioxide on the skin's enzymatic antioxidant defense system.

1.3.1 Copper-Zinc superoxide dismutase

Two families of enzymes exist for the disproportionation of the harmful superoxide radical ($O_2^{\bullet -}$). These are (1) the copper-zinc superoxide dismutases,

$$2\,O_2^{\bullet -} + 2\,H^+ \underset{}{\overset{SOD}{\rightleftharpoons}} H_2O_2 + O_2 \qquad (1)$$

CuZnSOD [Bannister (1987), Valentine (1981), Valentine (1985)] found in almost all eukaryotic cells and (2) the manganese and iron superoxide dismutases, MnSOD and FeSOD, the former found in the mitochondria of eukaryotic cells, and both found in many prokaryotes. The focus here is on CuZnSOD because it is the cytosolic form of SOD and hence more likely affected by radicals generated upon photoexcitation of titanium dioxide as opposite to MnSOD, which is located in the mitochondria.

1.3.1.1 Structure of CuZnSOD

CuZnSODs are highly stable enzymes. They are located in the cytosol, in lysosomes, in peroxisomes, in the nucleus, and in the space between the inner and outer mitochondrial membranes [Halliwell (1999)]. Table 2 lists some properties of bovine erythrocyte CuZnSOD, which is very similar to human CuZnSOD [Jabusch (1980), Steinman (1974)].

The enzyme contains two identical subunits held together by hydrophobic interactions [Bannister (1987), Valentine (1981), Valentine (1985)] (Figure 4). Each subunit consists of a flattened cylindrical barrel of β-pleated sheet from which three external loops of irregular structure extend (Figure 5). Each subunit contains one copper and one zinc atom bridged by the imidazolate ring of a histidyl side chain (Figures 5, 6 and 7). The copper lies at the bottom of a narrow channel that is large enough to admit only water, small anions, or small ligands (Figure 8). In addition to the positively charged Cu^{II} ion at the bottom of the channel, the positively charged side chain of Arg141 is part of the walls of the channel, which direct the superoxide anion towards the copper. Two positively charged lysine side chains (not shown in Figure 8) are close to the mouth of the channel. A disruption in the structure of the enzyme and of the channel should decrease the efficiency of the enzyme in directing anions toward the copper, thus leading to loss of enzyme activity.

Table 2. Molecular properties of bovine erythrocyte CuZnSOD [Valentine (1981)].

Property or Characteristic	Value		
Molecular weight	31 200 g/mol		
Isoelectric point	4.95		
Subunit composition	2 identical subunits with 151 amino acid residues each; one intra subunit disulfide bond		
Metal ion content	One Cu^{II} and one Zn^{II} per subunit		
Color	Native Cu^{II} protein, blue-green; apoprotein colorless		
Native Protein λ_{max} (nm)	258	250-270	680
	↓	↓	↓
Native Protein ε_{max} (M^{-1} cm^{-1})	10,300	Fine structure	300

Figure 4. 3D structure of CuZnSOD [http://davinci.ethz.ch/kissner/koppenol_group.html].

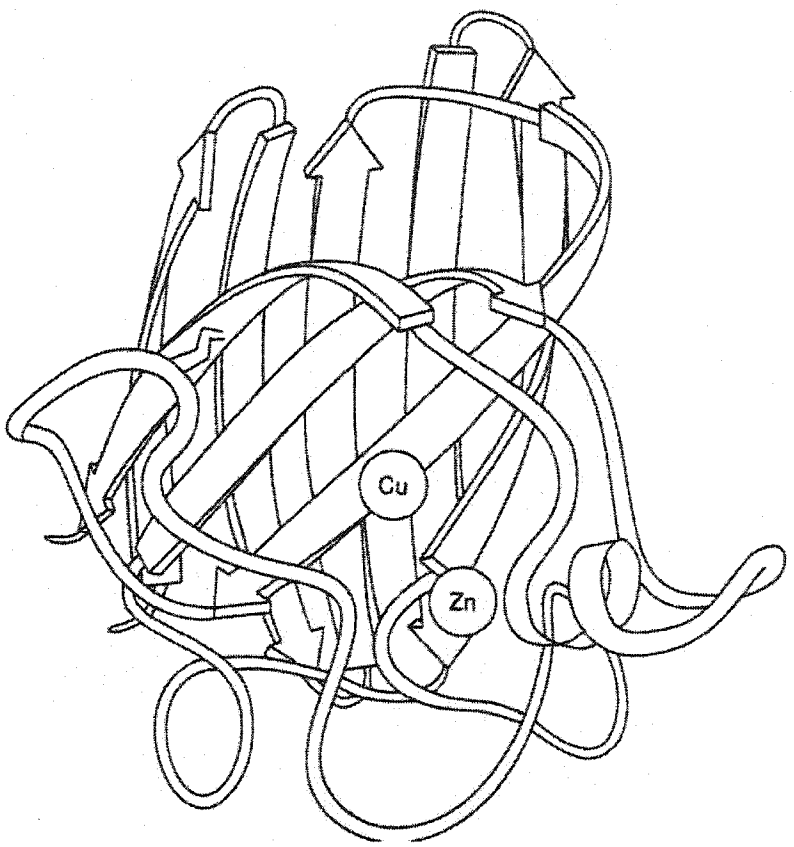

Figure 5. Schematic drawing of the polypeptide backbone of one of the two subunits of bovine CuZnSOD. The β-strands are shown as arrows. The active-site channel provides access to the copper site from the direction of the viewer [Tainer (1982)].

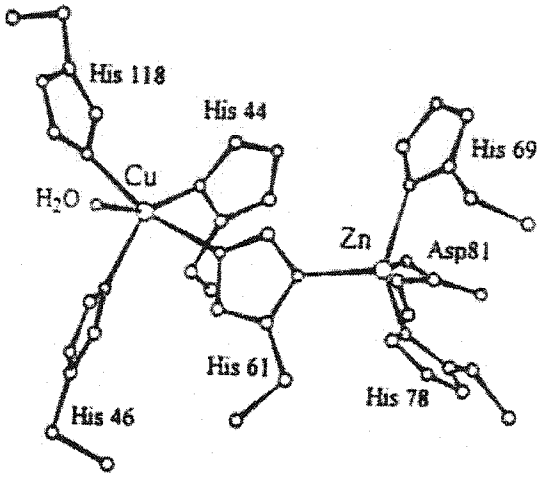

Figure 6. Representation of the metal-binding site of CuZnSOD [Bertini (1994)].

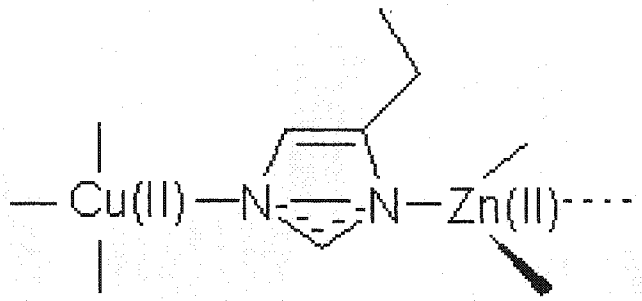

Figure 7. The copper and zinc binding sites share a common ligand, a deprotonated imidazole ring from a histidyl residue.

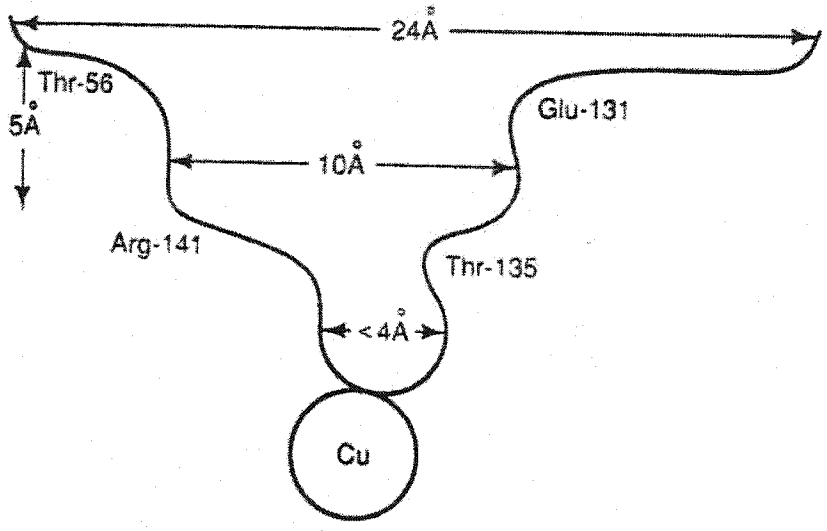

Figure 8. Schematic diagram of a cross section of the active-site channel in CuZnSOD [Bertini (1994)].

1.3.1.2 Activity of CuZnSOD

CuZnSOD protects cells from oxidative stress by removing superoxide via the mechanism shown in Equations 2 and 3. Effectively, one molecule of CuZnSOD transforms two molecules of superoxide per catalytic cycle. One molecule is oxidized (Reaction 2) while the other is reduced (Reaction 3).

$$E\text{-}Cu^{II} + O_2^{\bullet -} \rightleftharpoons E\text{-}Cu^{I} + O_2 \qquad (2)$$

$$E\text{-}Cu^{I} + O_2^{\bullet -} \rightleftharpoons E\text{-}Cu^{II} + H_2O_2 \qquad (3)$$

The role of the zinc ion in CuZnSOD appears to be primarily structural [Bertini (1994)]. There is no evidence that water, anions, or other potential ligands bind to the zinc, so it is highly unlikely that superoxide binds at this site. Moreover, removal of zinc under conditions where the copper ion remains bound to the copper site does not significantly diminish the SOD activity of the enzyme [Pantoliano (1982)]. However, such removal does result in diminished thermal stability. The zinc-depleted protein denatures at lower temperature than the native protein, supporting the hypothesis that the role of the zinc is primarily structural in nature [Roe (1988)].

1.3.2 Catalase

Antioxidant enzymes work in a complementary manner to protect cells from ROS. As discussed above, CuZnSOD converts superoxide radicals to hydrogen peroxide, an oxidizing agent that contributes to the aging process in animals. The function of catalase within cells is to prevent the accumulation of toxic levels of H_2O_2 by catalyzing its conversion to water and oxygen:

$$2\ H_2O_2 \xrightleftharpoons{\text{catalase}} 2\ H_2O + O_2 \qquad (4)$$

1.3.2.1 Structure of catalase

Catalase is a hemoprotein consisting of four identical subunits of equal size (MW 60-65 kDa) to yield a ~ 240 kDa protein (Figure 9). The bovine liver catalase monomer consists of a 506 residue polypeptide chain plus one heme (Figure 10) and one NADP group. The latter is on the surface and the heme is embedded in the middle of each monomer, ~ 20 Å below the molecular surface and ~ 23 Å from the center of the

tetramer. The catalase subunit is composed of 26% α-helix and 12% β-sheet and irregular structures include a predominance of extended single strands and loops that play a major role in the assembly of the tetramer. This is more complicated than a simple combination of monomers since changes in the folding pattern of each monomer occur to optimize packing interactions [http://www.clunet.Edu/BioDev/omm/catalase/frames/cattx. htm].

Although the heme group is deeply embedded in each subunit, it can be accessed through a funnel-shaped channel 30 Å long and 15 Å wide. The channel is lined with hydrophilic residues at the entrance and hydrophobic residues as the channel descends, constricting, towards the heme [http://www.clunet.Edu/BioDev/omm/catalase/frames/cattx.htm]. The hydrophilic residues at the entrance of the channel are thought to be involved in the initial binding of the heme while hydrophobic residues stabilize the iron and the shape of the cavity [http://www.clunet.Edu/BioDev/omm/catalase/frames/cattx.htm].

1.3.2.2 Activity of catalase

Catalatic activity is present in nearly all animal cells and organs in aerobic microorganisms. The chemistry of catalase catalysis has not been precisely described yet, but the following two-step mechanism has been proposed [http://www.clunet.Edu/BioDev/omm/catalase/frames/cattx.htm]:

$$E\text{-}Fe^{III} + H_2O_2 \rightleftharpoons E\text{-}Fe^{IV}{=}O + H_2O \quad (5)$$

$$E\text{-}Fe^{IV}{=}O + H_2O_2 \rightleftharpoons E\text{-}Fe^{III} + H_2O + O_2 \quad (6)$$

E-Fe represents the iron center of the heme attached to the rest of the enzyme (E).

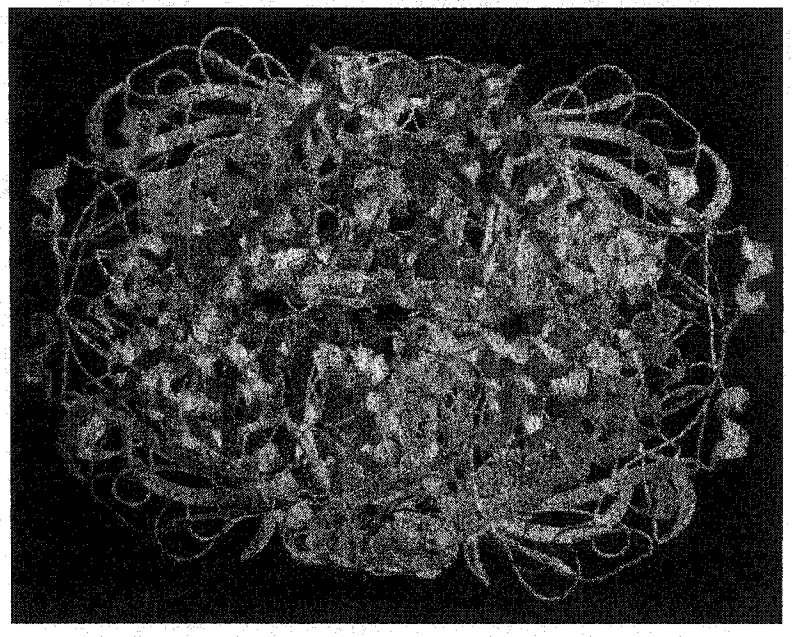

Figure 9. 3D structure of *E. coli* catalase [http://crystal.uah.edu/carter/enzyme/catalase.htm].

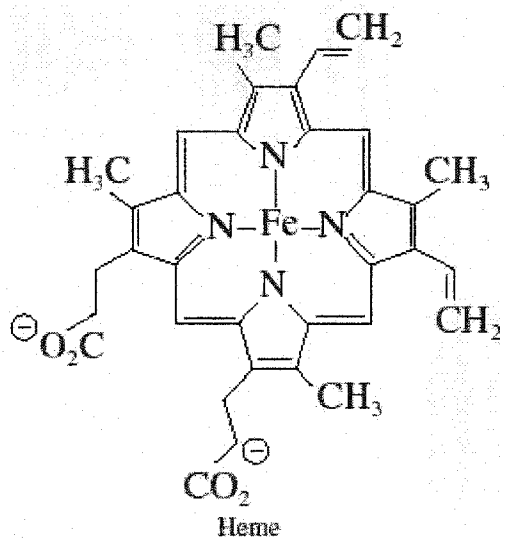

Figure 10. Structure of the protoporphyrin heme found in bovine catalase [http://www.callutheran.Edu/BioDev/omm/catalase/frames/cattx.htm].

H_2O_2, upon entering the heme cavity, is severely sterically hindered and must be positioned to interact with His74 and Asn147. Transfer of a proton from one oxygen of the peroxide to the other, via His74, elongates and polarizes the O-O bond, which cleaves heterolytically as a peroxide oxygen is coordinated to the iron center. This coordination

displaces water and forms what is called compound I, which possesses Fe^{IV}=O plus a porphyrin radical. Compound I, which is two oxidizing equivalents above the resting enzyme E-Fe^{III}, then reacts with a second molecule of hydrogen peroxide to reform E-Fe^{III} with the release of H_2O and O_2:

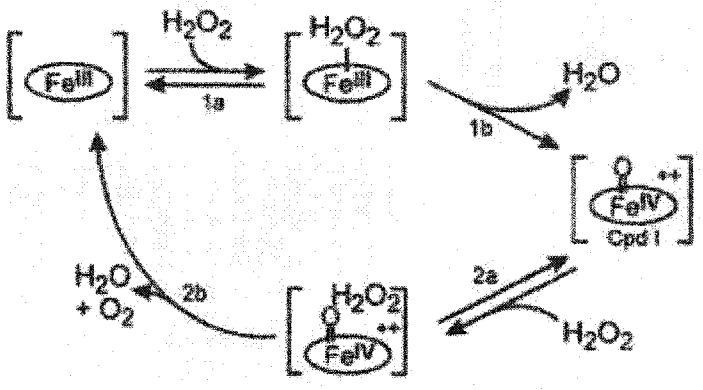

Figure 11. Catalase reaction scheme [Regelsberge (2000)].

1.4 Titanium dioxide (TiO_2)

As mentioned in Section 1.1.1, many different components are used in sunscreens to protect human skin from UV radiation. One such component consists of titanium dioxide (TiO_2) particles. Beside sunscreens, TiO_2 is widely used in cosmetic and industrial applications as discussed next.

1.4.1 Uses of TiO_2

The largest market for TiO_2 is in the manufacture of pigments. Because of its high refractive index, TiO_2 particles impart whiteness, opacity, and brightness to paints, varnishes and lacquers. TiO_2 is also used in face powder, beauty creams, lipsticks, emulsion bases, ointments, and in ingested products such as toothpaste [http://www.admmr.state.az.us/circ9titanium.htm]. TiO_2 is also a semiconductor that acts as a

photocatalyst in the degradation of pollutants [Kominami (1998), Litter (1999), Malato (2000)], in the photochemical splitting of water [Kudo (1987), Mallouk (1992)] and in photovoltaic solar cells [Amadelli (1990), Hagfeldt (2000)]. TiO_2 particles and other titanium compounds are additionally found in rubber tires, floor and wall coverings, glass fibers, ceramic capacitors, carbide cutting tools, and organotitanium catalysts.

The application of interest in this study is related to the light scatterering properties of TiO_2, the basis for its use in the cosmetic and paper industries. In fact, TiO_2 has the highest refractive index of all colorless substances known [http://www.psrc.usm.edu/macrog/coatings/tio2.htm] and it provides the best light scattering ability as well as the best hiding power. These properties have driven the use of TiO_2 as a safe physical sunscreen (US Federal Register, 43FR38206, 25 August 1978) because it reflects and scatters both UVB and UVA radiation. TiO_2 in sunscreens is formulated as "micronised" or "ultrafine" (20-50 nm) particles that scatter light according to Rayleigh's law, whereby the intensity of scattered light is inversely proportional to the fourth power of the wavelength [Judin (1993)]. Consequently, TiO_2 particles scatter UVB (290-320 nm) and UVA (320-400 nm) radiation more than the longer, visible wavelengths, preventing sunburn while remaining invisible on the skin. However, TiO_2 absorbs about 70% of the incident UV. In aqueous environments, this leads to the generation of hydroxyl radicals, which can initiate oxidation.

1.4.2 Structure of TiO_2

TiO_2 is polymorphous. It exists in three different forms, rutile, anatase and brookite but only two (rutile and anatase) of these forms are used. The rutile form is

actually used the most because the rutile crystal is more compact, with higher density (rutile has a density of 4.2 g/cc, while anatase has a density of 3.8 g/cc), higher refractive index (2.7) and greater opacity.

In a TiO_2 crystal, each titanium is surrounded by six oxygen ions located at the corners of an octahedron (Figure 12). Each oxygen ion is surrounded by three titanium ions lying in a plane at the corners of an equilateral triangle. The different crystalline forms of TiO_2 are due to the different linkages of the TiO_2 octahedron. In rutile, the structure is based on octahedrons of TiO_2, which share two opposite edges of the octahedron with other octahedrons and form chains; other chains are connected via corners common to three octahedral (Figure 13). In anatase, the octahedrons share four edges with neighbouring octahedral (Figure 14). This results in a more closely packed rutile crystal, hence its higher density compared to anatase.

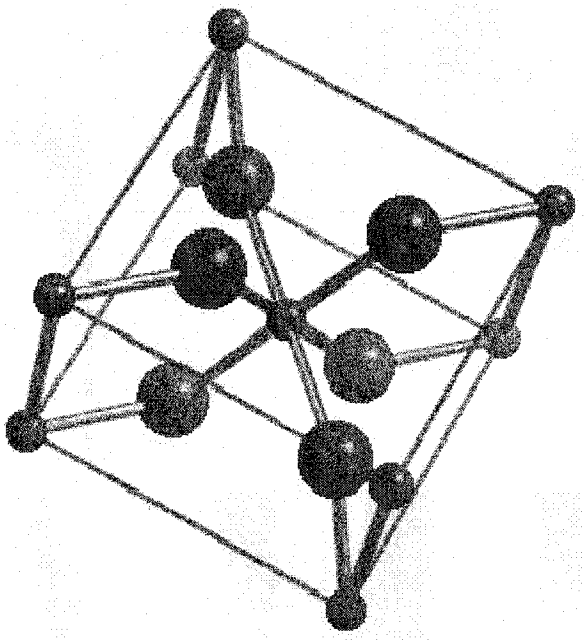

Figure 12. 3D representation of a TiO_2 octahedron [http://www.webelements.com/webelements/compounds/text/Ti/O2Ti1-13463677.html]. Larger balls are oxygen ions (ionic radius 0.65 Å) and smaller balls are titanium ions (ionic radius 1.45 Å).

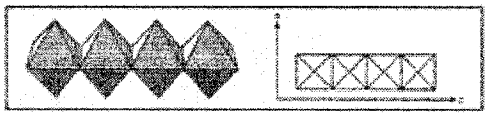

Figure 13. Representation of a rutile TiO_2 crystal [http://www.nl-ind.com/kronos/titanium3.html].

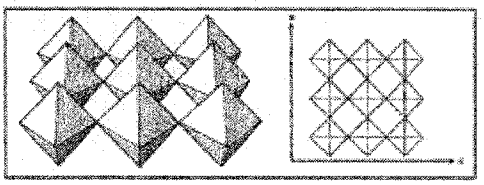

Figure 14. Representation of an anatase TiO_2 crystal [http://www.nl-ind.com/kronos/titanium3.html].

1.4.3 Reactivity of TiO_2

Upon exposure to UVA light lower than ~385 nm, TiO_2 is excited and electrons are promoted from the valence band to the conduction band, thus producing electron-hole pairs. Most of these pairs (~ 90%) recombine within picoseconds, but some are stable for a few nanoseconds [Serpone (1995)], leading to different reactions that produce reactive oxygen species such as superoxide, hydroxyl radicals and hydrogen peroxide:

$$TiO_2 \xrightarrow[\lambda = 350\ nm]{h\nu} hole^+ + e^- \quad (7)$$

$$hole^+ + H_2O \longrightarrow HO^\bullet + H^+ \quad (8)$$

$$O_2 + e^- \longrightarrow O_2^{\bullet -} \quad (9)$$

$$O_2^{\bullet -} + H^+ \longrightarrow HO_2^\bullet \quad (10)$$

$$HO_2^{\bullet} + HO_2^{\bullet} \longrightarrow H_2O_2 + O_2 \quad (11)$$

$$H_2O_2 + O_2^{\bullet -} \longrightarrow HO^- + HO^{\bullet} + O_2 \quad (12)$$

$$hole^+ + HO^- \longrightarrow HO^{\bullet} \quad (13)$$

$$H_2O_2 + e^- \longrightarrow HO^- + HO^{\bullet} \quad (14)$$

Beside their different crystal structures, rutile and anatase also have different reactivities. This was initially attributed to the different position of the conduction band (more positive for rutile) and to the higher recombination rates of the electron-hole pairs photoproduced in rutile [Kawaguchi (1984), Okamoto (1985)]. The band-gap energy (E_G) is 3.2 eV for the anatase and 3.02 eV for the rutile form of TiO_2, corresponding to the energy of light (E) of ≈ 385 nm and 400 nm, respectively (Equation 15).

$$E = h\nu c \quad (15)$$

where E is the energy of light, h is Planck's constant, ν is the wavenumber of the radiation and c is the speed of light.

It could be assumed that the rutile form is more reactive since its band-gap is smaller, so that less energy is required to promote an electron from the valence to the conduction band. However, anatase exhibits much higher photocatalytic activity than that of rutile in all types of reaction media and in the presence of O_2 as an oxidizing species [Augugliaro (1988), Kawaguchi (1984), Okamoto (1985)]. A possible explanation is that rutile is much less efficient in photoadsorbing O_2 than anatase [Sclafani (1996)].

Moreover, photoconductance measurements have clearly indicated that rutile is less efficient in creating electron-hole pairs than anatase [Sclafani (1996)]. The poorer O_2 adsorption capacity and lower electronic reactivity observed for rutile is attributed to its higher degree of crystallinity, which gives rise to fewer structured defects to act as electron sources or adsorption sites for the active oxygen precursor [Primet (1971)]. Thus, the higher activity of anatase with respect to rutile can be explained by its higher photoadsorption and photodesorption of O_2, and its lower electron-hole recombination rate.

Following electron-hole-pair formation and subsequent charge-carrier separation (Equation 16), a fraction of electrons and holes are trapped at lattice sites (oxygen vacancies, Ti^{4+}, and other defects) in competition with recombination. Some electrons and holes migrate to the surface where they are trapped to yield Ti^{3+} centers (trapped electrons in Ti^{4+} sites) and surface-bound radicals, respectively. $\{Ti^{IV}–O^{2-}–Ti^{IV}\}–O^{\bullet}$ or $\{Ti^{IV}–O^{2-}–Ti^{IV}\}–OH^{\bullet}$ species have been proposed based on low-temperature EPR measurements [Micic (1993)] and EPR spin-trap methods at ambient temperature [Jaeger (1979)].

Some of the events occurring at the TiO_2 particle surface following its irradiation are:

1. Charge-carrier generation and separation

$$TiO_2 + h\nu \rightarrow TiO_2\,(e^-/h^+) \rightarrow e^-_{CB} + h^+_{VB} \qquad (16)$$

where e^-_{CB} and h^+_{VB} are conduction-band electrons and valence-band holes, respectively, in TiO_2.

2. Charge-carrier migration to surface

$$e^-_{CB} \rightarrow e^-_S \quad (17a)$$

$$h^+_{VB} \rightarrow h^+_S \quad (17b)$$

$$e^-_S, h^+_S \rightarrow \text{surface migration} \quad (17c)$$

3. Charge-carrier trapping in shallow traps (ST)

$$e^-_{CB} + (ST)_e \rightarrow e^-_{TR} \quad (18a)$$

$$h^+_{VB} + (ST)_h \rightarrow h^+_{TR} \quad (18b)$$

$$e^-_S + A_S \rightarrow A^-_S \quad (18c)$$

$$h^+_S + D_S \rightarrow D^+_S \quad (18d)$$

where e^-_{TR} and h^+_{TB} represent trapped electrons and trapped holes, respectively, in TiO_2 and A_s and D_s are surface acceptors and surface donors, respectively.

4. charge-carrier recombination

$$e^-_{CB} + h^+_{VB} \rightarrow h\nu_1 + TiO_2 \quad (19a)$$

$$e^-_{TR} + h^+_{VB} \rightarrow h\nu_2 + TiO_2 \quad (19b)$$

$$e^-_{CB} + h^+_{TR} \rightarrow h\nu_3 + TiO_2 \quad (19c)$$

$$e^-_{TR} + h^+_{TR} \rightarrow h\nu_4 + TiO_2 \quad (19d)$$

Reaction 19d is responsible for most of the recombination process.

The number of e^-/h^+ pairs formed in Reaction 16 is strongly dependent on the TiO_2 particle size [Serpone (1995)]. Effectively, the average number of pairs per particle immediately after the excitation laser pulse is much higher for bigger particles (1504 pairs per 26.7-nm particle compared to 0.2 pairs per 2.1-nm particle). Moreover, the smaller the particle, the greater the fraction of e^-/h^+ pairs that recombine in 20 ps,

indicating that recombination is faster in small particles. By 10 ns, 100% of all e^-/h^+ pairs have recombined in the 2.1-nm particles versus ~ 90% in 13.3-nm and 26.7-nm particles.

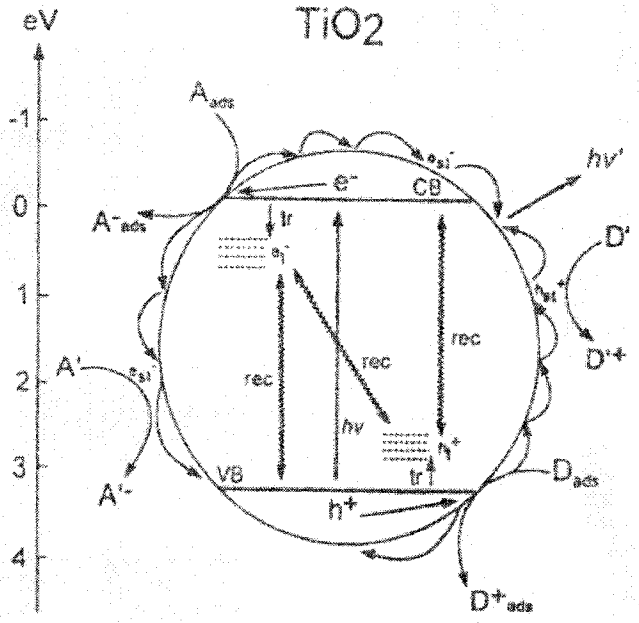

Figure 15. Diagram illustrating some of the events following irradiation of a TiO_2 particle [Serpone (1995)] (CB = conduction band, VB = valence band, rec = recombination, A = acceptor, D = donor, st = shallow trap).

It has also been shown that the production of $OH^\bullet$ radicals from irradiated TiO_2 differs in regard to the crystal form and size [Uchino (2002)]. More $OH^\bullet$ radicals are produced by anatase particles compared to rutile particles [Uchino (2002)]. The size of an anatase TiO_2 particle where $OH^\bullet$ radical generation is the greatest is ~ 30 nm, which is about the size of the TiO_2 particles found in sunscreens. In the case of the rutile form, the optimal size is ~ 90 nm. As expected, the amount of $OH^\bullet$ radical produced increased with higher UVA intensity and with increasing concentrations of TiO_2 [Uchino (2002)].

1.4.4 TiO_2 and skin

Studies have been conducted to measure TiO_2 absorption by the skin [Lademann (1999), Tan (1996)]. The levels of titanium were found to be higher in the skin of subjects who applied TiO_2-containing sunscreens than the levels found in controls. Most interestingly, TiO_2 was not only found at the level of the epidermis, but also in the dermis (Figure 2). However, the bulk of TiO_2 was present in the uppermost part of the stratum corneum. The TiO_2 concentration decreased rapidly with increasing depth of the stratum corneum and only a small amount of TiO_2 was found in its lowest layers. In these layers, the TiO_2 microparticles were localized exclusively in the follicle channels, at a concentration two orders of magnitude smaller than in the upper section of the stratum corneum. However, this cannot be interpreted as TiO_2 penetration into layers of living skin, since the follicular channel is covered with a stratum corneum barrier.

Other studies showed that when HeLa cells were exposed to TiO_2, particles were detected in the cytoplasm of the cells [Cai (1991)]. More important, HeLa cells were killed in the presence of irradiated TiO_2. It was concluded that the cells were killed by hydroxyl ($OH^{\bullet}$) and perhydroxyl ($HO_2^{\bullet}$) radicals produced from water by the irradiated particles (Reaction 7-14), and also that the cells were directly oxidized by photogenerated holes in TiO_2. In another study, the viability of chinese hamster ovary (CHO) cells decreased significantly after exposure to both UVA light and anatase TiO_2 [Uchino (2002)]. A high concentration of anatase (100 μg/mL) even showed cytotoxicity without UVA. It was demonstrated that photoexcited TiO_2 catalyzed oxidative damage to DNA *in vitro* and in cultured human fibroblasts [Dunford (1997)]. I*n vitro* inactivation of the

heme enzyme, horseradish peroxidase (HRP), was also detected in solutions containing TiO_2 following UVA irradiation [Hancock-Chen (2000)].

1.5 Zeolites

To reduce some of the adverse effects caused by sunscreen components, a new generation of sunscreens based on supramolecular chemistry was proposed. A zeolite, which is a porous material, serves to host the organic or inorganic sunscreens. Studies conducted at the University of Ottawa [Cosa (2002a), Cosa (2002b)] using zeolite hosts showed very promising results, since inactivation of HRP by zeolite-encapsulated TiO_2 was significantly less than in solutions containing free TiO_2.

1.5.1 Structure of zeolites

Zeolites are crystalline, porous aluminosilicates with the general composition

$$M_{x/n}Al_xSi_y\ O_{2(x+y)} \bullet (H_2O)_z$$

where M is an exchangeable cation of valence n and $(H_2O)_z$ represents the number of hydrated waters. Zeolites are made up of a series of SiO_4^{-4} and AlO_4^{-5} tetrahedra stacked in regular arrays to form channels. The way the stacking can occur is virtually limitless, and hundreds of unique structures are known. Figure 16 clearly shows the cavities that are formed within a zeolite.

Their uniform cavities and channels make zeolites highly versatile materials. They are used as molecular sieves in size-exclusion separations, as catalysts for reactions such as alkylation and isomerisation, as a matrix in the purification of proteins from

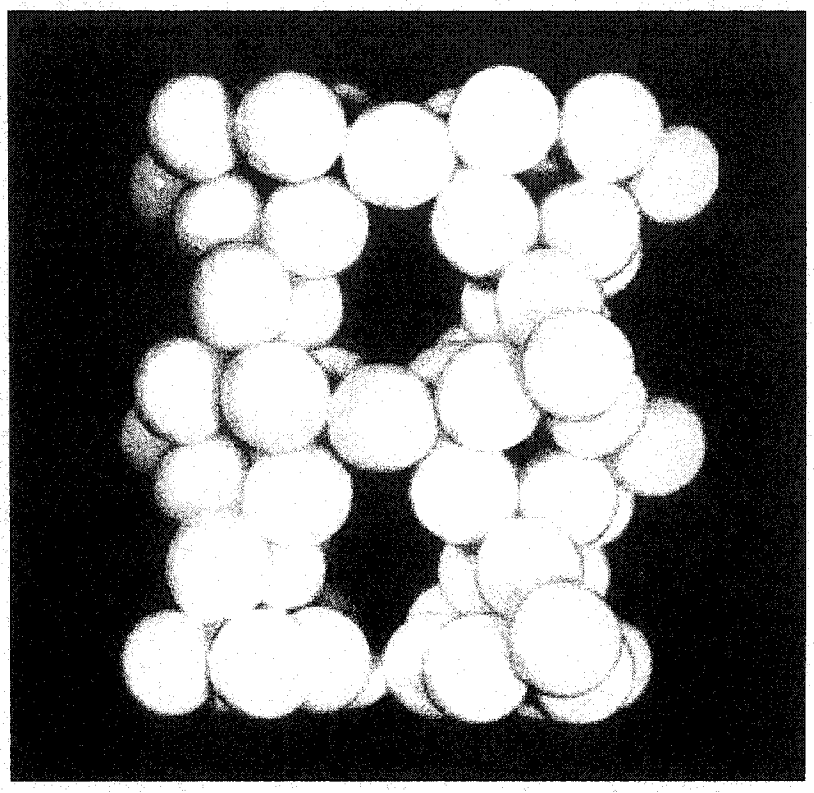

Figure 16. Model of a zeolite (edingtonite) showing the channels in the structure. The spheres represent oxygen atoms. The Si and Al atoms lie at the centers of O_4 tetrahedra and cannot be seen in this figure. [Cotton (1995)].

crude extracts [Klint (1994), Klint (1997)], and also as ion-exchangers. The lower valence of Al^{+3} relative to that of Si^{+4} creates a negative framework, which takes up cations to maintain electroneutrality. Using special techniques, the Si/Al ratio can be controlled to produce zeolites with less acidic sites. The Si/Al ratio is also an indicator of the hydrophobicity of the zeolite; the higher the ratio, the higher the degree of hydrophobicity and the lower the ion-exchange capacity. Near-neutral zeolites are preferred for sunscreen use since these are less likely to have adverse effects on the skin. Commercially available zeolites, whose Si/Al ratio can be altered, include faujasite (Y), mordenite and silicalite. The zeolites used in this work were faujasite (Figure 17) and

mordenite (Figure 18). Both these zeolites can be produced with substantially reduced aluminium content by postsynthetic treatment [Van Bekkum (1991)].

Typical zeolite particles are in the 500-2000 nm range, but particles as small as 20 nm can be produced. An important property of zeolites is that the cavity size and the window size are different. A zeolite particle can be viewed as a room. The cavity would represent the area inside the room while the window would represent the door. When molecules are incorporated into zeolites, they may be small enough to fit inside the cavity but too big to get out of the window after they react together. Zeolites with encapsulated TiO_2 can be produced by *ship-in-a-bottle* synthesis, a terminology that refers to the diffusion of small precursors into zeolites followed by reaction within the cavities to yield the desired product. The precursors $((Ti{=}O)K_2(C_2O_4)_2{\cdot}2H_2O$ or $(NH_4)_2(Ti{=}O)(C_2O_4)_2{\cdot}H_2O)$ are small enough to enter the cavities through the windows where they react together to produce TiO_2 particles that cannot exit.

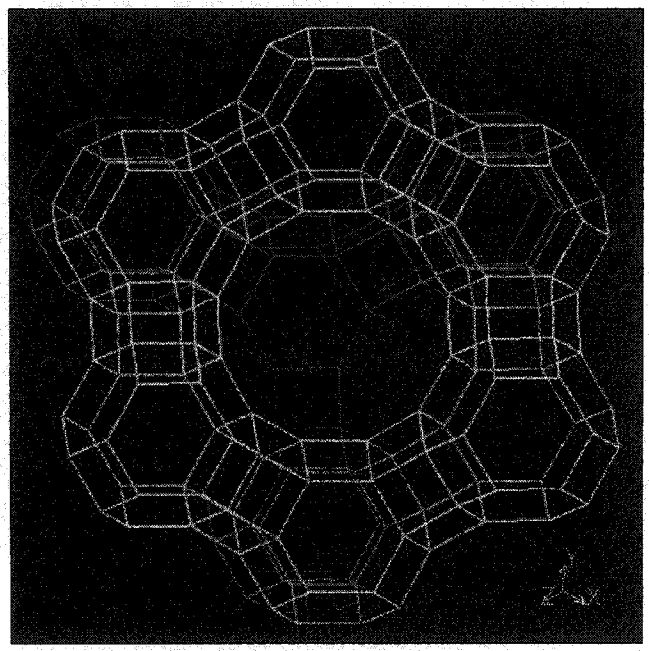

Figure 17. Structure of the zeolite faujasite (NaY) [http://www.kristall.ethz.ch/IZA-SC/Atlas/data/FAU.html].

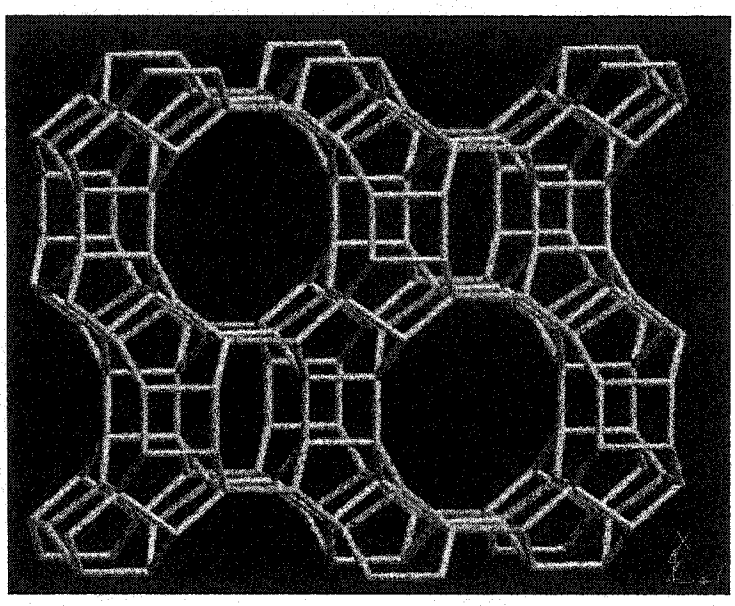

Figure 18. Structure of the zeolite mordenite [http://www.kristall.ethz.ch/IZA-SC/Atlas/data/MOR.html].

Faujasite has a three-dimensional channel system with the largest aperture (0.75 nm) of the zeolites. Mordenite has a one-dimensional channel system with an elliptical aperture of 0.7 * 0.65 nm. It is usually produced in particle sizes of ~ 1000 nm while zeolite NaY particles are usually between 500 and 1000 nm. Since the diameters of the cavity and window of faujasite are ~ 1.3 and 0.75 nm, respectively, many guests that can fit inside the cavity will be too big to leak out of the zeolite.

1.5.2 Advantages related to the uses of zeolites

There are many advantages in using zeolites to encapsulate the sunscreen components:

1) The first is related to the sunscreen fatigue. As mentioned in Section 1.1.2.1, the active sunscreen molecule can be destroyed during the skin protection

process, leading to the production of other compounds that may be harmful to the skin. By encapsulating the sunscreen, the degradation products will hopefully be trapped inside the zeolite, and will not come into direct contact with the skin.

2) The second advantage is that encapsulation will allow the use of sunscreen mixtures. Effectively, the zeolite will act as a barrier between the different sunscreens and reduce their interactions. Thus, the entire UV range can be covered by the use of more than one sunscreen without the fear of interactions.
3) Encapsulation will also prevent the direct contact of sunscreens with the skin.
4) Zeolites are effective in scattering light, which should increase the efficiency of the sunscreen.

1.5.3 Possible disadvantages related to the uses of zeolites

Although the use of zeolites presents several important advantages, there are some disadvantages to be considered:

1) The size of the zeolite must be acceptable in cosmetic preparations. Effectively, particles > 400 nm will be apparent on skin and will not be acceptable to the customer. The size of a zeolite can be controlled and it is possible to find small zeolite particles, commonly called nanocrystalline zeolites, with particle sizes of 20-30 nm. Such particles would be suitable for sunscreens, although their use brings up other considerations, such as skin and cell penetration. Studies conducted in our laboratory showed that faujasite

(500-1000 nm) did not penetrate skin cells (Biao Shen, unpublished results). Further studies are needed to test the penetration of smaller zeolites into skin cells.

2) Agglomeration and aggregation of the zeolite particles occurs. This would not be esthetically acceptable and it would also reduce the efficiency of a sunscreen due to uneven skin coverage. Investigation of suitable dispersing agents is therefore important.
3) Interaction of the zeolite particle with the skin has to be investigated. As mentioned in Section 1.5.1, zeolites contain acidic sites. Although it is possible to reduce the number of acidic sites by changing the Si/Al ratio, the effects of zeolites on the skin needs to be investigated.
4) The photophysics of organic molecules may be altered by encapsulation. However, studies conducted by our collaborators at the University of Ottawa suggest that the excited-state deactivation mechanisms of the commonly used sunblocks continue to operate within the zeolite cavity (Michelle Chrétien, unpublished results).

1.5.4 Current biological uses of zeolites

As specified in section 1.5.1, zeolites are used in many different applications such as the treatment of water and wastewater, the purification of gaseous hydrocarbons, and the preparation of catalysts for petroleum refining. Zeolites are also used in situations where they come in contact with biological material. For example, they are used as dietary supplements in animal nutrition [Onagi (1966), Kondo (1968), Pond (1995)].

Zeolite powder has been found to be effective in the treatment of athlete's foot [Lopez (1991)] and to decrease the healing time of wounds and surgical incisions [Maeda (1989), Ikeganmi (1993)]. These last three applications are relevant to our work on supramolecular sunscreens since all involve the application of zeolite-based creams on the skin.

Recently, an analysis of the biological and chemical reactivity of zeolite-based aluminosilicate fibers and particulates was reported [Fach (2002)]. This study showed that iron bound to the zeolite surface led to the production of hydroxyl radicals via Fenton chemistry. The amount of radical produced was found to depend on the type of zeolite due to variation in iron coordination, which affects the reduction potentials of the metal. It was also shown that rat pulmonary alveolar macrophage-derived cells died more rapidly in the presence of zeolites. However, the study did not indicate if removal of the iron from the zeolite surface decreased the amount of hydroxyl radicals produced. Thus, it is reasonable to assume that zeolites appropriately treated to remove any iron would be safe for topical use.

1.6 Scope and outline of this thesis

The goal of this thesis is to study the effects of UV light in combination with free or encapsulated-TiO_2 on two of the main enzymes involved in the skin's enzymatic antioxidant defense system, CuZnSOD and catalase. In the first instance, the assay used to measure CuZnSOD and catalase activity is described. Then, the effects of photoexcited free TiO_2 on both enzymes are presented followed by the results of an investigation of the inactivation mechanism of CuZnSOD and catalase. The effects of encapsulated TiO_2 on

both enzymes are then described. Finally, the results of a brief study on the effects of UVA light and TiO_2 on cells viability are reported. The research presented here is part of a larger project carried out in collaboration with Dr. Tito Scaiano and his group at the University of Ottawa towards the creation of zeolite-hosted supramolecular sunscreens.

Chapter 2

2. EXPERIMENTAL

2.1 Chemicals

Anatase titanium dioxide (TiO_2) with purity of 99.9 % was purchased from Alfa Aesar. The average particle size was 32 nm, which is comparable to that employed in sunscreens and cosmetics, and the surface area was ~ 45 m^2/g. Copper-zinc superoxide dismutase (CuZnSOD) from bovine erythrocytes (E.C. # 1.15.1.1) was purchased from Roche Molecular Biochemicals, as were horseradish peroxidase (HRP) (E.C. # 1.11.1.7) grade 1 and 2,2`-azino-di-[3-ethylbenzthiazoline sulfonate (6)] diammonium salt (ABTS). Pyrogallol (1,2,3-benzenetriol) was purchased from Fisher Scientific; hydrogen peroxide (30%) and copper standard 1000 ppm from ACP Chemicals Inc.; diethylenetriaminepentaacetic acid (DTPA) and Tris from ICN Biomedicals; cacodylic acid from Aldrich; catalase from bovine liver (E.C. # 1.11.1.6), glutathione (GSH), thiourea, DDC (diethyldithiocarbamic acid), Dulbecco's modified eagles's medium (DMEM), fetal calf serum (FCS), penicillin and streptomycin were purchased from Sigma; BSA (bovine serum albumin) was from Bio-Rad, rat keratinocytes (RK) from American Tissue Culture Collection (ATCC), and UHP argon from Praxair. All buffers were prepared using filtered Millipore water and treated with a chelating resin, Chelex 100 (100-200 mesh, sodium form, Bio-Rad) to remove any metal ions. Encapsulated TiO_2 in faujasite and mordenite as well as free faujasite were obtained from our collaborators at University of Ottawa. TiO_2 was encapsulated into zeolites using the procedure described by Cosa et al. (2002b).

2.2 Irradiated solutions

TiO_2 (0.3 mg/mL, 0.03 % w/w) and zeolite (3 mg/mL) suspensions were prepared in water. The concentration of TiO_2 incorporated into zeolites was not specified by our collaborators at Ottawa and a fixed ratio of weight of TiO_2@zeolite compared to free TiO_2 (10:1) was used in these experiments. CuZnSOD (ε_{258}=10 300 M^{-1} cm^{-1}) [McCord (1969)], HRP (ε_{403}=102 mM^{-1} cm^{-1}) [Schonbaum (1973)] and catalase (ε_{405}= 324 mM^{-1} cm^{-1}) [Samejima (1963)] solutions were prepared in 50 mM sodium phosphate buffer, pH 7.0 and quantitated spectrophotometrically. An equal volume of enzyme solution (the concentrations are given in Section 2.4 and 2.5) was mixed with the TiO_2 suspension, the zeolite suspension or water (control) prior to irradiation. During irradiation, the solutions were not stirred because the irradiation chamber could not accommodate the number of stirring plates required. Hence the TiO_2 or zeolites particles formed a deposit on the bottom of the well but before removing an aliquot, the suspensions were mixed with a pipet tip. Constant stirring during irradiation would have been preferable because this would have increased light scattering by the TiO_2 particles. Aliquots containing TiO_2 or zeolite were not centrifuged prior to measuring enzyme activities because only a small volume (10 µL) was added to 1 or 2 mL of assay solution. All absorption spectra were acquired on an Agilent diode-array spectrophotometer (Model 8453).

2.3 UVA irradiation

UVA irradiations were performed in a Luzchem (Ottawa) Model ICH-2 photoreactor (Figure 19). Ten 350-nm Luzchem UVA lamps noted "A" in Figure 19 were used with a turntable to ensure homogeneous irradiation. The spectrum of the lamps is

shown in Figure 20, and the total UVA output of the ten lamps was 4.7-5.0 mW/cm^2, an intensity similar to the UVA light that reaches the earth's surface in summer at noon. Dark (control) samples were foil-covered and placed in the chamber so that all samples were exposed to similar conditions. The 1-mL samples were placed in a 24-well polystyrene MULTIWELL^{TM} tissue culture plate (Becton Dickinson) permeable to UVA and the temperature of the photoreactor was maintained at 37 ± 1°C.

Aerobic irradiations were performed using solutions that were air equilibrated. For the anaerobic irradiations, the solutions were first purged with argon for 30 min and then transferred to a glove box under nitrogen (Plas Labs Model 818GB from Fisher Scientific). The tissue culture plates were filled in the glove box and sealed with Parafilm. Each plate was placed in a box (Beta work box 185 x 115 x 80 mm from Amersham Pharmacia Biotech) covered with a quartz lid (polished fused quartz, 110 x 190 mm, 1/8" thick from Technical Glass Products Inc.) and the box was transferred to the photoreactor. The box was purged with argon to maintain an inert atmosphere. The anaerobic samples were not rotated because the argon connection prevented any rotation of the Beta work box.

2.4 CuZnSOD activity assay

The literature procedure [Marklund (1974)] was followed with minor corrections. A pyrogallol stock solution (40 mM) was prepared in 10 mM HCl. This solution is stable for weeks when stored at –20°C. The CuZnSOD concentration in the irradiated samples was 620 nM (20.2 μg/mL) and this was diluted to 3 nM (100 ng/mL) for the assay. The assay was carried out in 3-mL quartz cuvettes with a 1-cm pathlength following addition

of 10 µL of the irradiated CuZnSOD solution to 2 mL of 50 mM Tris cacodylate buffer, pH 8.2 containing 1 mM DTPA. The spectrophotometer was blanked using buffer

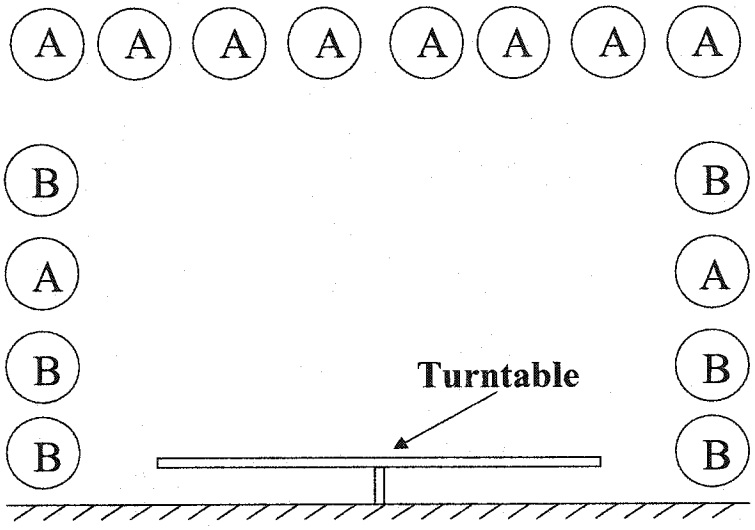

Figure 19. A schematic representation of the photoreactor. Only lamps "A" were used for sample irradiation.

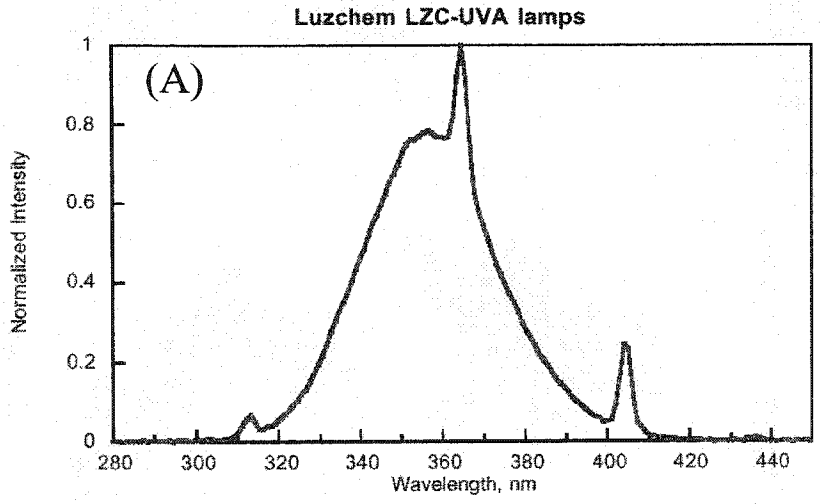

(B)

Region	Range (nm)	% energy
UVC	240-280	0.27
UVB	280-320	0.98
UVA	320-400	95.05
Visible	400-700	3.70

Figure 20. (A) Spectrum of light produced by the Luzchem LZC-UVA lamps used in the photoreactor. (B) Relative intensity of lamp output in specific regions of the spectrum.

without CuZnSOD. Finally, 10 µL of the pyrogallol stock solution was added at t=0.0 s, the solution shaken, and at t=10.0 s, the oxidation of pyrogallol was monitored at 320 nm. The final concentration of pyrogallol was 198 µM. The activity assays were performed using the kinetic mode of the Agilent spectrophotometer, which is controlled by a computer equipped with Chemstation software (Agilent). Measurements were made every 15 s over 90 s, and the slope over the first 60 s was used to calculate activity since this portion of the graph was linear. The slope of each sample was compared to the blank (no CuZnSOD present), in which pyrogallol oxidation is the fastest because CuZnSOD does not compete for the superoxide radicals generated on pyrogallol autoxidation. These radicals further oxidize pyrogallol in the absence of CuZnSOD. DTPA was added to chelate free trace metals that would catalyze pyrogallol oxidation. The equation used to measure CuZnSOD activity is related to its efficiency in preventing pyrogallol oxidation:

$$\% \text{ inhibition of pyrogallol oxidation} = \left[1 - \frac{\text{slope of blank}}{\text{slope of sample}} \right] * 100 \qquad (20)$$

However, SOD activities of the irradiated samples are reported related to the control (dark, no TiO_2):

$$\text{Relative \% SOD activity} = \left[\frac{\% \text{ inhibition of pyrogallol oxidation in sample}}{\% \text{ inhibition of pyrogallol oxidation in control}} \right] * 100 \qquad (21)$$

2.5 Catalase activity assay

A H_2O_2 stock solution (ε_{240}=39.4 $M^{-1}cm^{-1}$) [Heinecke (1993)] of 14 mM was prepared in 50 mM sodium phosphate buffer, pH 7.0. The catalase concentration in the irradiated samples was 130 nM (30.8 µg/mL). Before the assay, the instrument was blanked using the phosphate buffer. For the assay, 10 µL of the irradiated catalase

solution was added to 990 μL of 14 mM H_2O_2 in 1.5-mL quartz cuvettes with a 1-cm pathlength to give a final enzyme concentration of 1.3 nM (300 ng/mL) and the solution was shaken. A 10-s induction was allowed before starting the measurements. H_2O_2 depletion was followed at 240 nm every 15 s over 90 s. One unit of catalase will decompose 1 μmol of H_2O_2 per min at 25°C and pH 7.0. The activities were compared to a control sample (dark, no TiO_2).

2.6 Determination of H_2O_2

To measure the H_2O_2 concentration, a method based on HRP-catalyzed ABTS oxidation by H_2O_2 was used (Reaction 22). Since the rate of ABTS oxidation depends on

$$H_2O_2 + 2\,ABTS \xrightleftharpoons{HRP} 2\,H_2O + 2\,ABTS_{ox} \qquad (22)$$

the H_2O_2 concentration, it can be used to quantify H_2O_2. A 9.1 mM ABTS stock solution (ε_{340}= 36 600 M^{-1} cm^{-1}) [Kim (2001)] was prepared in 100 mM sodium phosphate buffer (pH 5.0), a 9.15 nM (403 ng/mL) HRP solution in 50 mM sodium phosphate buffer (pH 7.0), and a 10 mM H_2O_2 stock solution in H_2O. For the assay, 10 μL of the HRP solution was added to 550 μL of ABTS in a 1.5 mL quartz cuvette (1-cm pathlength) and the instrument was blanked using this solution. The H_2O_2 solution (50 μL) was added, the solution shaken, and a 10-s induction was allowed before starting the measurements. The final concentrations of HRP, ABTS and H_2O_2 in the assay solutions were 0.15 nM (6.6 ng/mL), 8.20 mM and 0.82-82 μM, respectively. ABTS oxidation was followed at 405 nm every 10 s over 90 s. The slope was measured using the points for the first 60 s, and

the H_2O_2 concentrations of the samples were determined from the calibration curve of ABTS oxidation rate versus H_2O_2 concentration of the standards.

For the H_2O_2 depletion experiment, a 600 μM H_2O_2 solution was prepared in 50 mM sodium phosphate buffer, pH 7.0 and placed in tissue culture plate at 37°C (Section 2.3) during exposure to UVA light. The concentration of TiO_2, when present, was 0.15 mg/mL. All solutions containing TiO_2 were centrifuged for 2 min at 12,000 rpm and the supernatant was used for the assay.

2.7 Determination of protein concentration

The Bio-Rad dye-binding assay was used to determine the total protein concentration by following the supplier's protocol. A calibration curve was prepared from BSA standards (200-1400 μg/mL) in 25 mM sodium phosphate buffer, pH 7.0 (the same buffer used during the irradiation of catalase). All solutions, including those without TiO_2, were centrifuged before the Bio-Rad assay was performed so that all samples were treated the same way. Solutions were centrifuged for 2 min at 12,000 rpm and the total protein in the supernatant was determined. The supernatant was also used to monitor heme destruction by monitoring the disappearance of the Soret peak of catalase at 405 nm.

Because of the lower sensitivity of the Bio-Rad total protein assay compared to the catalase activity assay described in Section 2.5, it was not possible to use the same solutions for both assays. Catalase solutions of 1000 μg/ml (4.2 μM) were irradiated and the total protein remaining in solution was determined using the Bio-Rad assay. The TiO_2 concentration of the solutions (when TiO_2 was present) was 2.5 mg/mL.

2.8 Determination of copper release from CuZnSOD

In order to measure the copper released from CuZnSOD, a colorimetric method using DDC was employed. This chelator binds free Cu^{II} to give a yellow complex that has an intense absorption peak at 450 nm. A copper calibration curve using Cu standards (1-50 μM) was prepared by adding 500 μM DDC to 1 mL of standard, and reading the absorbance at 450 nm after 10 min. Since the CuZnSOD concentration used during the irradiation procedure described in Section 2.4 was too low for the sensitivity of the DDC assay, it was increased to 17 μM (550 μg/mL) and the enzyme was irradiated with TiO_2 (2.4 mg/mL) as before. Before addition of DDC, the CuZnSOD solutions were centrifuged for 2 min at 12,000 rpm and then subjected to ultrafiltration using a Millipore Ultrafree-MC filter with a molecular mass cut-off of 5 kDa to remove any CuZnSOD. The copper content of the ultrafiltrate was determined to establish the amount of metal released from the dismutase.

Cu^{II}ZnSOD has a characteristic absorption peak at 680 nm due to a d-d transition of the active-site Cu^{II}. Therefore, Cu^{II}ZnSOD solutions were irradiated with UVA for different times and the absorbance at 680 nm measured. Since the extinction coefficient of the d-d transition is small (ε_{680}=300 $M^{-1}cm^{-1}$) [Valentine (1981)], the CuZnSOD concentration in the irradiated samples was increased to 250 μM (8.1 mg/mL) and the TiO_2 concentration was 5 mg/mL. The solutions were centrifuged for 2 min at 12,000 rpm before the absorbance at 680 nm was recorded.

2.9 Cell viability assay

Rat keratinocytes cells were grown in 24-well tissue culture plates in DMEM containing 5% FCS. The cells were exposed to the conditions given in Table 3. DMEM

Table 3. Cell viability assay conditions

DMEM + 5% FCS pH 7.4	PBS pH 7.2
$-TiO_2 \pm UVA$	$-TiO_2 \pm UVA$
$+TiO_2 \pm UVA$	$+TiO_2 \pm UVA$

containing 5% FCS, pH 7.4 and PBS, pH 7.2 were examined as media to determine which would be the most suitable for the cells. Every hour over a period of four hours, an aliquot of cells subjected to the different treatments was washed and treated with Trypan Blue. This vital stain is taken up by dead cells only, thereby allowing distinction between viable and non-viable cells. Cells were exposed to 0.5 mL of buffer containing 0.3 mg/mL TiO_2 at 37°C. After the desired exposure time, the supernatant was removed and the cells were washed with 500 µL of PBS buffer. The buffer was discarded and 200 µL of Trypan Blue was added for 5 min and discarded, and the cells were washed with another 500 µL of PBS buffer. Finally, the percentage of living cells was determined under a microscope.

2.10 Cell lysate activity

Rat keratinocytes (RK) were grown in DMEM, pH 7.4 containing 5% FCS, 100 units/mL penicillin and 100 µg/mL streptomycin. Cells were grown to confluence in sterile petri dishes, washed with PBS buffer, and lysed with a hypotonic buffer, consisting of 10 mM HEPES pH 7.9, 10 mM KCl, 1.5 mM $MgCl_2$, 0.5 mM DTT, 0.5

mM PMSF, 1% glycerol, 0.2% Nonidet-P40 and mini cocktail protease inhibitors [1 tablet (Roche) per 10 mL lysis buffer]. The cells were scraped off the dishes, frozen to –80°C and subjected to three cycles of freeze-thaw. The lysate was centrifuged at 5000 rpm for 10 min to pellet the cell debris. The supernatant was assayed for total protein using the BioRad dye-binding assay, aliquoted and stored at –80°C for further processing. The total protein concentration in the supernatant was found to be ~ 1 mg/mL.

Chapter 3

3. RESULTS

3.1 Assay method development

Different literature methods exist to measure the activities of CuZnSOD and catalase. Since the percent inactivation of the enzymes over time was the parameter of interest in this study, it was important to ensure that the enzyme activity was directly proportional to the concentration of active enzyme under the assay conditions. Therefore, the literature methods were optimized for the purpose of the project.

3.1.1 CuZnSOD

As mentioned in Section 1.3.1, the function of CuZnSOD is to remove superoxide radicals in living tissues. In order to determine the activity of the enzyme, an assay to measure the depletion of superoxide radicals was needed. However, it is not easy to directly measure their concentration spectrophotometrically. The method used in our laboratory was developed by Marklund and Marklund [Marklund (1974)]. Superoxide radicals oxidize an organic molecule, pyrogallol (Figure 21) to give a colored product

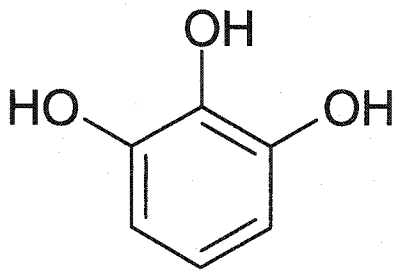

Figure 21. Structure of pyrogallol.

detectable spectrophotometrically. The smaller the concentration of superoxide radicals, the slower the oxidation of pyrogallol. Hence, in the presence of CuZnSOD, pyrogallol is oxidized more slowly since the enzyme removes superoxide radicals. The advantage of this assay is that it does not require the addition of compounds that generate superoxide radicals because these are formed during pyrogallol oxidation, which occurs in two reactions. In the first reaction, pyrogallol is oxidized by oxygen to give a superoxide radical (Reaction 23), which can oxidize another molecule of pyrogallol (Reaction 24).

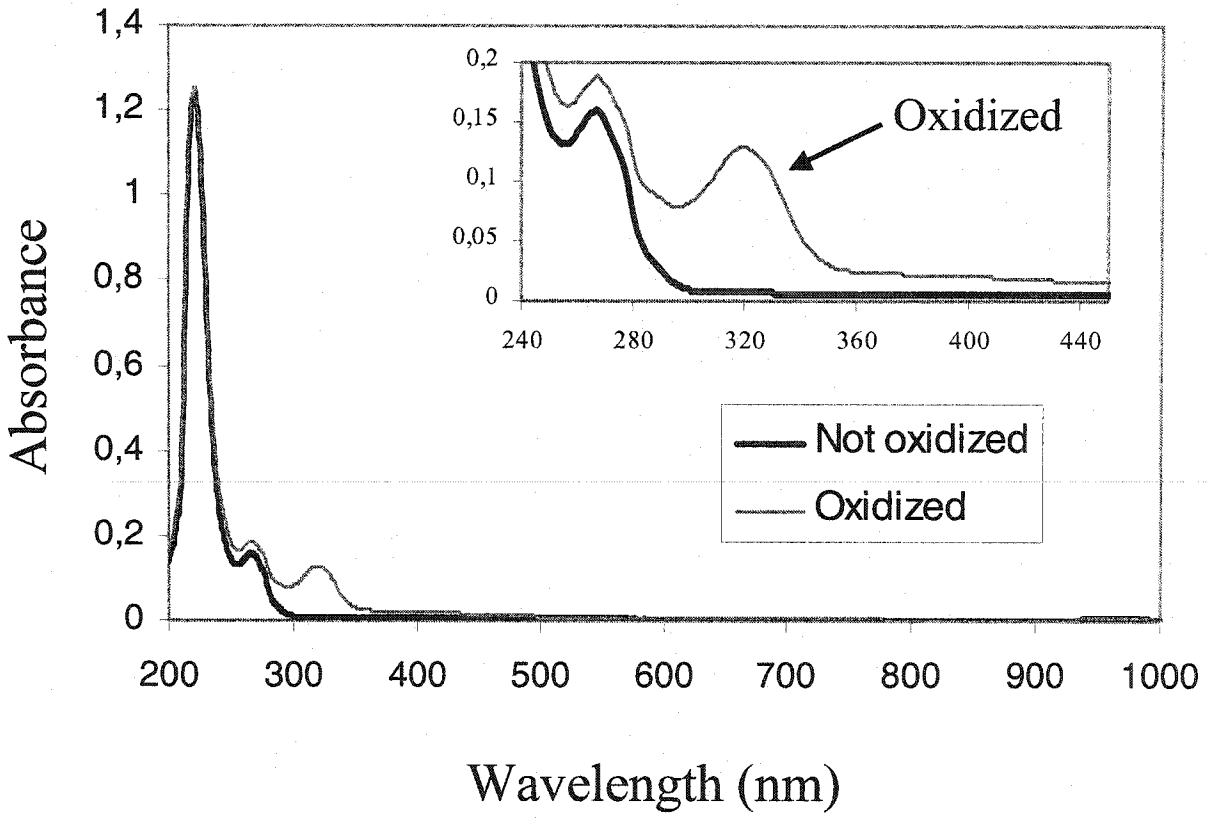

Figure 22. UV-Vis spectrum of oxidized pyrogallol after 90 s. At t=0 s, 198 µM pyrogallol was added to 50 mM Tris cacodylate buffer, pH 8.2 containing 1 mM DTPA. The spectrum was recorded at 0 s and 90 s after addition (Section 2.4).

Since CuZnSOD will compete for the $O_2^{\bullet -}$ formed in Reaction 23, any active enzyme

$$Py + O_2 \rightleftharpoons Py_{ox} + O_2^{\bullet -} \quad (23)$$

$$Py + O_2^{\bullet -} \rightleftharpoons Py_{ox} + O_2^{2-} \quad (24)$$

present in solution will slow down but not inhibit pyrogallol oxidation completely since autoxidation also occurs (Reaction 23).

The first modification of the assay was the wavelength used to monitor pyrogallol oxidation. A close look at the oxidized pyrogallol spectrum (Figure 22) revealed a maximum around 320 nm. Using that wavelength instead of 420 nm, as recommended [Marklund (1974)], the sensitivity of the assay was increased by a factor of ~ 9 (Figure 23) without affecting reproducibility and reliability.

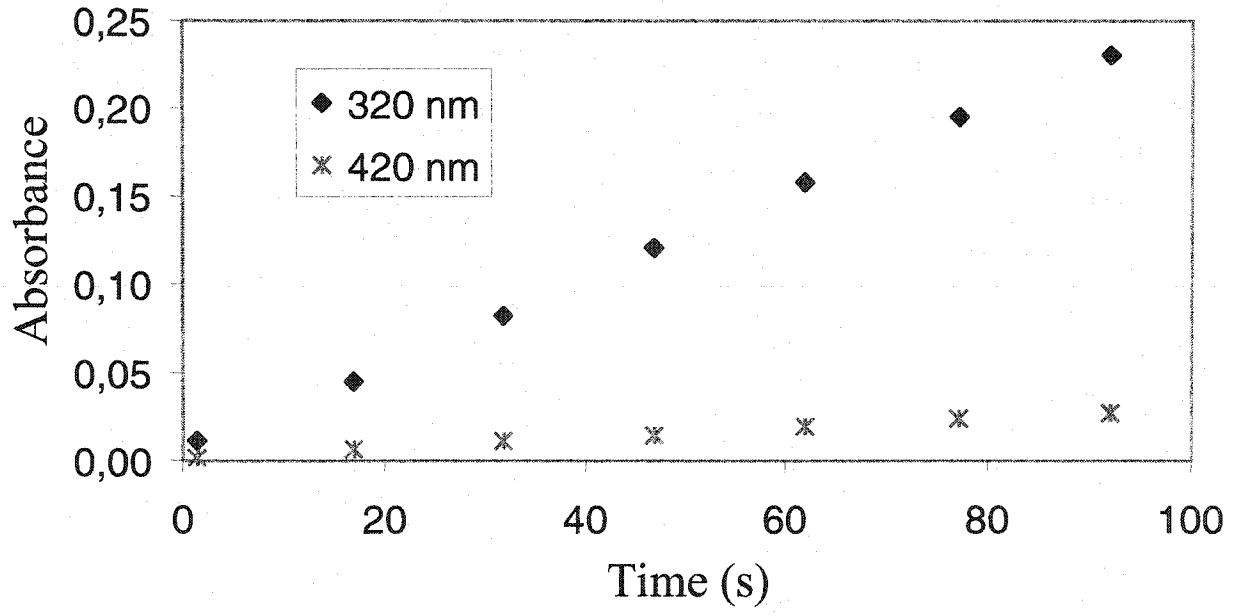

Figure 23. Pyrogallol oxidation followed at two different wavelengths. At t=0 s, 198 µM pyrogallol was added to 50 mM Tris-cacodylate buffer, pH 8.2 containing 1 mM DTPA. Measurements were started 10 s after addition and made every 15 s (Section 2.4).

The next step was to determine the appropriate concentration of enzyme to use. To accomplish this, the effect of CuZnSOD concentration on the percent inhibition of pyrogallol oxidation was examined (Figure 24). As expected, the rate of pyrogallol oxidation decreased with increasing concentrations of CuZnSOD. However, at high

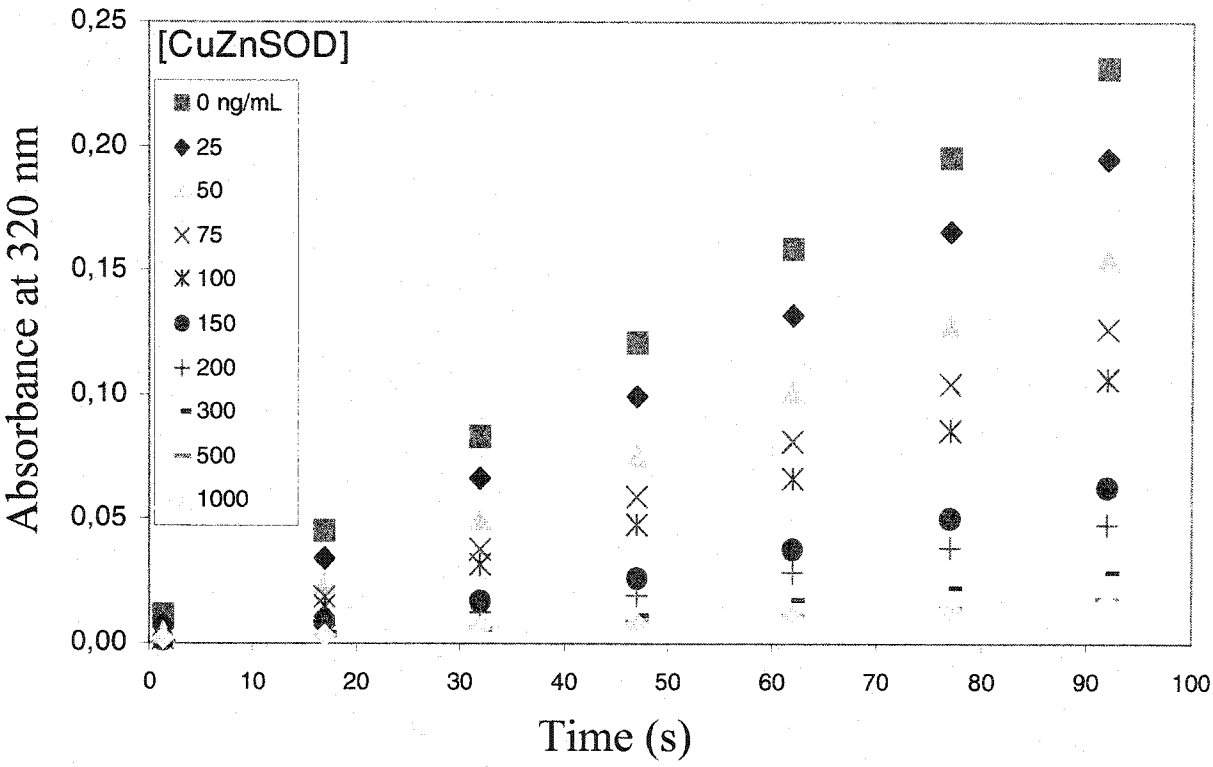

Figure 24. Pyrogallol oxidation vs time as a function of CuZnSOD concentration. Same conditions as described in caption of Figure 23 except that CuZnSOD was added at different concentrations ranging from 0 to 1000 ng/mL (Section 2.4).

concentrations of CuZnSOD (>150 ng/mL), the response of the assay is not linear anymore, as seen when the % inhibition of pyrogallol oxidation is plotted versus the CuZnSOD concentration (Figure 25). Effectively, the linear range of the assay was found to be 0-100 ng/mL of CuZnSOD. At >500 ng/mL, the oxidation rate of pyrogallol is

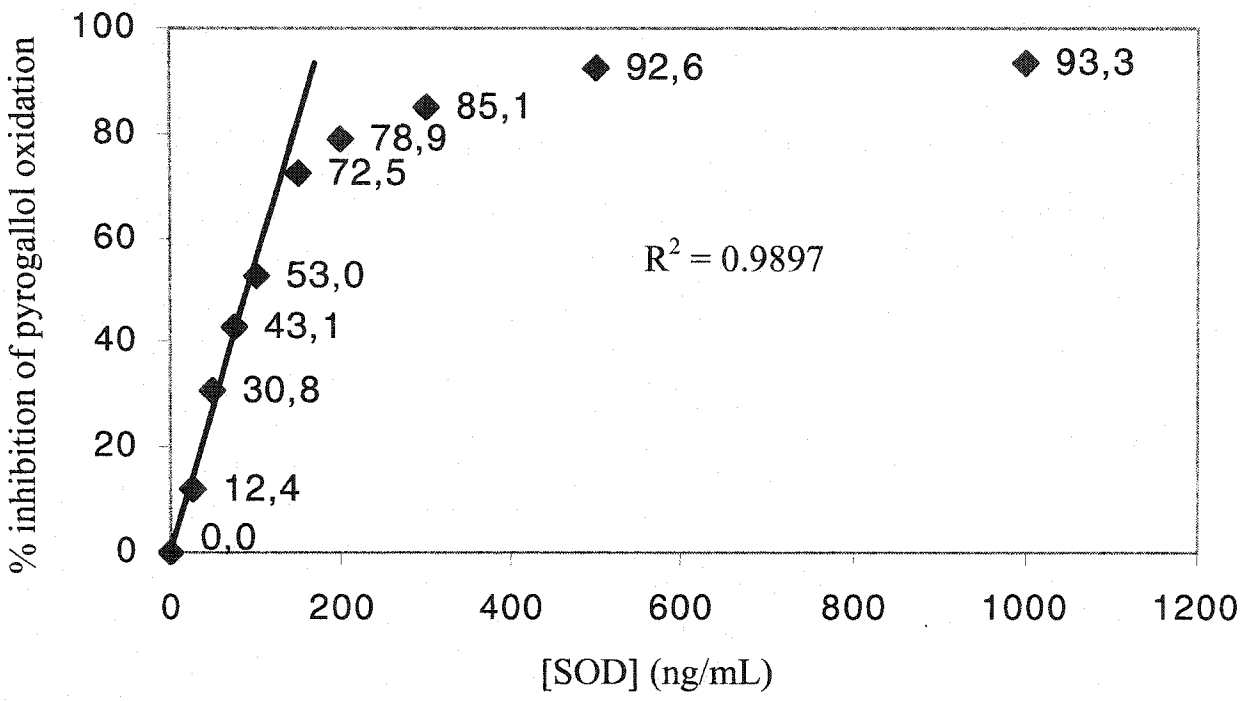

Figure 25. Calibration curve to establish linear range of CuZnSOD activity. Inhibition of pyrogallol oxidation is linear up to 100 ng/mL CuZnSOD. Experimental details are given in caption to Figure 24. The data points are the percent inhibition of pyrogallol oxidation by CuZnSOD compared to the blank (no CuZnSOD).

independent of CuZnSOD concentration, which can be explained by the mechanism defined by Reactions 22 and 23. Therefore, CuZnSOD cannot fully inhibit pyrogallol oxidation as reported [Marklund (1974)]. A concentration of CuZnSOD of 100 ng/mL (3 nM), which is at the high end of the linear range of the assay, was selected for the SOD assays carried out here, and correspond to ~ 50% inhibition of pyrogallol oxidation.

3.1.2 Catalase

As mentioned in Section 1.3.2, the reaction catalyzed by catalase is the conversion of hydrogen peroxide to water and oxygen. Hydrogen peroxide absorbs in the UV range so its depletion can be monitored directly over time spectrophotometrically. As noted in Section 2.5, one unit of catalase decomposes 1 μmol of H_2O_2 per min at 25°C and pH 7.0. However, the linear range of the assay had to be determined as for CuZnSOD so the effect of catalase concentration on H_2O_2 depletion was studied (Figure 26). As

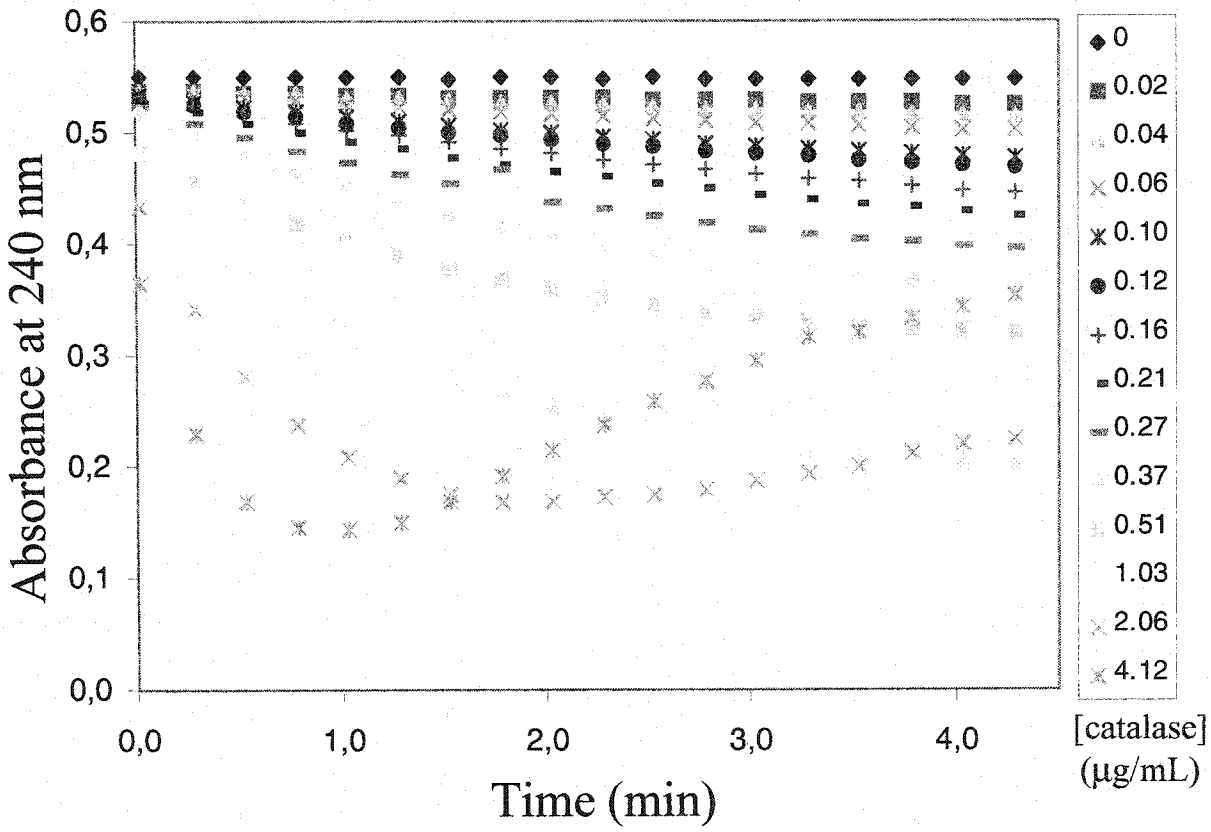

Figure 26. Rate of H_2O_2 depletion in function of catalase concentration. Catalase (0-4.12 μg/mL) was added to 50 mM sodium phosphate buffer, pH 7.0 containing 14 mM H_2O_2 (Section 2.5). After a 10-s induction, the absorbance at 240 nm was measured every 15 s.

expected, the H_2O_2 depletion rate increased with the catalase concentration. However, at high concentrations of the enzyme (>5 U/mL), the absorbance at 240 nm increased at longer times after an initial quick drop (Figure 26). During H_2O_2 turnover by catalase (Reaction 4), oxygen is produced. At high catalase concentrations, there is so much oxygen produced that bubbles are formed in the cuvette, causing light scattering, which is detected as an apparent increased absorbance. The calibration curve (Figure 27) shows that the assay is linear up to 350 ng/mL of catalase. An enzyme concentration of 300 ng/mL was used here to monitor catalase inactivation since it is close to the upper limit of the linear range of the assay.

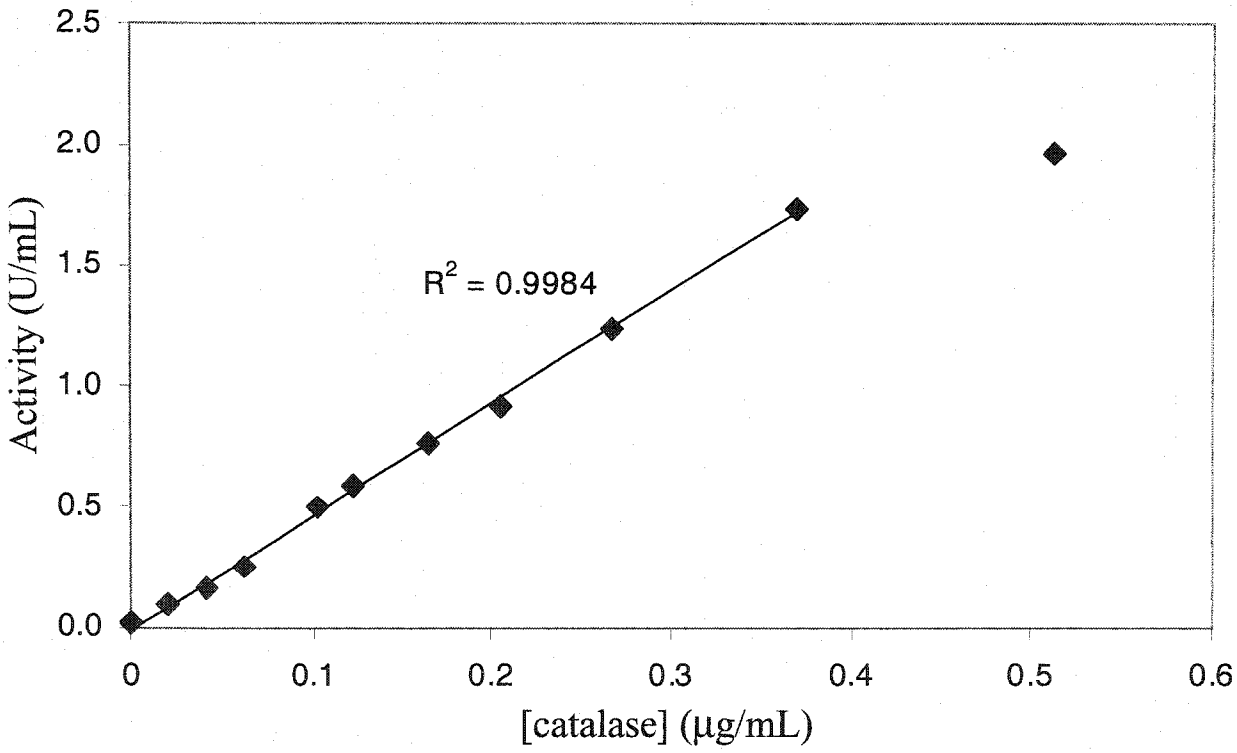

Figure 27. Calibration curve to establish the linear range of catalase activity. H_2O_2 depletion by catalase is linear up to 350 ng/mL catalase. Experimental details given in the caption to Figure 26.

While calibrating the catalase assay, an interesting observation was made. Effectively, catalase was found to adsorb on the surface of the TiO_2 particles, which caused a decreased in the observed catalase concentration upon centrifugation of the solution (Figure 28). This observation is important in explaining some of the results obtained below.

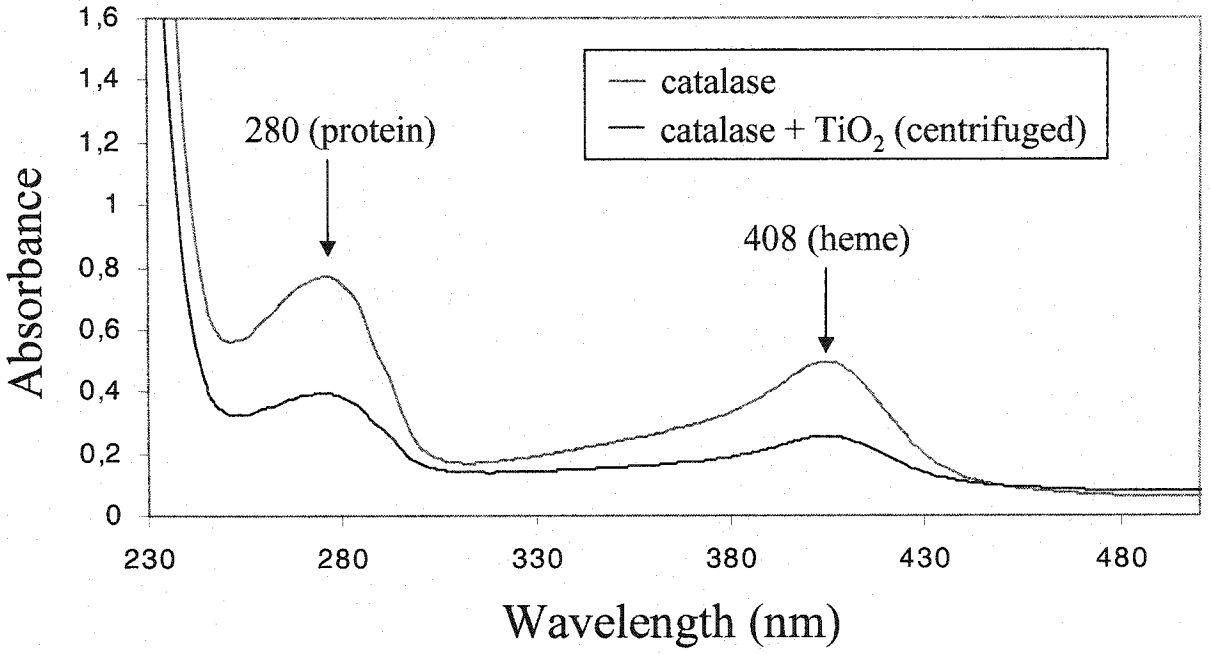

Figure 28. Effects of TiO_2 addition and centrifugation on the visible absorption spectrum of catalase. The enzyme (1.5 μM; 0.37 mg/mL) was exposed to TiO_2 particles (15 mg/mL) for 5 min at room temperature. The sample was centrifuged at 12 000 rpm for 2 min and the spectrum of the supernatant was recorded in a 1-cm cell.

3.1.3 UVA transparent container

Before any irradiation experiments could take place, containers that would transmit UVA light had to be found to hold the solutions under investigation. The first trial involved placing the samples in uncovered petri-dishes, which proved to be

unsuitable since the solvent evaporated, especially under UV light. A polyethylene petri-dish cover was tested to see if it transmitted UVA radiation (Figure 29). Since the cut-off of the cover was lower than 300 nm, it allowed UVA light to pass through. However, petri-dishes were not used because of their large volume (10 mL). Pyrex test tubes were also not suitable due to light scattering and the fact that most of the lamps were positioned on the top of the photoreactor (Figure 19). In attempts to find a smaller, UVA-transparent container, a 24-well polystyrene tissue-culture plate with a capacity of 2 mL per well was tried. The cover of the plate transmitted UVA light (Figure 29), thus enabling irradiation to be carried out on sealed containers. Experiments were then commenced on the two enzymes, CuZnSOD and catalase, since the conditions were optimized.

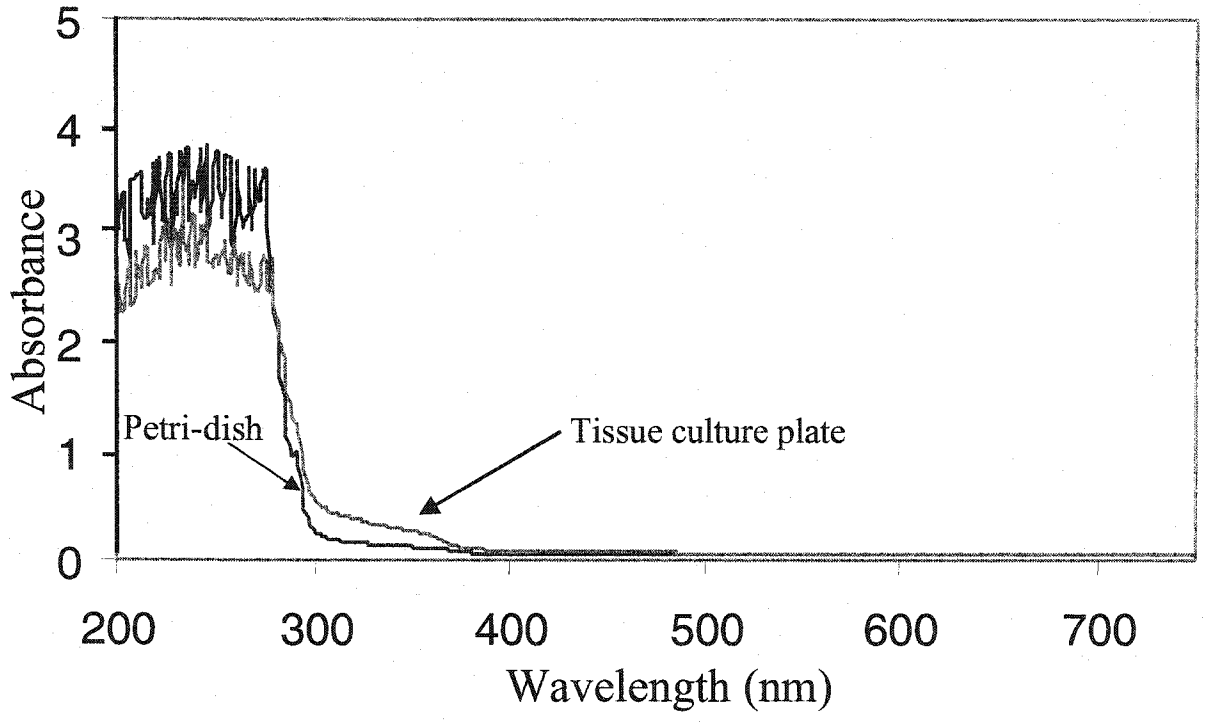

Figure 29. UV-Vis spectra of different containers. The cover of a polyethylene petri-dish and a 24-well polystyrene tissue culture plate were placed in the beam of a spectrophotometer and their UV-Vis spectra recorded.

3.2 Effects of photoexcited TiO_2 on enzymes

The first goal of our project was to investigate the effects of photoexcited TiO_2 on key antioxidant enzymes such as CuZnSOD and catalase.

3.2.1 CuZnSOD

The first enzyme investigated was CuZnSOD. An example of the data (from Figure 30) and the calculations performed to determine the relative SOD activity (Section 2.4) of a sample is as follows:

$$\% \text{ inhibition of pyrogallol oxidation of the control} = \left[1 - \frac{\text{slope of control}}{\text{slope of blank}} \right] * 100$$

$$= \left[1 - \frac{0.0785}{0.1407} \right] * 100 = 44.2\%$$

$$\% \text{ inhibition of pyrogallol oxidation of sample} = \left[1 - \frac{\text{slope of sample}}{\text{slope of blank}} \right] * 100$$

$$= \left[1 - \frac{0.1126}{0.1407} \right] * 100 = 20.0\%$$

$$\text{Relative \% SOD activity of sample} = \left[\frac{\text{\% inhibition of sample}}{\text{\% inhibition of control}} \right] * 100$$

$$= \frac{20.0}{44.2} * 100 = 45.3\ \%$$

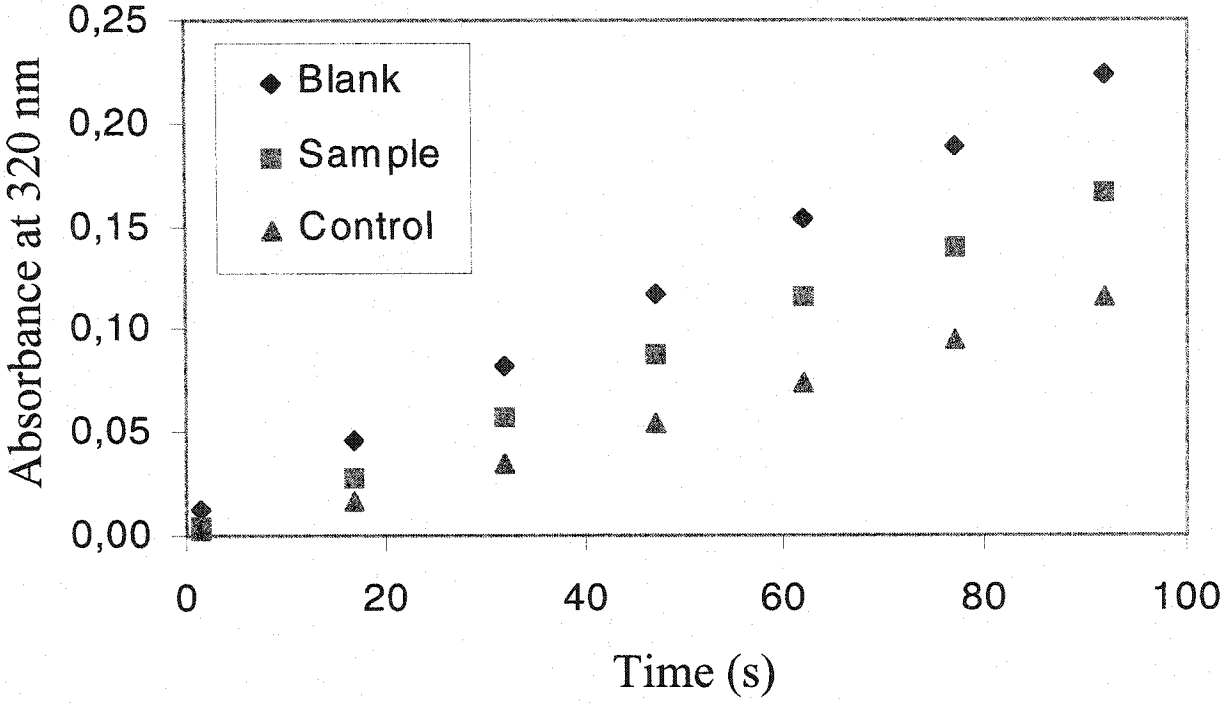

Figure 30. Pyrogallol oxidation vs time in different solutions. The blank did not contain CuZnSOD (slope = 0.1407). The control contained 3 nM (100 ng/mL) CuZnSOD that was not exposed to TiO_2 nor UVA light and the slope of absorbance at 320 nm vs time was 0.0785. The sample contained 3 nM (100 ng/mL) CuZnSOD exposed to 0.15 mg/mL TiO_2 and UVA light for 2 h (slope = 0.1126). The final pyrogallol concentration is 198 μM. The experimental procedures are given in the caption to Figure 23.

To determine the effect of irradiation time on CuZnSOD activity, the enzyme was irradiated and its activity tested every hour over 4 h (Figure 31). The activity was stable over time in the dark at 37°C and TiO_2 did not affect the SOD activity when the solution was not irradiated (Figure 31). However, when the CuZnSOD solution was exposed to UVA light, the enzyme lost >20% activity in 4 h. A dramatic loss of activity was observed over time when the sample was irradiated in the presence of TiO_2 (Figure 31).

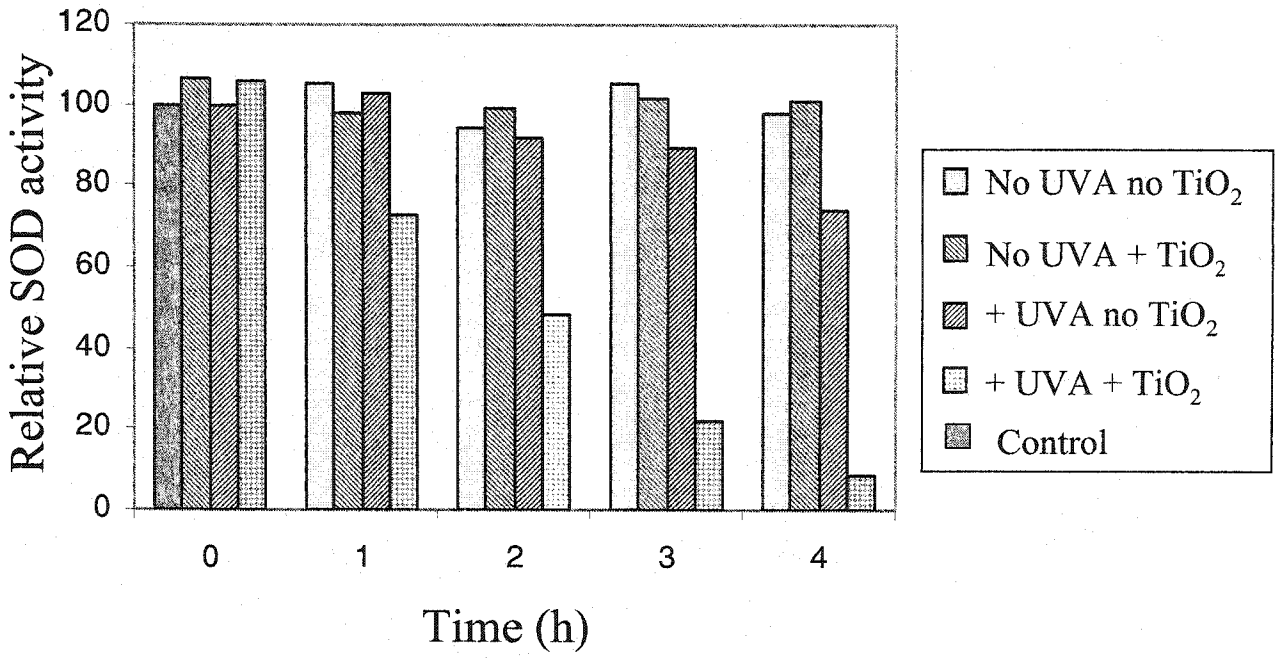

Figure 31. Effect of irradiation time on CuZnSOD activity. All activities are relative to the activity of the control (dark, 0 h). The experimental details are given in the caption to Figure 30. (n=1)

To confirm the results of the single experiment (n=1) shown in Figure 31, an irradiation time of 4 h was selected and the experiment was repeated several times. After 4 h UVA exposure, the remaining activity was 69 ± 8% (Figure 32), which clearly shows that UVA light by itself damages the enzyme and contributes to its inactivation. Again over 4 h, photoexcited TiO_2 caused a large decrease in the activity of CuZnSOD and the remaining activity was 19 ± 13% (Figure 32). Hence, the difference in inactivation levels (69 ± 8% – 19 ± 13%) when the enzyme was exposed to UVA light alone and UVA light combined with TiO_2 was ~ 50%.

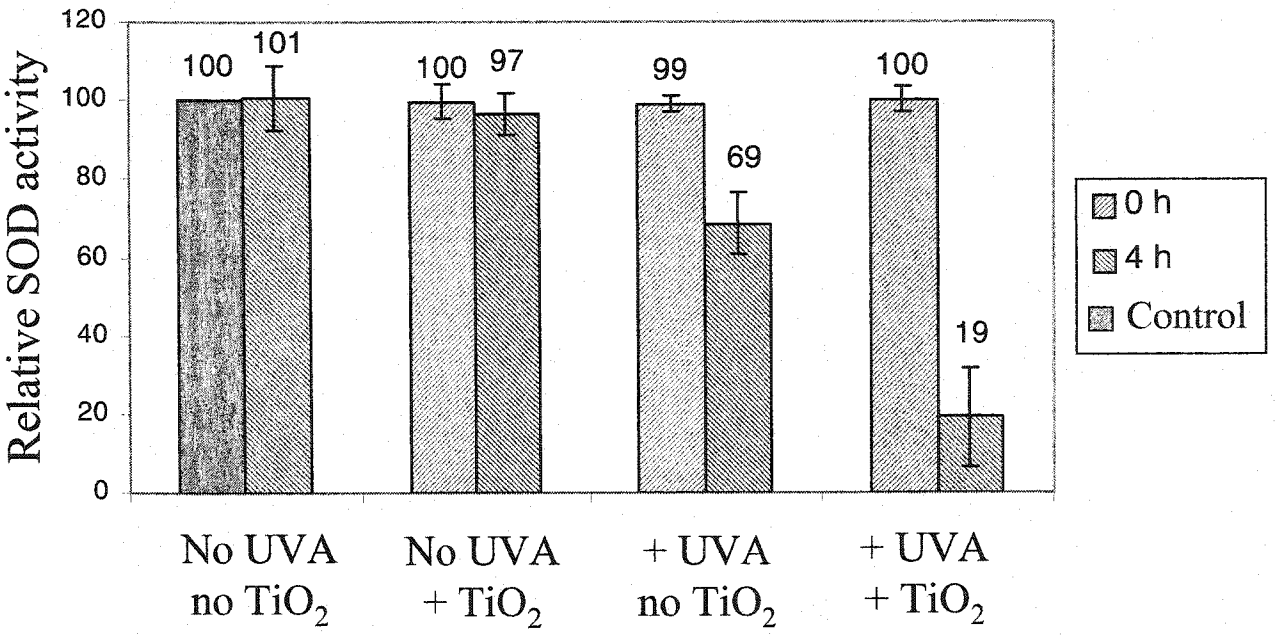

Figure 32. Effect of photoexcited TiO_2 on CuZnSOD activity after 4 h irradiation. All activities are relative to the activity of the control (dark, 0 h). The experimental details are given in the caption to Figure 30. (n=7)

3.2.2 Catalase

Another important enzyme in the enzymatic antioxidant defense of skin cells is catalase, as discussed in Section 1.3.2. Combined with CuZnSOD, catalase forms a very effective duo to remove ROS. Hence, the effects of irradiation time on the activity of catalase were also investigated (Figures 33 and 34). Catalase inactivation follows similar trends as that of CuZnSOD. Catalase was stable over 60 min when stored in the dark at 37°C (99 ± 5%) (Figure 34). TiO_2 alone had little effect on the activity of catalase, even though enzyme adsorption on the surface of TiO_2 was detected (Figure 28). When exposed to UVA light, catalase was inactivated more rapidly than CuZnSOD since its activity decreased to 62 ± 4% after only 60 min exposure (Figure 34) whereas CuZnSOD

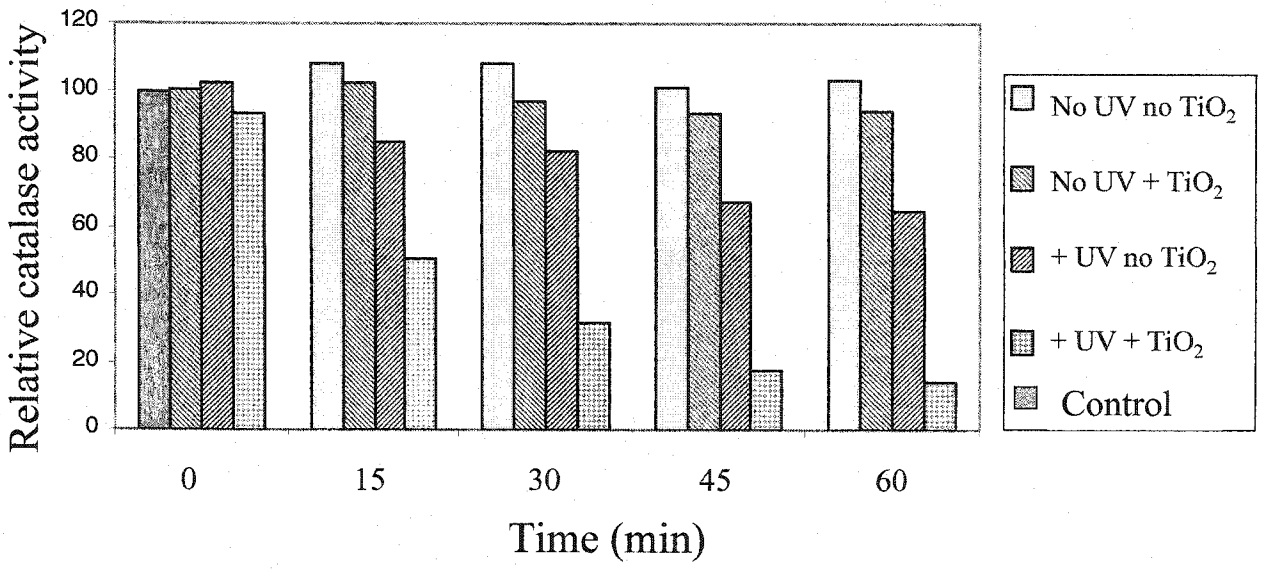

Figure 33. Effect of irradiation time on catalase activity. All activities are relative to the activity of the control (dark, 0 h). $[H_2O_2]$ = 14 mM, [catalase] = 1.3 nM (300 ng/mL) and $[TiO_2]$ = 0.15 mg/mL. The experimental details are given in the caption to Figure 26. (n=1)

retained 69% activity after 4 h exposure (Figure 32). As with CuZnSOD, the difference in inactivation levels (62%± 4% – 14% ± 7%) when the enzyme was exposed to UVA light alone and UVA light combined with TiO_2 was ~ 50%. These results call into question the safety of using TiO_2 in sunscreens.

3.3 Mechanisms of CuZnSOD and catalase inactivation

Once clear evidence was obtained that photoexcited TiO_2 caused inactivation of CuZnSOD and catalase, the next step was to study the inactivation mechanisms of these enzymes. Are the ROS generated upon TiO_2 excitation by UVA light (Reactions 7-14) responsible for inactivation of CuZnSOD and catalase?

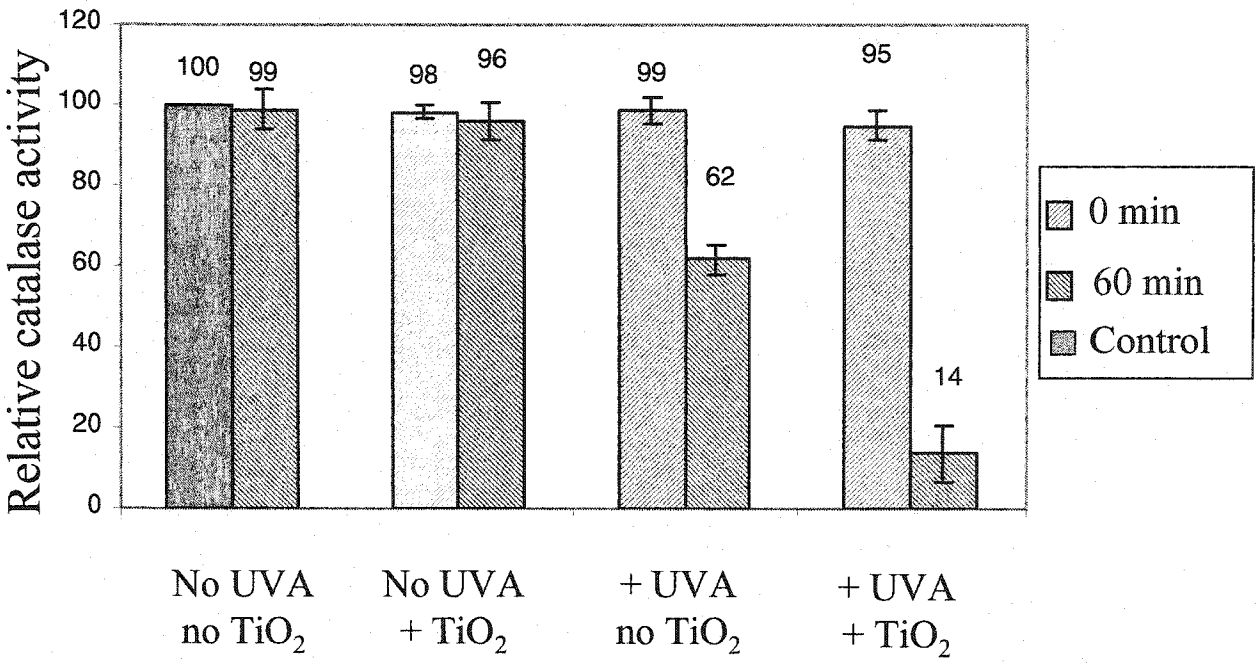

Figure 34. Effect of photoexcited TiO_2 on catalase activity after 60 min. All activities are relative to the activity of the control (dark, 0 h). The experimental details are given in caption to Figure 33. (n=3)

3.3.1 CuZnSOD

As seen in Figure 32, photoexcitation of TiO_2 caused 50% more inactivation of CuZnSOD than UVA light alone over a period of 4 h. The involvement of hydroxyl radicals ($OH^{\bullet}$) in the inactivation of CuZnSOD was investigated. A hydroxyl radical scavenger was added to the irradiated solutions and its effects on the activity of the enzyme were monitored. The scavenger used was thiourea (1 mM), which is known to bind $OH^{\bullet}$ radicals [Mello Filho (1984)]. To ensure that it did not absorb UVA light, the spectrum of 1 mM thiourea was recorded and no absorption above 300 nm was detected (data not shown). The scavenger also did not interfere with CuZnSOD activity since the enzyme activity after 4 h incubation with 1 mM thiourea was 105 ± 6% (Figure 35).

Hence, thiourea was added to specific solutions to determine if it was efficient in protecting the enzyme from inactivation by UVA light (Figure 35).

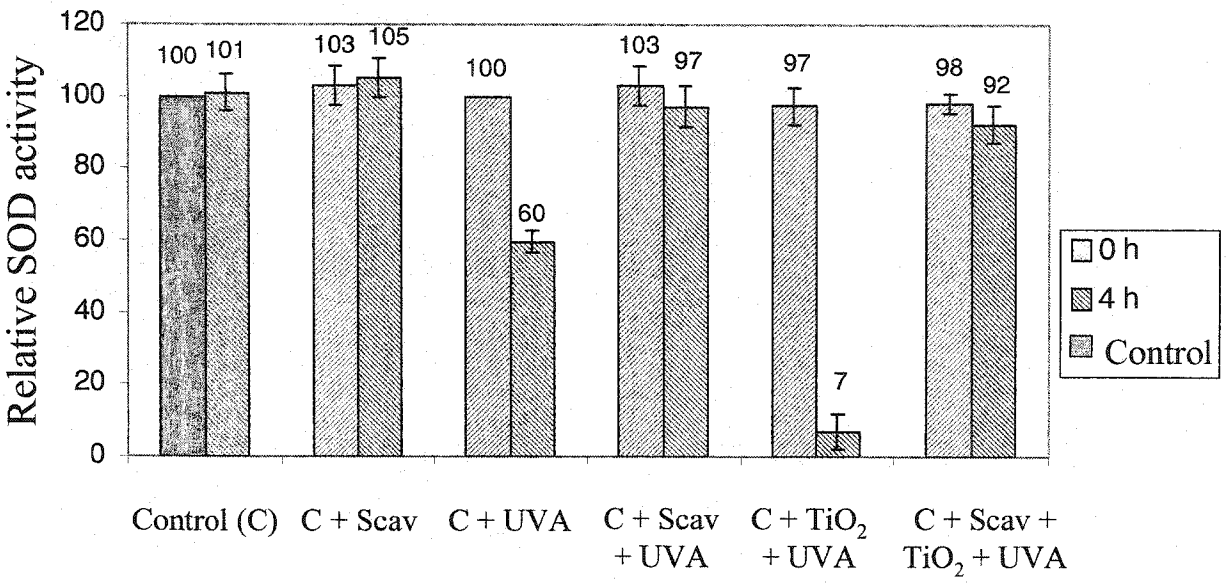

Figure 35. Effects of 1 mM thiourea, an $OH^{\bullet}$ radical scavenger on CuZnSOD activity. Experimental details given in the caption to Figure 30. (n=3)

Interestingly, it was first observed that thiourea is efficient in protecting the enzyme from UVA light alone (60 ± 3% activity without scavenger vs 97 ± 6% with scavenger) (Figure 35). The most dramatic result was the effect of thiourea on irradiated CuZnSOD plus TiO_2. Once again, the scavenger prevented CuZnSOD inactivation (7 ± 5% without scavenger vs 92 ± 5% with scavenger, Figure 35).

As seen in Equations 7 to 14, some of the $OH^{\bullet}$ radicals are generated from molecular oxygen. In order to measure the importance of O_2 in CuZnSOD inactivation, anaerobic irradiation of the samples was performed (Figure 36). The results in Figure 36 show that in absence of TiO_2, the UVA-induced inactivation of CuZnSOD was reduced

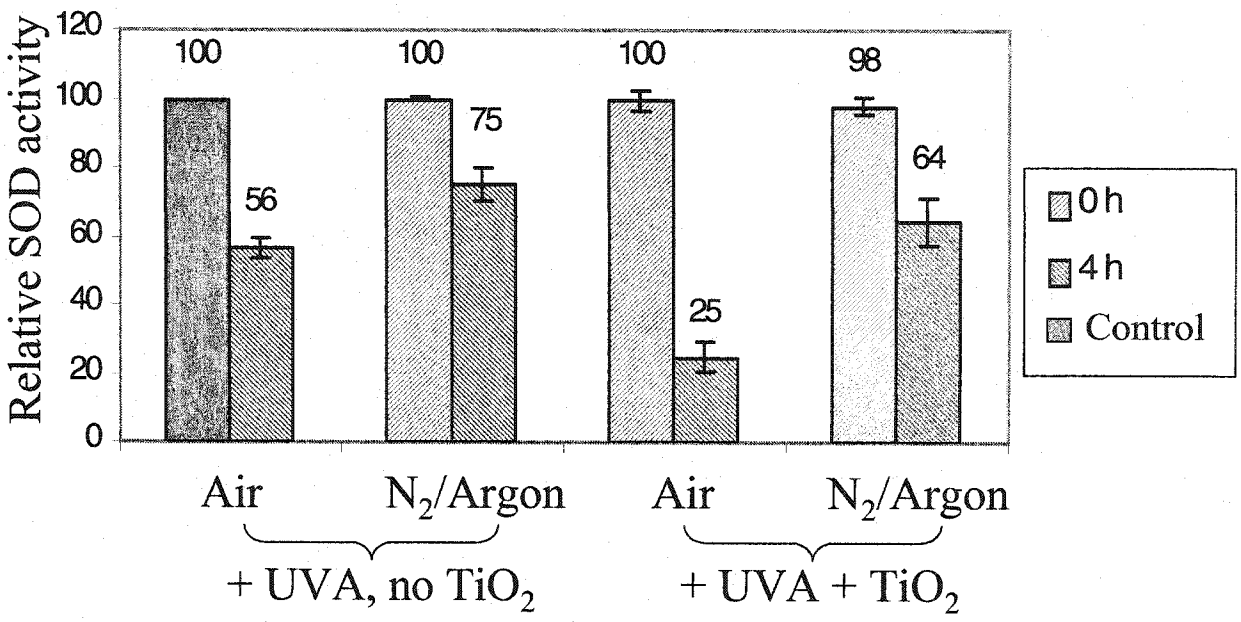

Figure 36. SOD activity following anaerobic irradiation of CuZnSOD. The buffer (50 mM sodium phosphate buffer, pH 7.0) was purged with argon and the samples were prepared in a glove box under nitrogen (Section 2.3). Experimental details are given in the caption to Figure 30. (n=3)

by ~ 20% in anaerobic solutions. The deleterious effects of O_2 were even greater when TiO_2 was present since a difference of ~ 40% (64 ± 7% – 25 ± 5%) inactivation of the enzyme was observed between the anaerobic and aerobic solutions containing TiO_2. Also, addition of DTPA, a metal chelator, increased CuZnSOD activity by 26% in solutions when exposed to UVA light and TiO_2 (Figure 37).

Upon inactivation, copper can be released from the active-site of CuZnSOD [Eum (1999), Kang (2000), Kwon (2000)]. CuZnSOD exhibits an absorption peak at 680 nm due to the d-d transition of the active-site Cu^{II}. Since the extinction coefficient for this peak is low (Section 1.3.1), a high concentration of enzyme was required so the experiment was performed only on a control (dark, no TiO_2) (Figure 38) and in the

presence of photoexcited TiO_2 (Figure 39), where the amount of copper released is expected to be the highest. The 680-nm absorbance of the control changed little over time

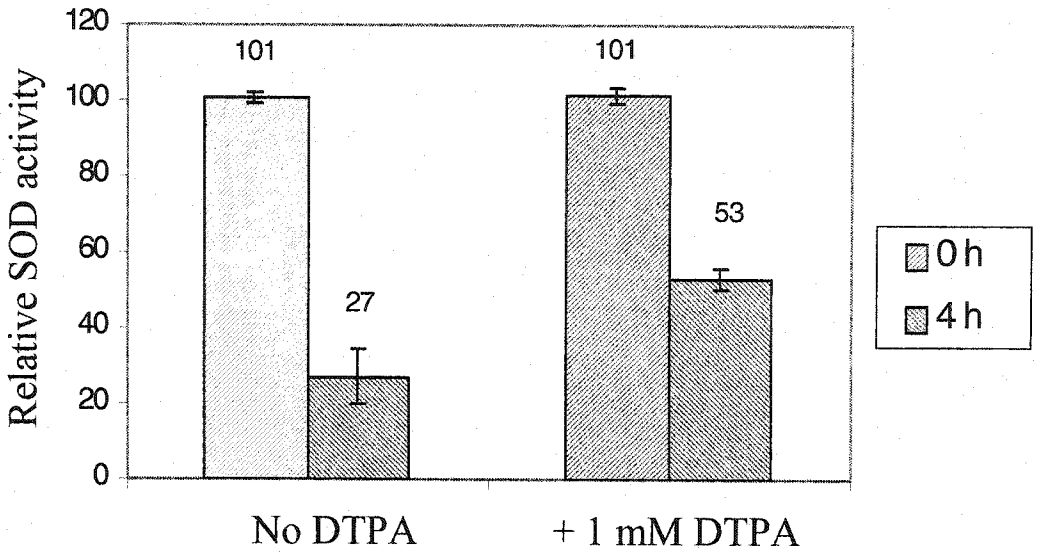

Figure 37. Effect of DTPA on SOD activity following irradiation of CuZnSOD. All solutions were exposed to UVA light and contained 0.15 mg/mL TiO_2. [DTPA] = 1 mM. Experimental details are given in the caption to Figure 30. (n=5)

(Figure 38), showing the stability of the enzyme under these conditions. However, upon exposure to both UVA and TiO_2, the 680-nm peak decreased dramatically (Figure 39), suggesting copper release from CuZnSOD.

To confirm copper release, another chelator, DDC was used. Upon chelation of copper, DDC gives a product with a strong absorption peak around 450 nm (ε_{450}=15 000 M^{-1} cm^{-1}) [Cobine (2002)]. The control as well as a sample that was exposed to TiO_2 in the dark released 1.1-2.5% copper over a 4-h period (Figure 40). Copper release increased to 3.9% on UVA-irradiation for 4 h, and in the presence of TiO_2, CuZnSOD released 7.7% copper after 4-h UVA-exposure (Figure 40).

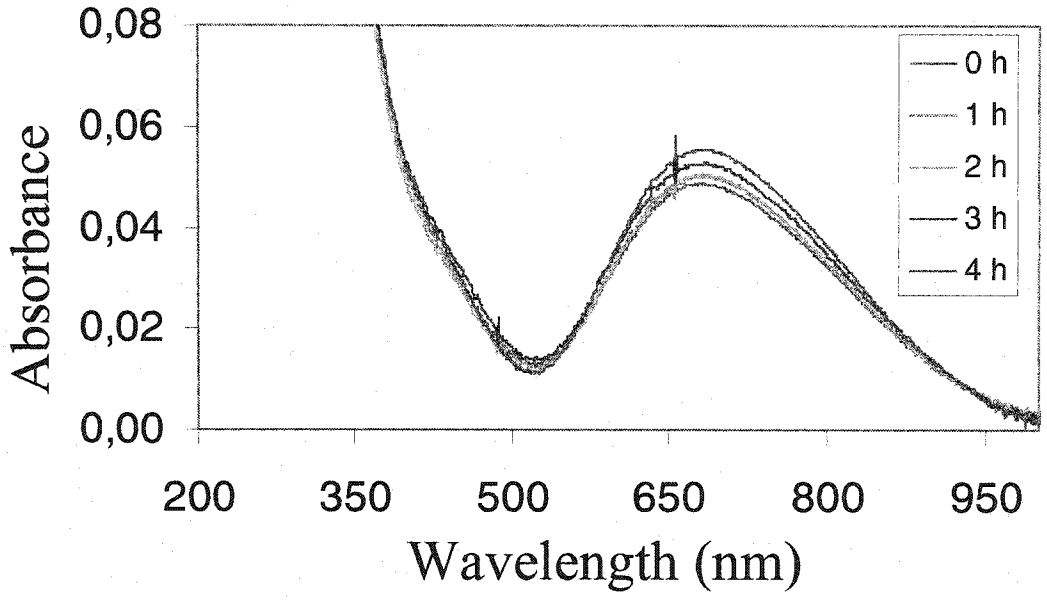

Figure 38. Cu^{II} d-d absorption of 250 μM (8.1 mg/mL) CuZnSOD in 50 mM sodium phosphate buffer, pH 7.0. The sample was stored in the dark at 37°C in the absence of TiO_2. The spectra were recorded in a 1-cm pathlength cuvette at the times indicated.

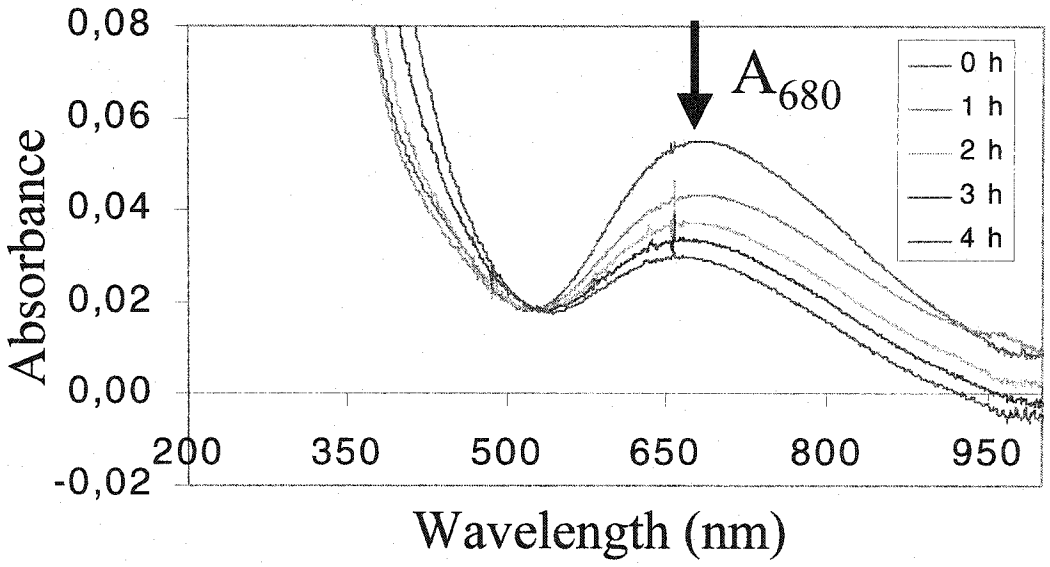

Figure 39. Cu^{II} d-d absorption of 250 μM (8.1 mg/mL) CuZnSOD in 50 mM sodium phosphate buffer, pH 7.0. The sample was exposed to 5.0 mg/mL photoexcited TiO_2 at 37°C. The sample was centrifuged at 12 000 rpm for 2 min and the spectrum of the supernatant was recorded at the times indicated in a 1-cm cell.

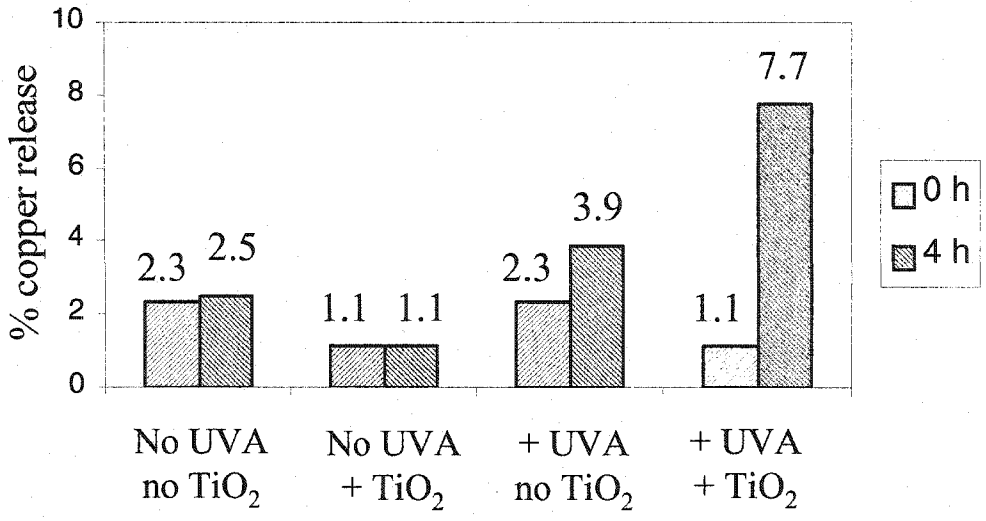

Figure 40. Copper release from CuZnSOD measured by the formation of a DDC-Cu complex. Before addition of 500 μM DDC, the CuZnSOD solutions (17 μM, 550 μg/mL) were centrifuged for 2 min at 12,000 rpm and then subjected to ultra-filtration using a Millipore Ultrafree-MC filter with a molecular weight cut-off of 5 kDa in order to remove any CuZnSOD. [TiO_2] = 2.4 mg/mL. (n=1)

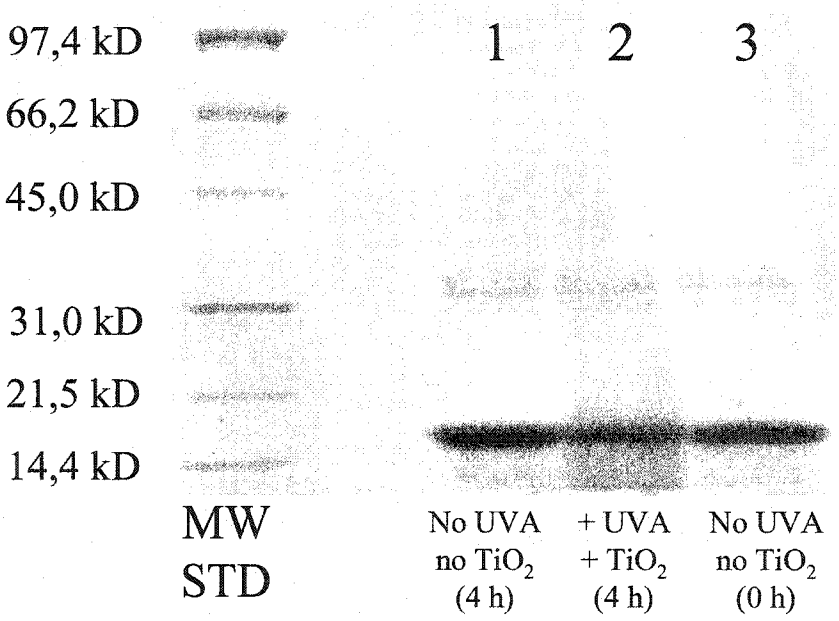

Figure 41. 4-15% SDS-PAGE analysis of CuZnSOD before and after inactivation. Experimental details are given in the caption to Figure 39. About 5 μg of CuZnSOD were loaded in each lane. Lane 1: CuZnSOD after 4 h in the dark without TiO_2. Lane 2: CuZnSOD after 4 h exposure to photoexcited TiO_2. Lane 3: Control CuZnSOD (no UVA, no TiO_2, 0 h).

Degradation of CuZnSOD upon inactivation was also investigated. The enzyme exposed to various conditions was analyzed by SDS-PAGE, and degradation products were observed in the sample exposed to photoexcited TiO_2 (Figure 41, lane 2).

3.3.2 Catalase

A number of the experiments performed with CuZnSOD were repeated with catalase. To see if the $OH^{\bullet}$ radical scavenger thiourea also protected catalase, its effects on the activity of the enzyme exposed to photoexcited TiO_2 were investigated (Figure 42).

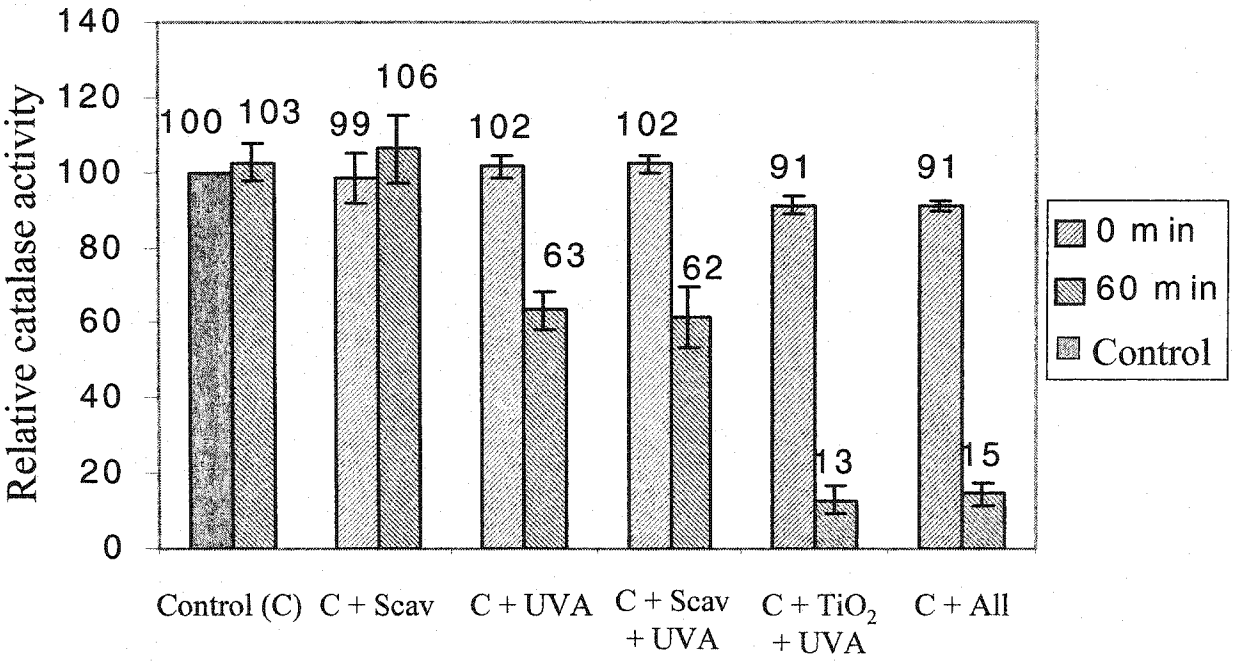

Figure 42. Effects of 1 mM thiourea, an $OH^{\bullet}$ radical scavenger, on catalase activity. Experimental details are given in the caption to Figure 33. (n=3)

Thiourea did not have any effect on the activity of catalase (106 ± 9%) after a 1 h incubation in the absence of both UVA and TiO_2 (Figure 42). Surprisingly, thiourea was not efficient in preventing catalase inactivation (Figure 42). Another well known $OH^{\bullet}$

radical scavenger, glutathione (GSH), was tested to see if it was more efficient in protecting catalase than thiourea (Figure 43). A lower concentration of scavenger was used (10 μM) because 1 mM GSH reduced the enzyme, thereby affecting its activity. This concentration of GSH was not more efficient in protecting catalase than 1 mM thiourea (Figure 43). Also, anaerobic vs aerobic irradiation had little effect on catalase activity (Figure 44).

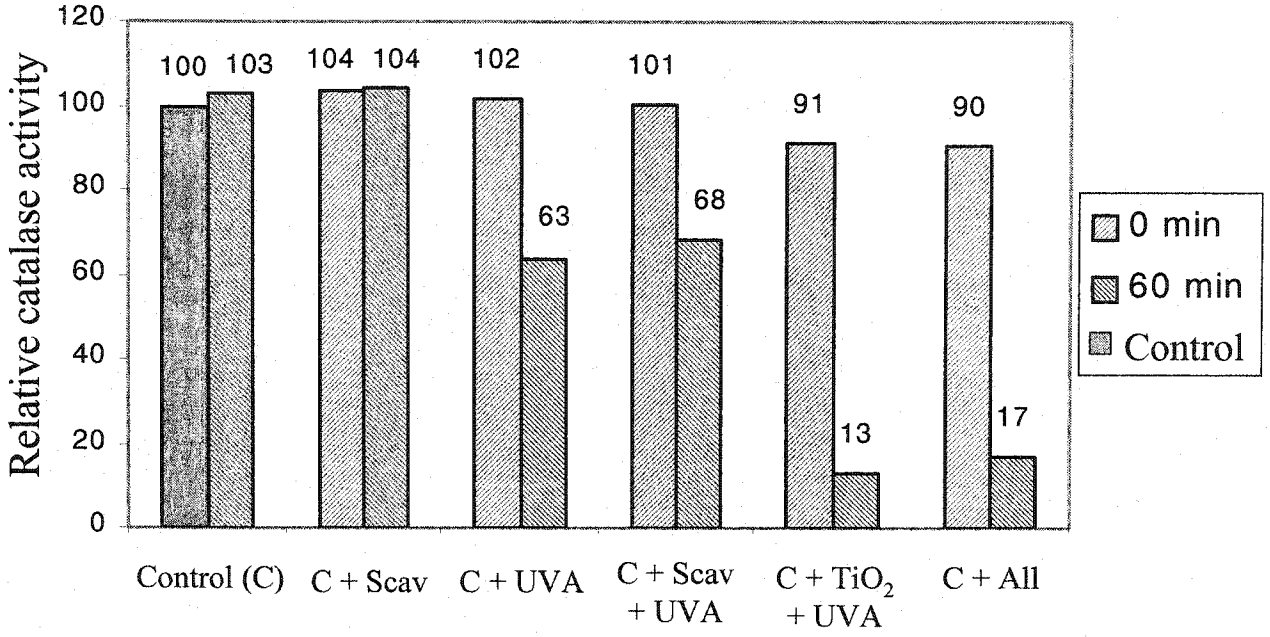

Figure 43. Effect of 10 μM GSH, an $OH^{\bullet}$ radical scavenger, on catalase activity. Experimental details are given in the caption to Figure 33. (n=1)

Since catalase was adsorbed onto the TiO_2 particles (Figure 28), UV-induced crosslinking of the enzyme to the oxide was considered. The protein concentration was measured in the supernatant of samples exposed to TiO_2 before and after irradiation (Figure 45). UV-induced crosslinking should lead to a reduction in protein concentration after exposure to UVA light. Obviously, this was not the case since the protein

concentration remained the same before and after 60 min irradiation. However, the enzyme concentration was lower when TiO_2 was present due to adsorption (Figure 45).

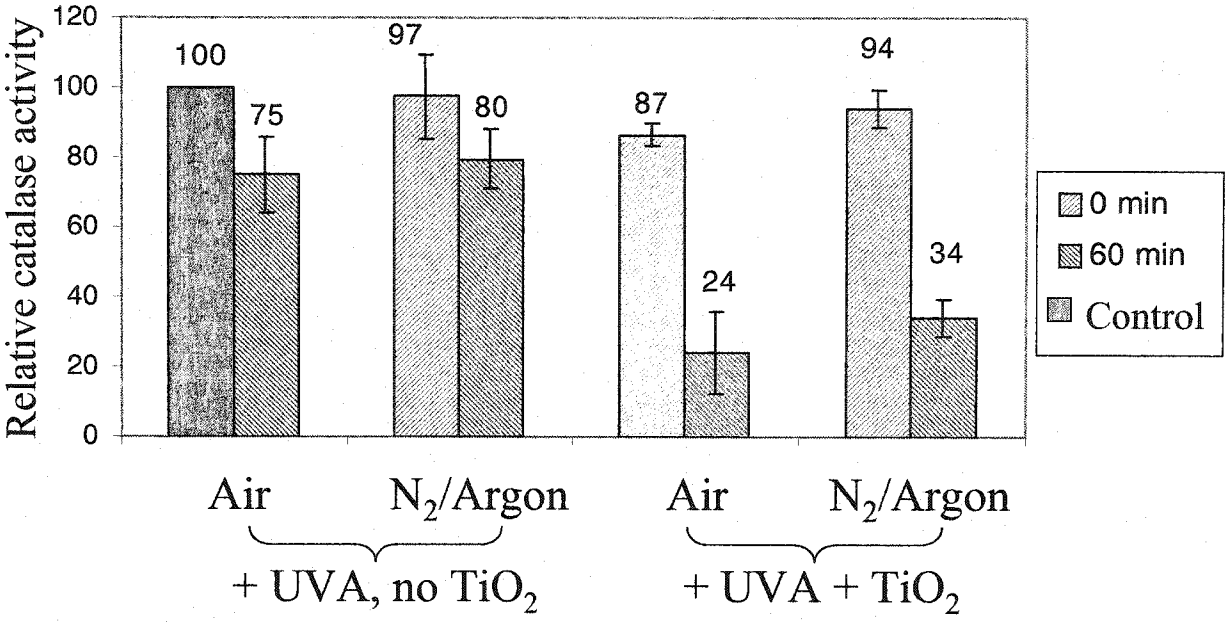

Figure 44. Activity following anaerobic irradiation of catalase. The buffer (50 mM sodium phosphate buffer, pH 7.0) was purged with argon and the samples were prepared in a glove box under nitrogen (Section 2.3). Experimental details are given in the caption to Figure 33. (n=3)

Catalase requires heme for activity. The heme group exhibits a strong absorption peak at 405 nm, which provides a rapid method of evaluating whether catalase inactivation is related to heme destruction. In the control and the sample containing only TiO_2 (Figures 46a and 46b), the heme absorption was stable over time. However, when catalase was exposed to UVA light, the heme degraded slowly (Figure 46c), and the inactivation rate increased when photoexcited TiO_2 was present (Figure 46d).

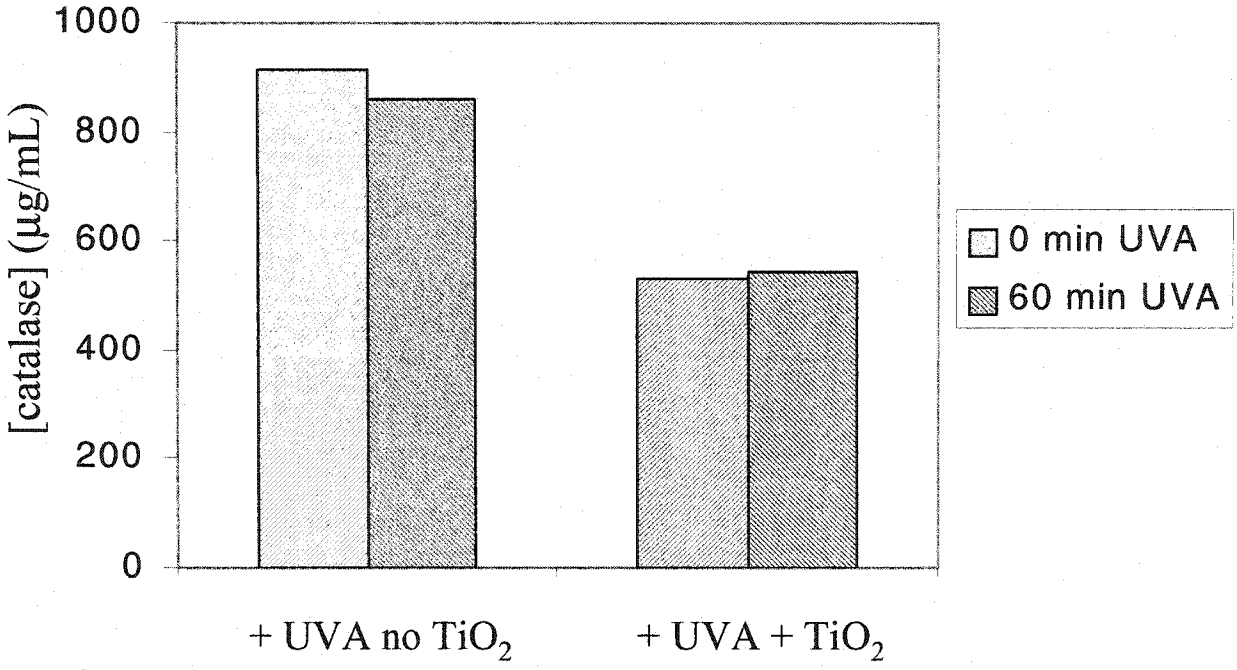

Figure 45. Catalase concentration in solution before and after exposure to UVA light and to photoexcited TiO_2. All samples were centrifuged prior to the Bio-Rad assay. Experimental procedure are given in Section 2.7. [Catalase] = 900 µg/mL, [TiO_2] = 2.5 mg/mL. (n=1)

As with CuZnSOD, the effect of a metal chelator (DTPA) on catalase inactivation was investigated. DTPA (Figure 47) was added but no changes in catalase inactivation were observed.

The final experiment performed to elucidate the mechanism of catalase inactivation was to run an SDS-PAGE of the enzyme exposed to various conditions (Figure 48). When the enzyme was kept in the dark or exposed to TiO_2 only, the same amount of protein in the catalase band at ~ 60 kDa was detected (lanes 1 and 2, Figure 48). When exposed to UVA only, a decrease in the quantity of catalase was observed (lane 3). However, the amount of enzyme observed when photoexcited TiO_2 was present

was significantly less (lane 5). A slight shift to higher mass is observed in lanes 3 and 5 and this may be due to catalase oxidation. Protein oxidation would likely contribute to enzyme inactivation.

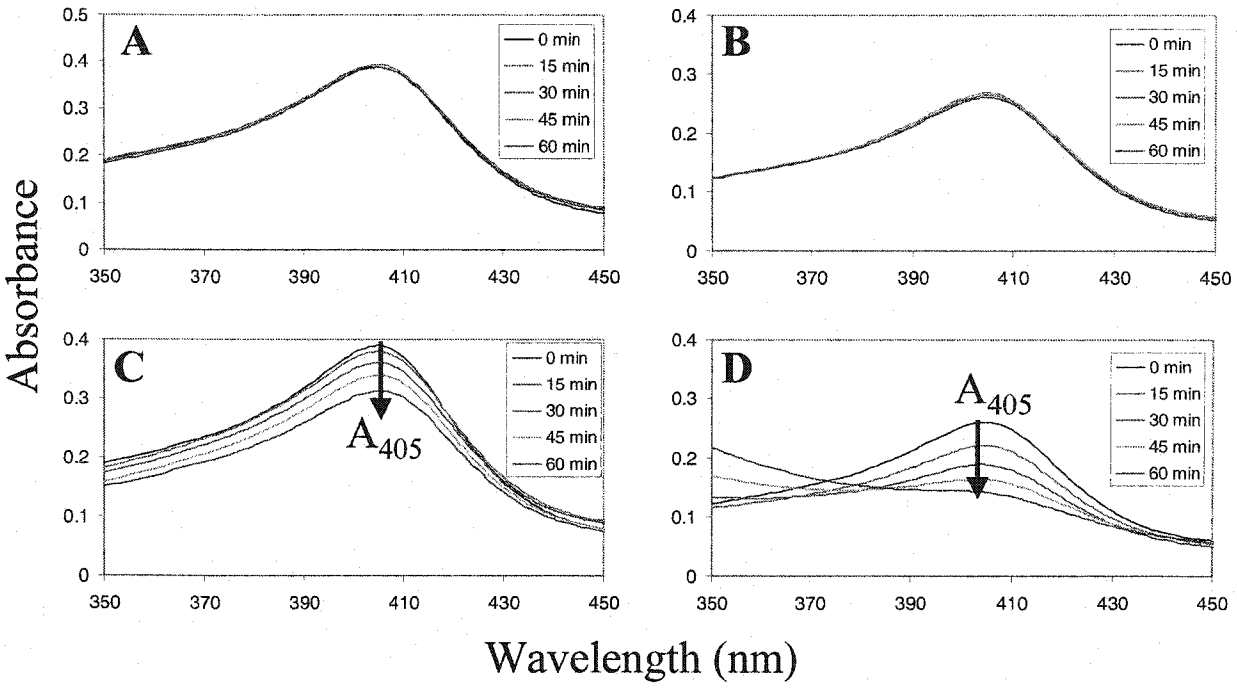

Figure 46. Heme absorption of 4.2 μM (1 mg/mL) catalase in 50 mM sodium phosphate buffer, pH 7.0. Samples were centrifuged at 12 000 rpm for 2 min and the spectrum of the supernatant was recorded at the times indicated in a 1-cm cell. [TiO_2] = 2.5 mg/mL Experimental procedure are given in Section 2.7. (A) Control (no UVA, no TiO2); (B) No UVA + TiO_2; (C) + UVA, no TiO_2; (D) + UVA + TiO_2

3.3.3 H_2O_2 depletion by photoexcited TiO_2

The concentration of H_2O_2 produced upon photoexcitation of TiO_2 (Reaction 11) was of interest because it is known that large amounts of H_2O_2 can be harmful to enzymes. However, negligible H_2O_2 was detected in photoexcited TiO_2 solutions (data

not shown), raising the question as to whether H_2O_2 was stable in the presence of TiO_2. A known amount of H_2O_2 was exposed to different conditions and the remaining concentration measured after 60 min (Figure 49). TiO_2 and UVA alone had little effect on the H_2O_2 level. However, in the presence of photoexcited TiO_2, H_2O_2 was completely depleted after 60 min.

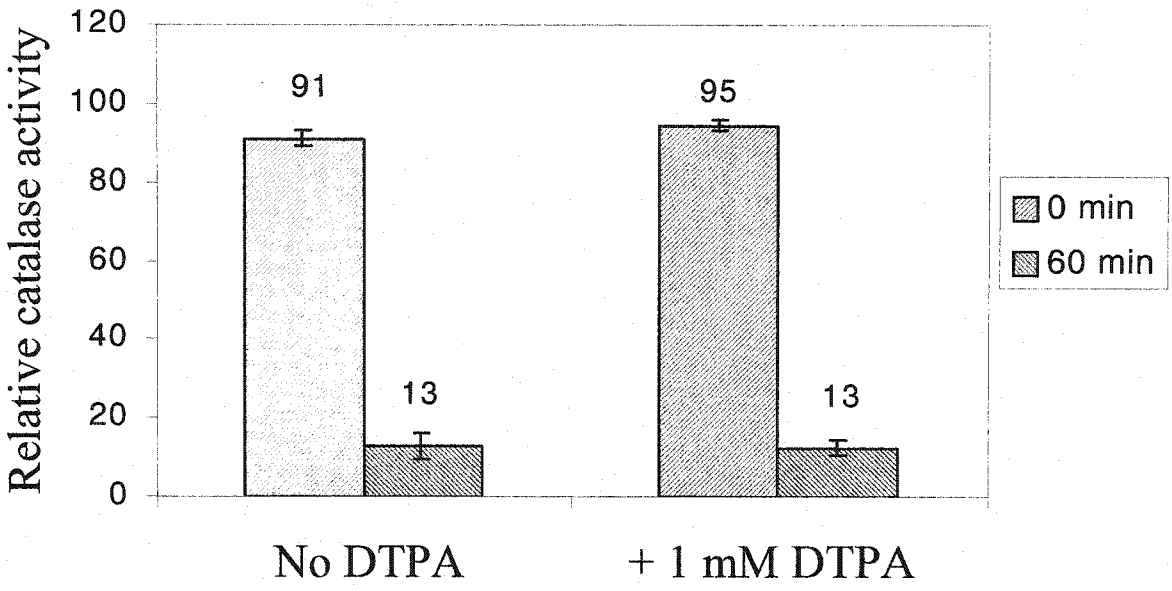

Figure 47. Effect of DTPA on catalase activity following irradiation. All solutions were exposed to UVA light and contained 0.15 mg/mL TiO_2. [DTPA] = 1 mM. Experimental details are given in the caption to Figure 33. (n=3)

3.4 Effect of encapsulated TiO_2 on enzymes

In this investigation, the effects of UVA-irradiation of solutions containing TiO_2 encapsulated in two zeolites, faujasite and mordenite, on CuZnSOD and catalase activities were studied.

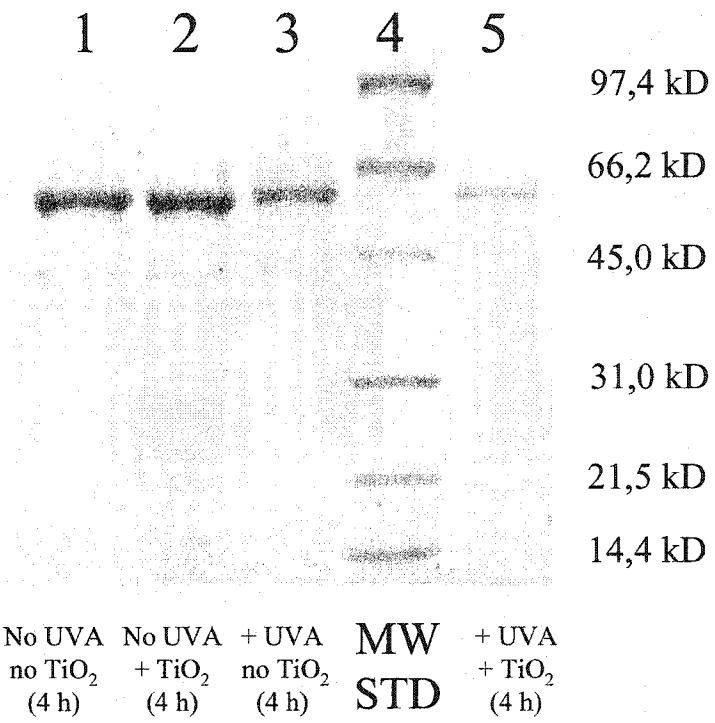

Figure 48. 4-15 % SDS-PAGE analysis of catalase after inactivation. Experimental details are given in the caption to Figure 46. About 5 µg of catalase were loaded in each lane. Lane 1: catalase after 4 h in the dark without TiO_2. Lane 2: catalase after 4 h exposure to TiO_2 in the dark. Lane 3: catalase after 4 h exposure to UVA without TiO_2. Lane 4: molecular weight standards. Lane 5: catalase after 4 h exposure to photoexcited TiO_2.

3.4.1 CuZnSOD

The effects of free zeolites, as well as TiO_2 encapsulated in the zeolites, on CuZnSOD activity was investigated under different conditions (Figure 50). Free faujasite does not affect UVA-induced inactivation of CuZnSOD (51 ± 17% and 58 ± 15% in the presence and absence of faujasite, respectively, Figure 50) even though the particles were expected to scatter the UVA light. However, the solutions were not stirred during the experiment and the zeolite particles settled to the bottom of the plates and therefore did

not act as effective light scatters. For the same reason, free faujasite did not inhibit the inactivation of CuZnSOD by irradiated free TiO_2 (11 ± 11% when both present vs 11 ± 14% when only TiO_2 was present, Figure 50). However, encapsulation of TiO_2 in both

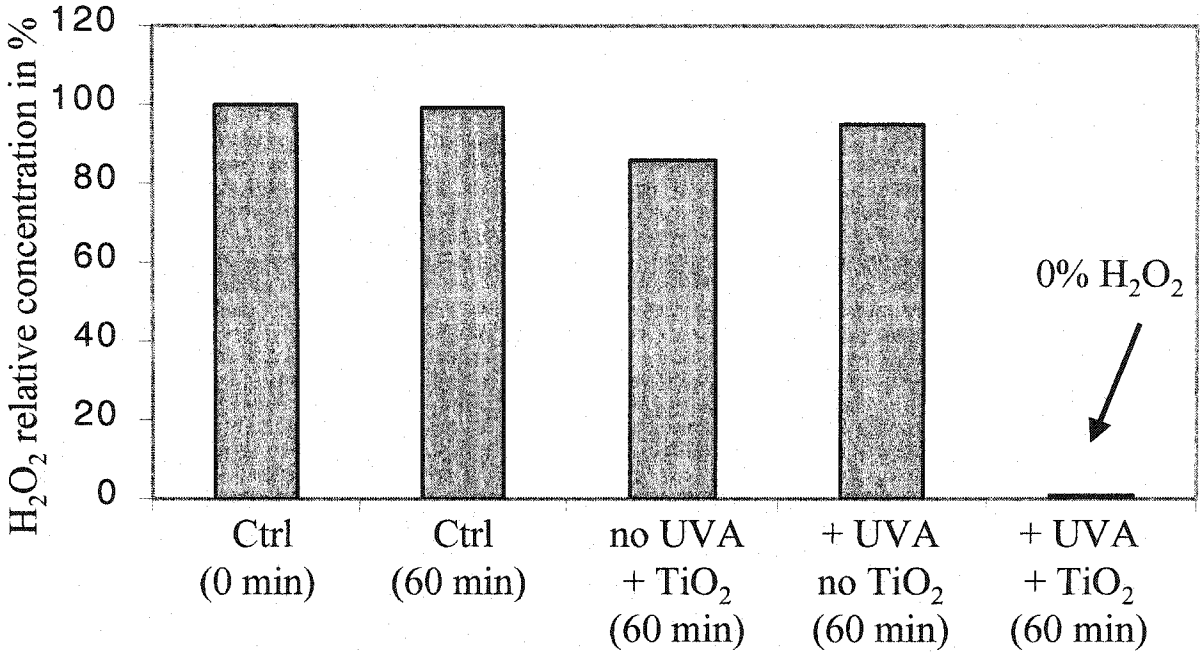

Figure 49. Relative H_2O_2 concentrations in different solutions after 60 min. The initial concentration of H_2O_2 was 600 μM in 50 mM sodium phosphate buffer, pH 7.0. [TiO_2] = 0.15 mg/mL. (n=1)

faujasite and mordenite protected the enzyme against inactivation by photoexcited TiO_2, and the activity observed was the same as that in UVA-irradiated solutions in the absence of free TiO_2 (62 ± 10%, 61 ± 16%, 58 ± 15% activity, respectively in the presence of irradiated TiO_2@faujasite, TiO_2@mordenite, and buffer only, Figure 50).

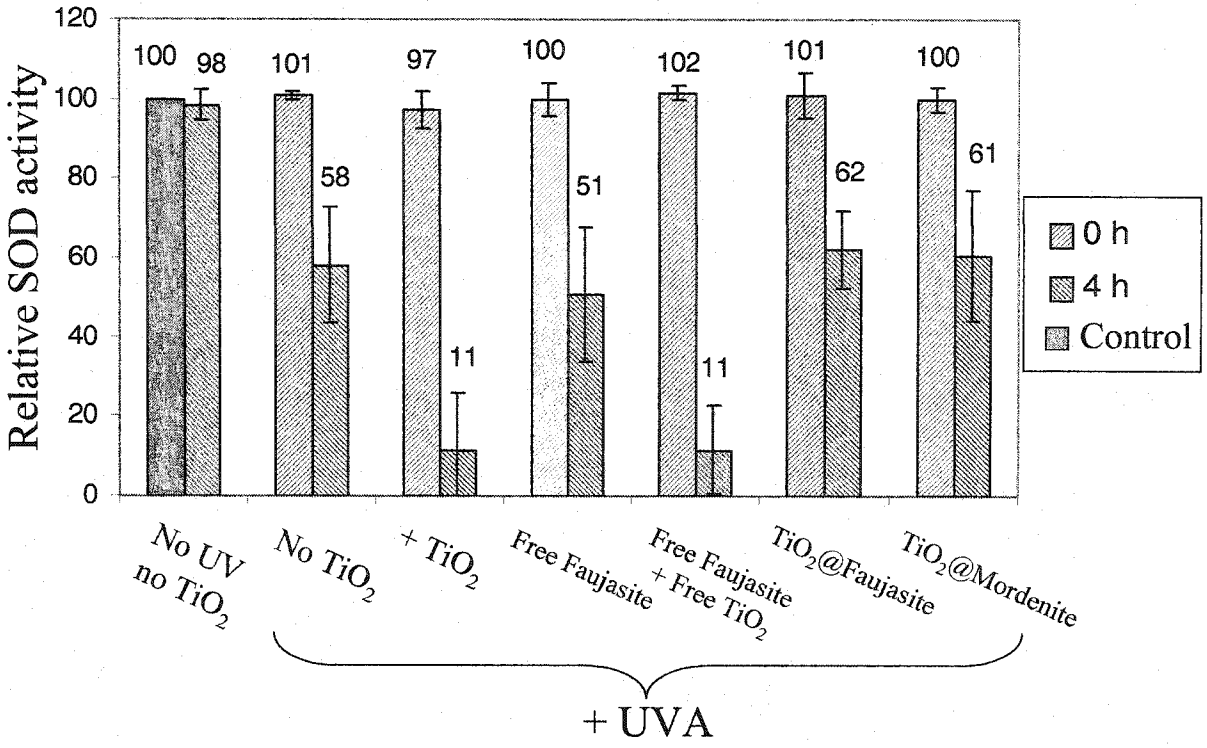

Figure 50. Effects of free zeolites and TiO_2 encapsulated in zeolites on CuZnSOD activity. [zeolite] = 1.5 mg/mL. Experimental details are given in the caption to Figure 30. (n=3)

3.4.2 Catalase

The effects of encapsulated TiO_2 on catalase activity were also investigated (Figure 51). Free faujasite did not protect catalase from UVA-induced damage in buffer only (40 ± 7% vs 49 ± 5% with and without free faujasite, respectively, Figure 51) or in the presence of free TiO_2 (14 ± 4% vs 11 ± 3% with and without free faujasite, respectively, Figure 51). Encapsulated TiO_2 in faujasite did protect catalase from inactivation (40 ± 5% and 11 ± 3% in the presence of irradiated encapsulated TiO_2 and free TiO_2, respectively, Figure 51). Interestingly, mordenite decreased catalase activity, since even before irradiation, the activity of the enzyme was 76 ± 7% (Figure 51). This could be due to adsorption of catalase on the surface of the mordenite particles, which

could alter the quaternary structure and/or the active-site conformation. However, TiO_2 encapsulation in mordenite decreased the inactivating effects of TiO_2 (Figure 51).

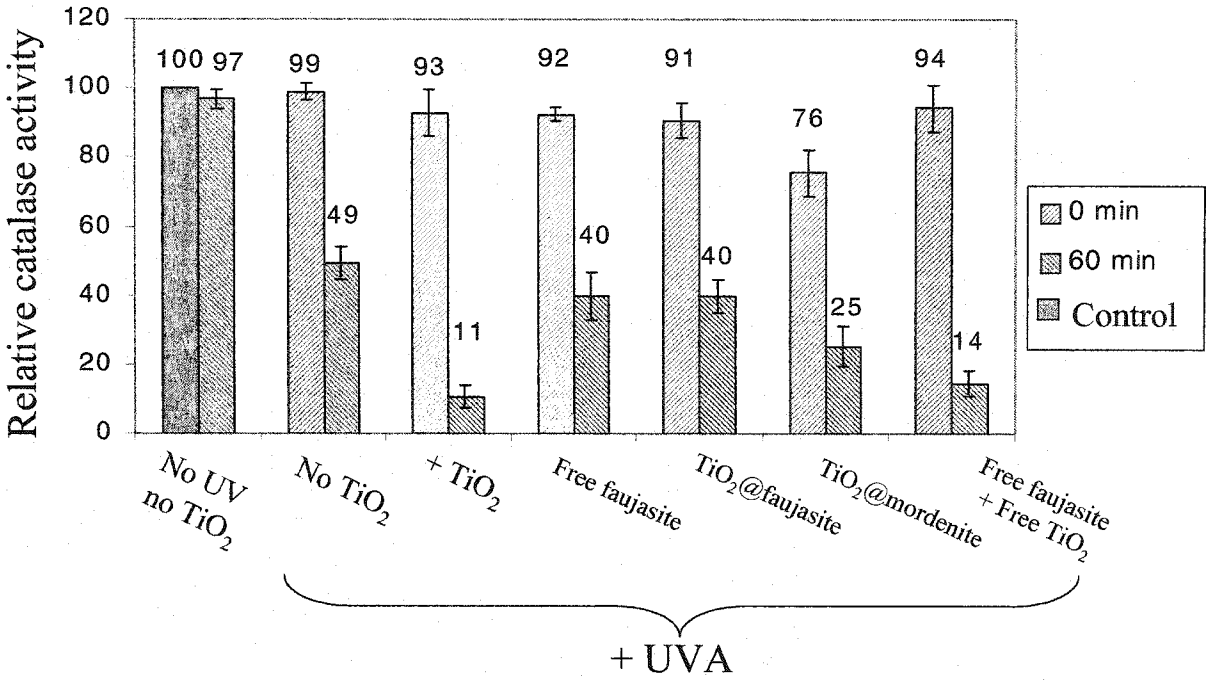

Figure 51. Effects of free zeolites and TiO_2 encapsulated in zeolites on catalase activity. [zeolite] = 1.5 mg/mL. Experimental are details given in the caption to Figure 33. (n=3)

3.5 Viability of cells exposed to TiO_2 and UVA light

Photoexcited TiO_2 inactivated isolated antioxidant enzymes and encapsulation of TiO_2 decreased the extent of inactivation (Figures 50 and 51). The effects of TiO_2 on living cells were next investigated. Rat keratinocytes were exposed to TiO_2 in two different buffers, DMEM at pH 7.4 and PBS at pH 7.2. DMEM contains nutrients that help cells to survive and divide, but PBS does not contain any nutrients. The purpose of the first set of experiments was to determine which buffer maximized cell viability during irradiation.

3.5.1 DMEM buffer

Rat keratinocytes in DMEM were irradiated by UVA light in presence and absence of TiO_2 (Table 4). The cells were stable over 4 h when stored at 37°C in the dark (Table 4, no UVA, no TiO_2). When exposed to free TiO_2, 85% of the cells died within 4 h (Table 4). The cytotoxicity of TiO_2 in the absence of UVA has also been reported by Uchino et al. (2002) and Cai et al. (1991). Cell death may be caused by TiO_2 aggregation on the cell surface and/or by penetration of TiO_2 particles into the cell [Cai et al. (1991)], which could damage organelles. UVA light with and without photoexcited TiO_2 killed all the cells within 1 h (Table 4). Changes in cell morphology were also observed on irradiation. The cells decreased in size and the cell membrane lost its smooth appearance (data not shown).

3.5.2 PBS

The viability of cells in PBS was also examined. The cells were found to be stable over 4 h when kept at 37°C in the dark (Table 5, no UVA, no TiO_2). When exposed to free TiO_2, cells died within 1 h, even in the absence of UVA light (Table 5). Exposure to UVA light and photoexcited TiO_2 also killed the cells within 1 h. Thus, DMEM is a more suitable medium for rat keratinocytes than PBS.

3.6 Preliminary studies on enzyme activity in cell lysates

The experiments conducted so far were performed on isolated enzymes. The activities of antioxidant enzymes (SOD, catalase and peroxidase) in rat keratinocytes were measured to compare the effects of UVA on enzymes *in vitro* and *in vivo*.

Table 4. Effects of TiO_2 and UVA light on the viability of rat keratinocytes in DMEM (pH 7.4) containing 5% FCS at 37°C.

	No UVA		+ UVA	
Time (h)	No TiO_2	+ TiO_2	No TiO_2	+ TiO_2
0	< 1%	< 1%	< 1%	< 1%
1	< 3%	< 4%	100%	100%
2	< 1%	< 2%	100%	100%
3	< 2%	< 4%	100%	100%
4	< 1%	≈ 85%	100%	100%

The numbers reported are the percentage of dead cells as determined by Trypan Blue uptake. Between 100 and 700 cells were observed at each time point, and the experimental procedures are described in Section 2.9. [TiO_2] = 0.15 mg/mL.

Table 5. Effects of TiO_2 and UVA light on the viability of rat keratinocytes in PBS (pH 7.2) at 37°C.

	No UVA		+ UVA	
Time (h)	No TiO_2	+ TiO_2	No TiO_2	+ TiO_2
0	< 1%	< 1%	< 1%	< 1%
1	< 3%	100%	100%	100%
2	< 10%	100%	100%	100%
3	< 5%	100%	100%	100%
4	< 7%	100%	100%	100%

The numbers reported are the percentage dead cells as determined by Trypan Blue uptake. Between 100 and 700 cells were observed at each time, and the experimental procedures are described in Section 2.9. [TiO_2] = 0.15 mg/mL.

3.6.1 SOD activity

As mentioned in Section 1.3.1, there are two types of SOD in eukaryotic cells, CuZnSOD and MnSOD. Using different inhibitors, it is possible to measure only CuZnSOD or MnSOD activity. Here, we are interested in total SOD activity in cells. A rat keratinocyte cell lysate containing ~ 1 mg/mL of total protein was prepared as described in Section 2.10, and 100 µL of this was added to 1.9 mL of SOD assay buffer (Section 2.4) to give a final protein concentration of 50 µg/mL. SOD activity, as measured by pyrogallol oxidation (Section 2.4), was observed (Figure 52); thus it should be possible to measure changes in SOD activity in cells after UVA and TiO_2 exposure.

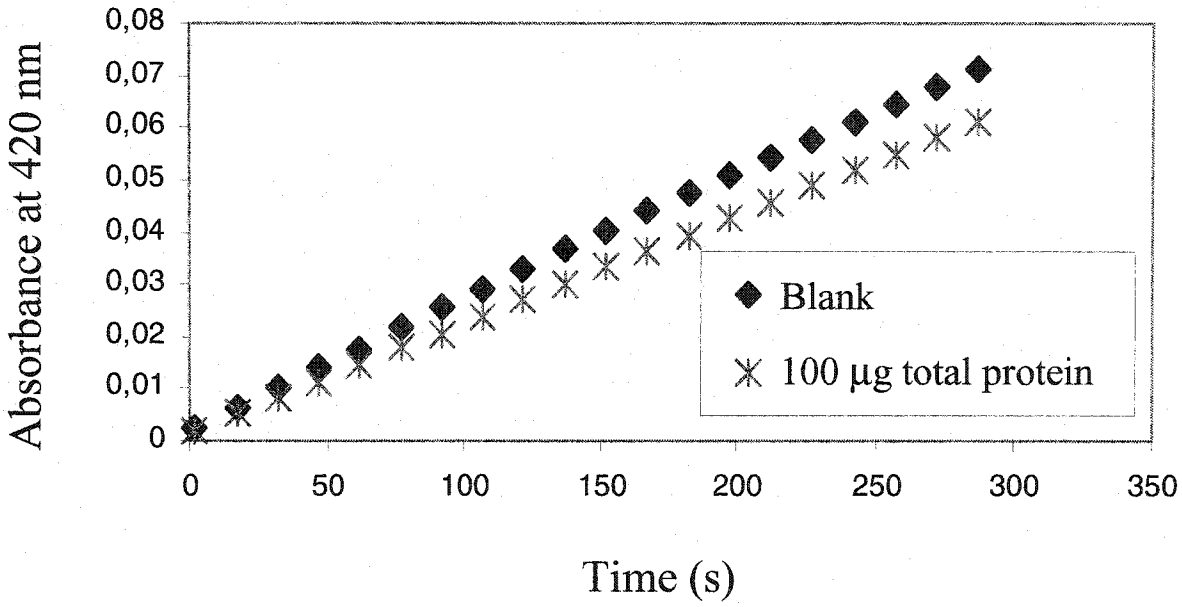

Figure 52. SOD activity in 50 µg/mL of total protein from a rat keratinocyte cell lysate. A 100-µL aliquot of a 1-mg/mL lysate was added to 1.9 mL of 50 mM Tris-cacodylate buffer (pH 8.2) containing 1 mM DTPA in a 1-cm cuvette. Pyrogallol was added to a final concentration of 198 µM and the total volume in the cuvette adjusted to 2.0 mL. Measurements of the absorbance at 420 nm were commenced at t=10 s and recorded every 15 s (Section 2.4).

3.6.2 Catalase and peroxidase activity

Catalase and peroxidase activities in rat keratinocytes were also measured. The same rat keratinocyte cell lysate (1 mg/mL) used to test SOD activity was used to monitor catalase and peroxidase activity. A 50-μL aliquot of cell lysate was added to 950 μL of 14 mM H_2O_2 in 50 mM sodium phosphate buffer (pH 7.0) to give a final protein concentration of 50 μg/mL after the volume was adjusted to 1.0 mL. Figure 53 shows that 50 μg of protein is adequate to measure H_2O_2 depletion within detectable limits. Assuming that only catalatic activity ($2\ H_2O_2 \rightarrow 2\ H_2O + O_2$) consumes H_2O_2 in the absence of added peroxidase donor substrates, catalase activity should be readily monitored in cells after different treatments.

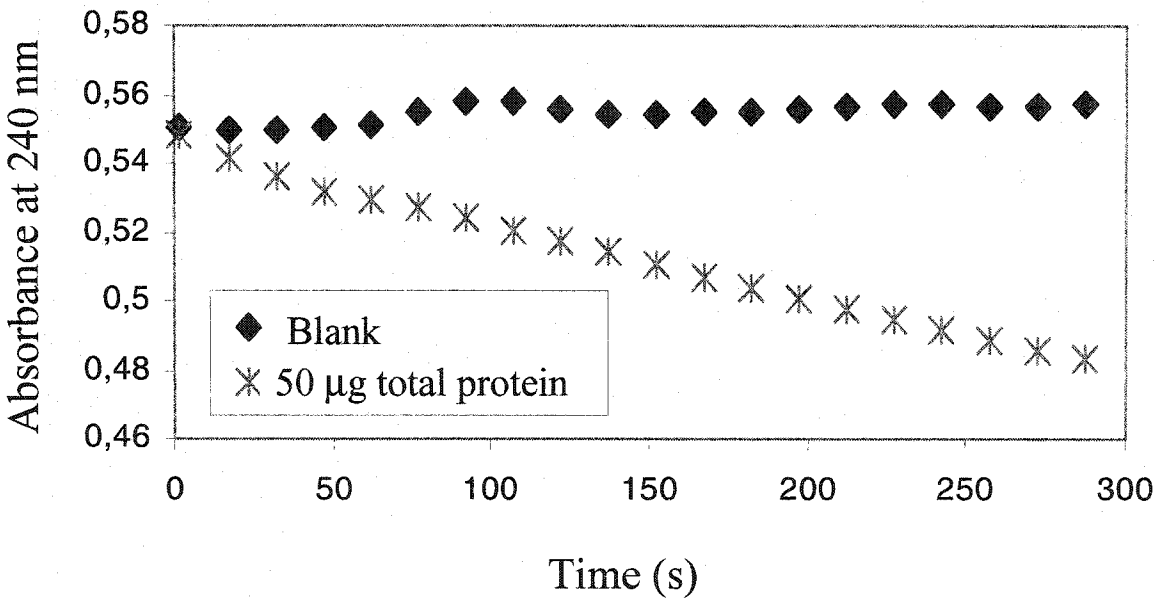

Figure 53. Catalase activity in 50 μg/mL of total protein from a rat keratinocyte cell lysate. A 50-μL aliquot of a 1 mg/mL lysate was added to 950 μL of 14 mM H_2O_2 in 50 mM sodium phosphate buffer (pH 7.0) in a 1-cm cuvette and the volume adjusted to 1.0 mL. Measurements of the absorbance at 240 nm were commenced at t=10 s and recorded every 15 s (Section 2.5).

The cell lysate was then tested for total peroxidase activity (Section 2.6) using ABTS as a donor substrate. A 50-µL aliquot of the cell lysate was added to 920 µL of 9.1 mM ABTS in 100 mM sodium phosphate buffer (pH 5.0) in a 1-cm cuvette, followed by 30 µL of 100 mM H_2O_2 in water, and the volume was adjusted to 1.0 mL. The rate of ABTS oxidation in the sample containing 50 µg/mL total protein was greater than in the blank (Figure 54) indicating that the lysate possessed peroxidase activity.

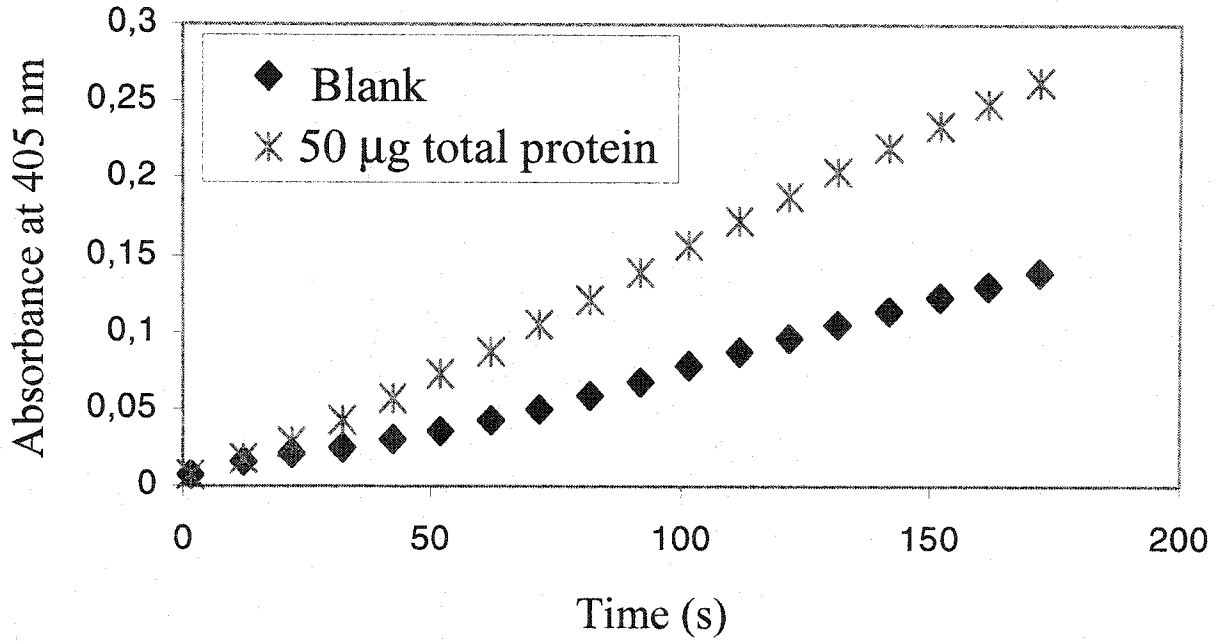

Figure 54. Peroxidase activity in 50 µg/mL of total protein from a rat keratinocyte cell lysate. A 50-µL aliquot of a 1 mg/mL lysate was added to 920 µL of 9.1 mM ABTS in 100 mM sodium phosphate buffer (pH 5.0) in a 1-cm cuvette. Then 30 µL of a 100 mM H_2O_2 solution in water was added, and the volume adjusted to 1.0 mL. Measurements of the absorbance at 405 nm were commenced at t=10 s and recorded every 15 s (Section 2.6).

From these preliminary results, it should be possible to measure differences in SOD, catalase and peroxidase activities in rat keratinocytes following exposure to UVA light and TiO_2. Measurements of the activity of these enzymes in cells should be more representative of the behavior of antioxidant enzymes in living tissues exposed to photoexcited TiO_2.

Chapter 4

4. DISCUSSION

4.1 Effect of photoexcited TiO_2 on enzymes

As discussed in Section 1.4, TiO_2 can be excited by light of wavelengths shorter than 385 nm. Once excited, an electron is promoted from the valence band to the conduction band and in solution, this leads to the generation of different reactive oxygen species (ROS) that can be harmful to skin proteins and cells. A few studies have already shown that photoexcitation of TiO_2 caused inactivation of the enzyme HRP *in vitro* [Hancock-Chen (2000), Cosa (2002a), Cosa (2002b)] and that it catalyzed oxidative damage to DNA *in vitro* and in cultured human fibroblasts [Dunford (1997)]. Some of the ROS produced following TiO_2 photoexcitation can be removed by enzymes found in our skin such as CuZnSOD, which removes superoxide radicals, and catalase, which catalyses the elimination of hydrogen peroxide. Inactivation of these enzymes by photoexcited TiO_2 would call into question the protective role of TiO_2 as a sunscreen.

When CuZnSOD and catalase were exposed to TiO_2 in the dark, no effect on the activity of the enzymes was observed (Figures 32 and 34). This is not surprising since ROS production by TiO_2 requires UV light. However, UVA irradiation affected both enzymes. The activity of catalase decreased to 62 ± 4% after only 60 min UVA-irradiation (Figure 34) whereas 69% CuZnSOD activity remained after 4 h exposure (Figure 32). This difference in stability can be explained by the fact that catalase contains heme groups that are photosensitive as shown in Figure 46c. The rapid UVA-induced inactivation of catalase is one reason to protect our skin from UV light.

In the presence of photoexcited TiO_2, almost complete inactivation was observed for both enzymes within 4 h (Figures 32 and 34). This clearly shows that photoexcited TiO_2 damages rather than protects the enzymes. Since TiO_2 is absorbed by the skin [Lademann (1999), Tan (1996)] and since UVA light penetrates the skin (Figure 3), TiO_2-containing sunscreens may enhance UV-induced aging of the skin.

4.2 Mechanisms of enzyme inactivation

A few studies conducted so far have shown that hydroxyl radicals ($OH^{\bullet}$) are produced upon photoexcitation of TiO_2 and that these radicals can cause degradation of organic molecules [Al-Ekabi (1988)] and damage cells and DNA [Dunford (1997), Salih (2002), Uchino (2002)]. The inactivation mechanism of both CuZnSOD and catalase was investigated to determine whether $OH^{\bullet}$ radicals were responsible for their inactivation.

4.2.1 CuZnSOD

The $OH^{\bullet}$ radical scavenger, thiourea, prevented CuZnSOD from inactivation when the enzyme was exposed to photoexcited TiO_2 (Figure 35). This provides evidence that free $OH^{\bullet}$ radicals are produced upon photoexcitation of TiO_2 and that these radicals are involved in the inactivation of CuZnSOD.

To establish whether the $OH^{\bullet}$ radicals were derived from O_2 and H_2O, anaerobic irradiation was performed (Figure 36). Obviously, O_2 is a major source of the $OH^{\bullet}$ radicals generated by photoexcited TiO_2 since 40% less inactivation of CuZnSOD was observed under anaerobic conditions. Upon removal of O_2, Reactions 9 to 14 are prevented because they are initiated by O_2 (Reaction 9). Hence, when O_2 is present, more

$OH^{\bullet}$ radicals are produced, which explains why more enzyme inactivation occurred under aerobic conditions. The ~ 10% greater inactivation of CuZnSOD in the presence of photoexcited TiO_2 (Figure 36) can be attributed to Reactions 7 and 8. The $hole^{+}$ generated upon TiO_2 photoexcitation can react with water to give $OH^{\bullet}$ radicals, without any oxygen consumption. However, $OH^{\bullet}$ generation via O_2-consuming reactions (Reactions 9-14) must be considerably greater than via H_2O-consuming reactions (Reactions 7-8) given the greater protection of CuZnSOD afforded by removing O_2 than TiO_2 (Figure 36).

An interesting observation made during the study of CuZnSOD inactivation was that DTPA, a metal chelator, partially protected the enzyme from inactivation (Figure 37). A few hypotheses that could explain this result were formulated. The first hypothesis was that DTPA absorbed part of the UVA light, but a UV-Vis spectrum of DTPA at the same concentration used in the experiment showed no absorption above 250 nm (data not shown). Perhaps DTPA was altering the rate of pyrogallol oxidation? Trace metals are known to catalyze pyrogallol oxidation [Marklund (1974)], which would affect the results. However, this hypothesis was also rejected since although DTPA was not present in all the irradiated solutions, the chelator was always present in the assay solutions. The last hypothesis that could explain the observed protective effect of DTPA is that trace metals are involved in the inactivation of CuZnSOD. However, since all buffers were treated with chelating resin, the enzyme itself was the suspected source of trace metal ions. It has been reported that upon inactivation of CuZnSOD by ROS such as $OH^{\bullet}$ radicals and H_2O_2, copper can be released from the active-site into the solution [Eum (1999), Kang (2000), Kwon (2000)]. Free cuprous ions are also known to react with H_2O_2

to produce $OH^{\bullet}$ radicals (Fenton reaction) according to Reactions 25 and 26. Since DTPA stabilizes Cu^{II}, the binding of copper by DTPA would inhibit Reaction 26 and thus, $OH^{\bullet}$ radical production.

$$H_2O_2 + Cu^{I} \rightleftharpoons OH^{\bullet} + OH^{-} + Cu^{II} \quad (25)$$

$$O_2^{\bullet -} + Cu^{II} \rightleftharpoons O_2 + Cu^{I} \quad (26)$$

To probe for copper loss from the enzyme, the 680-nm band due to the d-d absorption by the active-site Cu^{II} was monitored on exposure to both UVA and TiO_2. The intensity of this band decreased dramatically (Figure 39), suggesting copper release from CuZnSOD. This was confirmed when free copper was measured in solutions following exposure of CuZnSOD to photoexcited TiO_2 (Figure 40). However, the amount of free copper detected indicated that only 7% of the total active-site copper was released from the enzyme compared to 80% inactivation of the enzyme (Figure 32). Thus, inactivation may involve $OH^{\bullet}$ attack on amino acid residues that alter the enzyme (Figure 8) and lead to some copper release. The hypothesis that DTPA inhibits the Fenton reaction by binding copper is possible if CuZnSOD inactivation is autocatalytic. Inactivation is accompanied by copper release, which further increases Fenton chemistry (Reactions 25 and 26) and CuZnSOD inactivation.

Finally, CuZnSOD degradation upon exposure to photoexcited TiO_2 was detected by SDS-PAGE (Figure 41). With this result, it is possible to correlate copper release to enzyme degradation.

4.2.2 Catalase

Catalase acts in tandem with CuZnSOD to remove ROS. As mentioned in Section 1.3.2, catalase is a hemoprotein and this plays a major role in its inactivation mechanism, as will be discussed.

It was first observed that $OH^{\bullet}$ radical scavengers are not efficient in preventing catalase inactivation (Figures 42 and 43), although $OH^{\bullet}$ scavenging fully protected CuZnSOD from inactivation (Figure 35). This was the first major difference observed between the inactivation of the two enzymes. Another major difference was that oxygen does not affect catalase inactivation in presence of photoexcited TiO_2 (Figure 44). This result was quite surprising since most of the ROS produced in irradiated TiO_2 solutions are formed from oxygen (Reactions 9 to 14). It was mentioned in Section 3.1.2 that catalase (but not CuZnSOD) is adsorbed on the surface of TiO_2. This may be the key factor in explaining their different inactivation behaviour. Close contact between the heme groups of catalase and the TiO_2 particles could allow direct reaction between the heme and the holes (h^+) formed on radiation of the oxide. Rapid electron transfer between the adsorbed enzyme and the h^+ centres would compete with $OH^{\bullet}$ formation so that inactivation would be independent of $OH^{\bullet}$ scavenger and O_2 concentrations. Interestingly, catalase adsorption on TiO_2 (Figure 28) was found not to be sensitive to UVA exposure (Figure 45). Thus, no UVA-induced crosslinking between TiO_2 and catalase likely takes place.

As mentioned earlier, the two antioxidant enzymes studied here differ in that catalase is a hemoprotein whereas CuZnSOD that owes its activity to its active-site copper. It was observed that when catalase was exposed to photoexcited TiO_2, rapid

heme degradation occurred (Figure 46). Thus, inactivation of catalase can be linked to heme destruction. Since heme contains iron (Figure 10), the release of the metal was investigated since free iron could catalyze Fenton chemistry like free copper (Reactions 25 and 26). As with CuZnSOD, the effect of the metal chelator DTPA on catalase inactivation was investigated. No changes in the extent of catalase inactivation were observed in the presence and absence of DTPA (Figure 47), suggesting that free iron was not involved.

A correlation between activity loss and protein degradation was also investigated for catalase. Surprisingly, no degradation products and no species at high mass were observed (Figure 48). Possible explanations are that the degradation products were so small (< 10 kDa) that they ran off the gel, or they were adsorbed more strongly than the native enzyme on TiO_2.

4.2.3 H_2O_2 depletion by photoexcited TiO_2

According to Equation 11, H_2O_2 is formed in solution upon photoexcitation of TiO_2. It is known that H_2O_2 can lead to enzyme inactivation [Bray (1974)]. Surprisingly, no H_2O_2 was detected in photoexcited TiO_2 solutions, but added H_2O_2 was found to be completely depleted after 60 min in contact with photoexcited TiO_2. This can be explained by considering Equation 14, which indicates that electrons generated upon photoexcitation of TiO_2 react with H_2O_2 to produce $OH^{\bullet}$ radicals. Since H_2O_2 does not build up in TiO_2 photoexcited solutions, it does not directly contribute to enzyme inactivation.

4.3 Effect of encapsulated TiO_2 on enzymes

Evidence has been presented to show that photoexcited TiO_2 causes inactivation of two major enzymes involved in the skin's enzymatic antioxidant defense, CuZnSOD and catalase. TiO_2, which is marketed as a safe and efficient sunscreen component (US Federal Register, 43FR38206, 25 August 1978), could be harmful to biological materials if absorbed by the skin and excited by UV light. Thus, TiO_2 particles were encapsulated into zeolites to prevent direct contact of the particles with living tissues.

As seen in Section 3.2.1 and 3.2.2, photoexcited free TiO_2 inactivated CuZnSOD and catalase by ~ 80% after 4 h and 60 min exposure, respectively. Two zeolites were used as hosts for TiO_2, faujasite and mordenite. Although enzyme inactivation due to UVA exposure still occurred, encapsulation of TiO_2 in either zeolite protected both enzymes from the damaging effects of TiO_2. Hence, encapsulation represents a promising technology for the development of new and safer types of sunscreens.

The encapsulation of TiO_2 was expected to reduce the inactivation of catalase by eliminating direct interaction between the TiO_2 particles and the enzyme. However, TiO_2 encapsulation likely prevents enzyme inactivation because the bandgap for TiO_2 particles in zeolites shows a remarkable increase in energy. Effectively, the anatase TiO_2 bandgap is 3.2 eV compared to 4.66-4.81 eV for TiO_2 in zeolite Y [Cosa (2002b)]. Thus, UV light below 385 nm can excite free anatase TiO_2 particles but UV light below 260-265 nm is required to excite encapsulated TiO_2. The latter wavelengths fall within the UVC range and, as mentioned in Section 1.2.1, UVC light is absorbed by the ozone layer and none reaches the earth's surface. A trivial explanation for the protection afforded by

encapsulation is UVA scattering by the zeolites, thus decreasing the efficiency of TiO_2 excitation and ROS production.

Given the inhibition of UVA-induced ROS production by TiO_2, encapsulation may lead to safer and more efficient sunscreens. These results are promising but further study to measure the effects of encapsulated TiO_2 on cells and on living tissues will be required to fully evaluate its potential use in sunscreens.

4.4 Conclusions

Titanium dioxide is one of many components used today in sunscreens. It was described as a safe and efficient sunscreen in 1978 (US Federal Register, 43FR38206, 25 August 1978). However, the present study has shown that when TiO_2 particles are excited by UVA light, they cause inactivation of the key enzymes, CuZnSOD and catalase, involved in the skin's enzymatic antioxidant defense. Thus, instead of protecting the skin, TiO_2-based sunscreens might do the opposite if absorbed by the skin. It has been demonstrated that free $OH^{\bullet}$ radicals and oxygen are involved in the inactivation mechanism of CuZnSOD, which resulted in the degradation of the enzyme and a partial release of active-site copper into solution. Moreover, these copper ions played a role in the inactivation of the enzyme presumably by increasing the production of $OH^{\bullet}$ radicals generated from H_2O_2 by Fenton-type chemistry. Surprisingly, free $OH^{\bullet}$ radicals are not involved in the inactivation of catalase since an $OH^{\bullet}$ radical scavenger was not efficient in preventing enzyme inactivation. This can be explained by the fact that catalase adsorbs on the surface of TiO_2 and reacts directly with the holes generated in the oxide on exposure to UVA light. $OH^{\bullet}$ production would not compete with this process so scavengers would not be efficient in protecting the enzyme. This study also shows that the loss of catalase activity is due to heme degradation.

To render TiO_2 a safer sunscreen, particles were encapsulated in zeolites. When TiO_2 was encapsulated in the zeolites, faujasite and mordenite, the inactivation of CuZnSOD as well as catalase was much lower. In fact, the inactivation observed can be attributed to UVA exposure and not to excitation of TiO_2. These results are very

promising and could lead to the creation of a new generation of safer and more efficient sunscreens.

4.5 Should TiO_2 be used in sunscreens?

As introduced in Section 1.4, TiO_2 is used in sunscreens because it has good scattering properties. However, throughout this study, it was clearly shown that excitation of TiO_2 particles by UVA light leads to inactivation of enzymes such as CuZnSOD and catalase. However, does this mean that TiO_2-based sunscreens should be completely avoided? Unlike the particles used here, the TiO_2 particles used in the formulation of sunscreens are coated with materials such as SiO_2 and Al_2O_3 [Cui (1999)]. This reduces the photochemical activity of the particles and also favours dispersiveness and weather resistance. Although coating the TiO_2 particles reduces their photochemical activity [Dunford (1997)], it is hard to say if the remaining activity is dangerous to the skin. Further studies are required to compare differences in the effects of coated and uncoated TiO_2 on biological materials.

4.6 Proposed future work

In order to complete the study that was started in this thesis, a number of experiments are proposed for future research:

- Since $OH^{\bullet}$ radicals are involved in the inactivation of CuZnSOD, it would be interesting to compare the concentration of $OH^{\bullet}$ radicals produced upon UVA exposure of anatase TiO_2 and encapsulated TiO_2 in zeolites. A spin trap

(DMPO) could be used to measure $OH^{\bullet}$ radicals and electron spin resonance (ESR) could be used to quantify the spin adduct [Uchino (2002)].

- Antioxidant enzyme activities in rat keratinocytes were investigated briefly (Section 3.5 and 3.6). The effects of TiO_2 and UVA light on enzymes in cells needs to be measured. However, some method development will be necessary to optimize the assay conditions for each enzyme.
- It would be interesting to study another hemoprotein to see if its inactivation mechanism is similar to that of catalase.
- TiO_2 was the main focus of the study in this thesis. However, as mentioned in Section 1.1, there are many other compounds used in sunscreens to block UV radiation. It is important to investigate encapsulated organic molecules because organic- and inorganic-based sunscreens protect the skin from harmful UV radiation via different mechanisms.
- As discussed in Section 4.5, the TiO_2 particles found in sunscreens are coated in order to reduce their photochemical activity. It would be interesting to compare the effects of coated TiO_2 on CuZnSOD and catalase activities with the results from this study using uncoated TiO_2.

REFERENCES

Al-Ekabi, H., Serpone, N., *J. Phys. Chem.*, **1988**, *92*, 5726-5731.

Amadelli, R., Argazzi, R., Bignozzi, C. A., Scandola, F., *J. Am. Chem. Soc.*, **1990**, *112*, 7099-7103.

Augugliaro, V., Palmisano, L., Sclafani, A., Minero, C., Pelizzetti, E., *Toxicol. Environ. Chem.*, **1988**, *16*, 89-109.

Bannister, J. V., Bannister, W. H., Rotilio, G., *CRC Crit. Rev. Biochem.*, **1987**, *22*, 111-180.

Bertini, I, Gray, H.B., Lippard, S.J., Valentine, J.S., *Bioinorganic Chemistry*; University Science Books: Mill Valley, California, 1994.

Bray, R. C., Cockle, S. A., Fielden, E. M., Roberts, P. B., Rotilio, G., Calabrese, L., *Biochem. J.*, **1974**, *139*, 43-48.

Cai, R., Hashimoto, K., Itoh, K., Kubota, Y., Fujishima, A., *Bull. Chem. Soc. Jpn.* **1991**, *64*, 1268-1273.

Cobine, P.A., Gearge, G.N., Jones, C.E., Wickramasinghe, W.A., Solioz, M., Dameron, C.T., *Biochemistry,* **2002**, *41*, 5822-5829.

Cosa, G., Chrétien, M. N., Galletero, M. S., Fornés, V., Garcia, H., Scaiano, J. C., *J. Phys. Chem. B*, **2002**, *106*, 2460-2467.

Cosa, G., Galletero, M. S., Fernandez, L., Marquez, F., Garcia, H., Scaiano, J. C., *New J. Chem.*,**2002**, *26*, 1448-1455.

Cotton, F. A., Wilkinson, G., Gaus, P. L., *Basic Inorganic Chemistry*; 3th ed.; Wiley & Sons: New York, 1995.

Cui, A., Wang, T., Jin, Y., *Engineering Chemical & Metallurgy*, **1999**, *20*, 178-181.

Dunford, R., Salinaro, A., Cai, L., Serpone, N., Horikoshi, S., Hidaka, H., Knowlan, J., *FEBS Letters* **1997**, *418*, 87-90.

Eum, S. W., Kang, J. H., *Mol. Cells*, **1999**, *9*, 110-114.

Fach, E., Waldman, W. J., Williams, M., Long, J., Meister, R. K., Dutta, P. K., *Environmental Health Perspectives*, **2002**, *110*, 1087-1096.

Food and Drug Administration (1993) Sunscreen and drug products for over the counter human use; tentative final monograph. *Fed. Reg.* **59**, 28194-28302.

Frain-Bell, W., *Cutaneous Photobiology*, Oxford University Press, New York, 1985.

Gasparro, F. P., *Photodermatology*, **1985**, *2*, 151-157.

Gasparro, F.P., Mitchnick, M., Nash, J.F., *Photochemistry and Photobiology*, **1998**, *68*, 243-256.

Hagfeldt, A., Gratzel, M., *Acc. Chem. Res.*, **2000**, *33*, 269-277.

Halliwell, B., Gutteridge, J. M. C., *Free Radicals in Biology and Medecine: Third Edition*; Clarendon Press: Oxford, 1999.

Hancock-Chen, T., Scaiano, J. C., *J. Photochem. Photobiol. B*, **2000**, *57*, 193-196.

Heinecke, J.W., Li, W., Daehnke, H.L., Goldstein, J.A., *J. Biol. Chem.*, **1993**, *268*, 4069-4077.

Ikeganmi, K., Koide, M., *Japanese Patent*, **1993**, JP 05, 298, 209.

Jabusch, J. R., Farb, D. L., Kerschensteiner, D. A., Deutsch, H. F., *Biochemistry*, **1980**, *19*, 2310-2316.

Jaeger, C. D., Bard, A., *J. Phys. Chem.*, **1979**, *83*, 3146-3152.

Judin, V. P. S. *Chem. Brit.* **1993**, *29*, 503-505.

Kang, J. H., Eum, W. S., *Biochimica et Biophysica Acta*, **2000**, *1524*, 162-170.

Kawaguchi, H. *Environ. Technol. Lett.* **1984**, *5*, 471-474.

Kim, H.-J., Koh, M., *Bull. Korean. Chem. Soc.*, **2001**, *22*, 362-366.

Kitazawa, M., Podda, M., Thiele, J. J., Traber, M. G., Iwasaki, K., Sakamoro, K., Packer, I., *Photochem. Photobiol.*, **1997**, *65*, 355-365.

Klint, D., Arvidsson, P., Blum, Z., Eriksson, H., *Protein Expression and Purification*, **1994**, *5*, 569-574.

Klint, D., Eriksson, H., *Protein Expression and Purification*, **1997**, *10*, 247-255.

Kominami, H., Murakami, S., Kera, Y., Ohtani, B., *Catal. Lett.*, **1998**, *56*, 125-129.

Kondo, N., Wagai, B., *Yotonkai*, **1968**, 1-4.

Kudo, A., Domen, K., Maruya, K., Onishi, T., *Chem. Phys. Lett.*, **1987**, *133*, 517-519.

Kwon, H. Y., Choi, S. Y., Won, M. H., Kang, T.-C., Kang, J. H., *Biochimica et Biophysica Acta*, **2000**, *1543*, 69-76.

Lademann, J.; Weigmann, H.; Rickmeyer, C.; Barthelmes, H.; Schaefer, H.; Mueller, G.; Sterry, W. *Skin Pharmacol Appl Skin Physiol* **1999**, *12*, 247-56.

Litter, M. I., *Appl. Catal., B*, **1999**, *23*, 89-114.

Lopez, D. Z., *Program & Abstracts: Zeolites '91* (Int. Conf. Nat. Zeolites. Havana, Cuba), 1991, p. 187 (abstr.).

Maeda, K., *Eur. Patent Appl.*, **1989**, EP 298, 726.

Malato, S., Blanco, J., Richter, C., Maldonado, M. I., *Appl. Catal., B*, **2000**, *25*, 31-38.

Mallouk, T. E., Yonemoto, E. H., Riley, R. L., Kim, Y. I., Atherton, S. J., Schmehl, R. H., *J. Am. Chem. Soc.*, **1992**, *114*, 8081-8087.

Marklund, S., Marklund, G., *Eur. J. Biochem.*, **1974**, *47*, 469-474.

McCord, J.M., Fridovich, I., *J. Biol. Chem.*, **1969**, *244*, 6049-6055.

Mello Filho, A.C., Meneghini, R., *Biochim Biophys Acta.*, **1984**, *781*, 56-63.

Micic, O. I., Zhang, Y., Cromack, K.R., Trifunac, A.D., Thurnauer, M.C., *J. Phys. Chem.* **1993**, *97*, 13284.

Okamoto, K., Yamamoto, Y., Tanaka, H., Tanaka, M., Itaya, A., *Bull. Chem. Soc. Jpn.* **1985**, *58*, 2015-2022.

Onagi, T., *Rep. Yamagata Stock Raising Inst.*, **1966**, 11-22.

Pantoliano, M. W., Valentine, J. S., Burger, A. R., Lippard, S. J., *J. Inorg. Biochem*, **1982**, *17*, 325-341.

Pond, W. G., *Natural Zeolites '93: Occurrence, Properties, Use*; eds. Ming, D.W. & Mumpton, F. A., (Int. Comm. Nat. Zeolites, Brockport, New York), 1995, 449-457.

Primet, M., Pichat, P., Matthieu, M. V., *J. Phys. Chem* **1971**, *75*, 1216-1220.

Regelsberge, G., Jakopitsch, C., Ruker, F., Krois, D., Peschek, G. A., Obinger, C., *The Journal of Biological Chemistry*, **2000**, *275*, 22854-22861

Roe, J. A., Butler, A., Scholler, D. M., Valentine, J. S., Marky, L., Breslauer, K. J., *Biochemistry*, **1988**, *27*, 950-958.

Salih, F. M., *Journal of Applied Microbiology*, **2002**, *92*, 920-926.

Salter, L. F., Martincigh, B. S., Bolton, K., Aliwell, S. R., Clemmett, S. J., *Biological Effects and Physics of Solar and Galactic Cosmic Radiation,* Part A; Plenum Press: New York, 1993.

Samejima, T., Tsi Yang, J., *J. Biol. Chem.,* **1963**, *238*, 3256-3261.

Scharffetter-Kochanek, K., Wlaschek, M., Brenneisen, P., Schauen, M., Blaudschun, R., Wenk, J., *Biol. Chem.,* **1997**, *378*, 1247-1257.

Schonbaum, G. R., *J. Biol. Chem.*, **1973**, *248*, 502-511.

Sclafani, A., Herrmann, J. M., *J. Phys. Chem.* **1996**, *100*, 13655-13661.

Serpone, N., Lawless, D., Khairutdinov, R., Pelizzeti, E., *J. Phys. Chem* **1995**, *99*, 16655-16661.

Shaw, A. A., Wainschel, L. A., Shetlar, M. D., *Photochem. Photobiol.*, **1992**, *55*, 657-663.

Stadtman, E.R., *Science*, **1992**, *257*, 1220-1224.

Steinman, H. M., Naik, V. R., Abernethy, J. L., Hill, R. L., *J. Biol. Chem.*, **1974**, *249*, 7326-7338.

Sutherland, J.C., Griffin, K.P., *Photochem. Photobiol.*, **1984**, *40*, 391-394.

Tainer, J. A., Getzoff, E. D., Beem, K. M., Richardson J. S., Richardson, D. C., *J. Mol. Biol.*, **1982**, *160*, 191-217.

Tan, M. H.; Commens, C. A.; Burnett, L.; Snitch, P. J. *Australas J Dermatol* **1996**, *37*, 185-187.

Uchino, T., Tokunaga, H., Ando, M., Utsumi, H., *Toxicology in Vitro*, **2002**, *16*, 629-635.

Valentine, J. S., Pantoliano, M. W., *Copper Proteins*; Wiley: New York, 1981.

Valentine, J. S., Mota de Freitas, D., *J. Chem. Ed.*, **1985**, *62*, 990-997.

Van Bekkum, H., Flanigen, E. M., Janses, J. C., *Introduction to Zeolites Science and Practice*; Elsevier Science: New York, 1991.